ENGINEERING-PDH.com
ONLINE CONTINUING EDUCATION

COLD-FORMED STEAL SEISMIC DESIGN RECOMMENDATIONS - VOL 2 OF 3

Main Category:	Civil Engineering
Sub Category:	Structural
Course #:	STR-118
Course Content:	141 pgs
PDH/CE Hours:	7

OFFICIAL COURSE/EXAM

(SEE INSTRUCTIONS ON NEXT PAGE)

WWW.ENGINEERING-PDH.COM
TOLL FREE (US & CA): 1-833-ENGR-PDH (1-833-364-7734)
SUPPORT@ENGINEERING-PDH.COM

STR-118 EXAM PREVIEW

- TAKE EXAM! -

Instructions:

- At your convenience and own pace, review the course material below. When ready, click "Take Exam!" above to complete the live graded exam. (Note it may take a few seconds for the link to pull up the exam.) You will be able to re-take the exam as many times as needed to pass.
- Upon a satisfactory completion of the course exam, which is a score of 70% or better, you will be provided with your course completion certificate. Be sure to download and print your certificates to keep for your records.

Exam Preview:

1. According to the reference material, the static cyclic testing does not account for dynamic effects that will be experienced in real earthquakes.
    a. True
    b. False
2. The article, "A Rational Approach for Deter-mining Response Modification Factors for Seismic Design of Building Using Current Code Provisions" requires a series of nonlinear time-history analyses of representative building frames to determine what R coefficient is needed for a given structural system to achieve a 90% probability of collapse prevention for the 2% probability of exceedance in __ year seismic hazard.
    a. 10
    b. 25
    c. 50
    d. 75
3. Using Table 8-6. Coupon test results for materials used in shake table model shear panels, what was the yield stress for the diagonal straps used in the study?
    a. 71 ksi
    b. 53.6 ksi
    c. 54.5 ksi
    d. 48.0 ksi
4. Unlike seismic loads, Wind loads are well understood by structural engineers. Statistics on wind velocities are recorded regularly and have been for nearly 100 years.
    a. True
    b. False

5. The total (inelastic) lateral strength of a typical cold-formed steel building may be 2 times greater than the design value while the total strength of a moment frame building may be __ times greater than the design.
    a. 3
    b. 4
    c. 5
    d. 6
6. For panels that have an aspect ratio less than 1, a mid-height horizontal compression member should be installed that should reduce bending loads on the columns
    a. True
    b. False
7. According to the reference material, specifically discussing the Panel G configuration, the diagonal tension field should develop at close to a __ degree angle, so panels that have an aspect ratio of 1 would be most efficient.
    a. 20
    b. 30
    c. 45
    d. 60
8. According to the reference material, at least three coupons of each material shall be tested. Coupons shall be prepared and tested following the provisions of ASTM A___ (ASTM 2014b).
    a. 290
    b. 370
    c. 380
    d. 450
9. Using Table D-5. Acceptance criteria for shear panels based on μ, Ω, and ϱ1, what is the acceptance requirement for panel overstrength Ω.
    a. ≥1.3
    b. ≥1.5
    c. ≥1.7
    d. ≥1.9
10. According to the reference material, the current design codes are based on a maximum considered earthquake (MCE) earthquake with a return period of 2,475 years.
    a. True
    b. False

Contents

8 Shake Table Model Verification Test

In October 2000, ERDC-CERL began a project to characterize the inelastic response of structural systems. Ductile behavior is critical to good structural performance of buildings in earthquakes. Current building code provisions recognize degrees of assumed ductile behavior through the use of a seismic response modification coefficient, R. Seismic loads used to design the vast majority of buildings (linear static or dynamic design) are inversely proportional to this coefficient. Values for these coefficients vary from a low of 1.25 (e.g., steel ordinary cantilever column systems) to a maximum of 8.0 (e.g., steel eccentrically braced frames) in ASCE/SEI 7-10, Table 12.2-1. These values are intended to represent the degree of ductility, overstrength, redundancy, and energy dissipation capacity of the structural system. These coefficients have a tremendous impact on the design of buildings, yet there is a no rational basis for defining the values. FEMA P-750, section C12.1.1, states "the R values in the standard are based largely on engineering judgment of the performance of the various materials and systems in past earthquakes. The R factor for a specific project should be chosen and used with care." The article, "A Rational Approach for Determining Response Modification Factors for Seismic Design of Building Using Current Code Provisions" (Foutch and Wilcoski 2005), proposes a rational approach for defining the R coefficient. This approach builds on the probabilistic procedures for design and assessment of steel moment-resisting frame buildings developed for the SAC project. This approach requires a series of nonlinear time-history analyses of representative building frames to determine what R coefficient is needed for a given structural system to achieve a 90% probability of collapse prevention for the 2% probability of exceedence in 50 year seismic hazard. The series of analysis cases with various ground motions and building configurations is needed to establish the probabilistic data. This nonlinear analysis is used to define both the deformation capacity and demand for each of the analysis cases that use ground motions representative of the seismic hazard.

The proposed procedure was applied to the cold-formed steel structural system, based on the seismic design recommendations presented in this report. The capacity is defined based on a hysteretic load-versus-deformation characterization of critical components of the lateral-load-resisting system. This hysteretic characterization is based on cyclic testing

in a laboratory. Full-scale cold-formed steel shear panels were tested at ERDC-CERL (see Chapter 7), and they provided very predictable hysteric behavior that could be readily modeled in the example analysis (see Chapter 5).

However, the static cyclic testing does not account for dynamic effects that will be experienced in real earthquakes. The hysteretic load-versus-deflection plots of cold-formed steel shear panels are severely pinched, because the main panel lateral-load-resisting elements are thin diagonal straps that only offer resistance under tensile load. After a deformation cycle that causes strap yielding, the panel will have little resistance until deformations have cycled in the opposite direction to amplitudes that the opposite straps become taut. While the straps are slack, the structure above the panel can develop significant velocity, and the straps can snap when they become taut again. This will cause large accelerations and apply large impulsive loads to the joints. The strap connections to the columns must not fail; the columns must not buckle; or the anchors of the columns must not fail. Any of those failures could be brittle, and are not represented by the ductile hysteretic behavior defined in the laboratory. Other structural systems that have pinched hysteretic envelopes may have similar issues.

The static cyclic tests also do not represent the large P-delta-related overturning moments that could result at large deformations of multistory building frames. Therefore shake table testing of a full-scale model was needed to evaluate the effectiveness of the nonlinear analysis in representing the dynamic response of structures at large deformations. This verification testing evaluated the ability to define the deformation demand and capacity of the lateral-load-resisting system. A new analytical procedure was developed for the SAC work called incremental dynamic analysis (IDA) for defining the deformation capacity, and this same procedure is used in the proposed approach for defining R coefficients for all structural systems. The IDA procedure was never experimentally validated for the SAC project. The verification testing should be at full scale to avoid introducing errors associated with scaling relationships and component behavior that will differ with much different scale section properties. This chapter documents a two-story, full-scale shake table verification model that was tested with one of the more severe ground motions used in the analysis presented in Foutch and Wilcoski (unpublished).

8.1 Shake table model configuration

Figure 8-1 shows a photograph of the cold-formed steel shake table model assembled on the ERDC-CERL Triaxial Earthquake and Shock Simulator (TESS shake table). The model is full scale, consisting of two framing lines of two-story cold-formed steel shear panels. Supplemental weight was added above and below the floor slabs.

Figure 8-2 shows an elevation view drawing of the model. This model was shaken with uniaxial motions, in the in-plane direction relative to this drawing. The model consists of two identical two-story, one bay wide frames, which are separated from each other by 154 in. on center in the out-of-plane direction. The second-story frame is identical to the first story, though the loads on first story are greater so that significant nonlinear response would occur on the first story only, where it could be more easily observed during the test. Figure 8-3 presents an out-of-plane view of this model, showing these two frames. A heavy reinforced concrete slab diaphragm was installed at the top of each floor level. The concrete slabs were 8 in. thick and 14.5 ft square. The slabs were designed to be very stiff, representing a beam at the top of the wall panels. Each slab weighed 21,000 lb. In a typical building shear panels might be installed in one of every 5 or 10 bays. Therefore, additional weights were added to the slabs in order to model the mass that might come from other bays of a typical building. All the available steel plate and lead weights at ERDC-CERL that could be easily installed to the model were evenly distributed on the two slabs. This was approximately 24,000 lb of steel plates and 40,000 lb of lead, plus channels to hold them in place. Figure 8-3 shows that 13,000 lb of steel weights (plates with channels) were attached to the bottom of each floor slab. This figure shows 22,700 lb of lead weights (lead plus steel channels) attached to the top of the first-floor slab and 23,200 lb at the top of the second floor slab. The weight of the shear panels was 400 lb, so that the effective model weight at the first floor was 57,500 lb (21,000 lb + 13,000 lb + 22,700 lb + 2 x 2 x 400 lb/2), and the effective weight at the second floor was 57,600 lb (21,000 lb + 13,000 lb + 23,200 lb + 2 x 400 lb/2). Figure 8-4 through Figure 8-7 are plan views of the first- and second-story slabs, showing the locations of the supporting channels and steel weights below the slabs and lead weights above the slabs. Figure 8-8 illustrates safety restraints built into the experiment to address the unlikely event of brittle failure of shear panel straps that might result in a collapse of the model. Figure 8-8 also shows the backup pipe columns that would “catch” the first-floor slab if the first-floor cold-formed steel columns buckled.

Figure 8-1. Photograph of the cold-formed steel verification model mounted on the ERDC-CERL TESS (viewed from northeast corner).

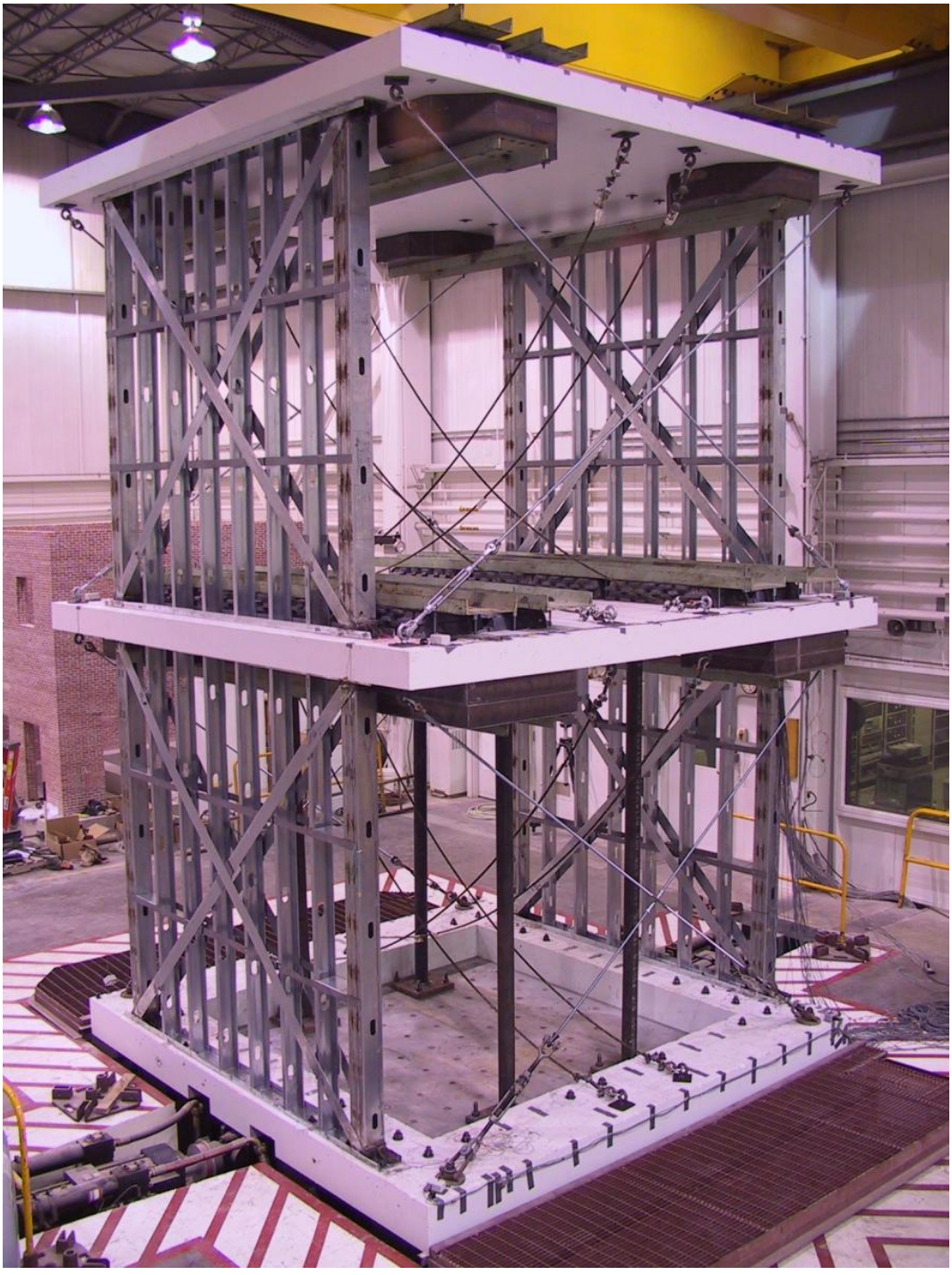

Figure 8-2. In-plane elevation drawing of the verification model.

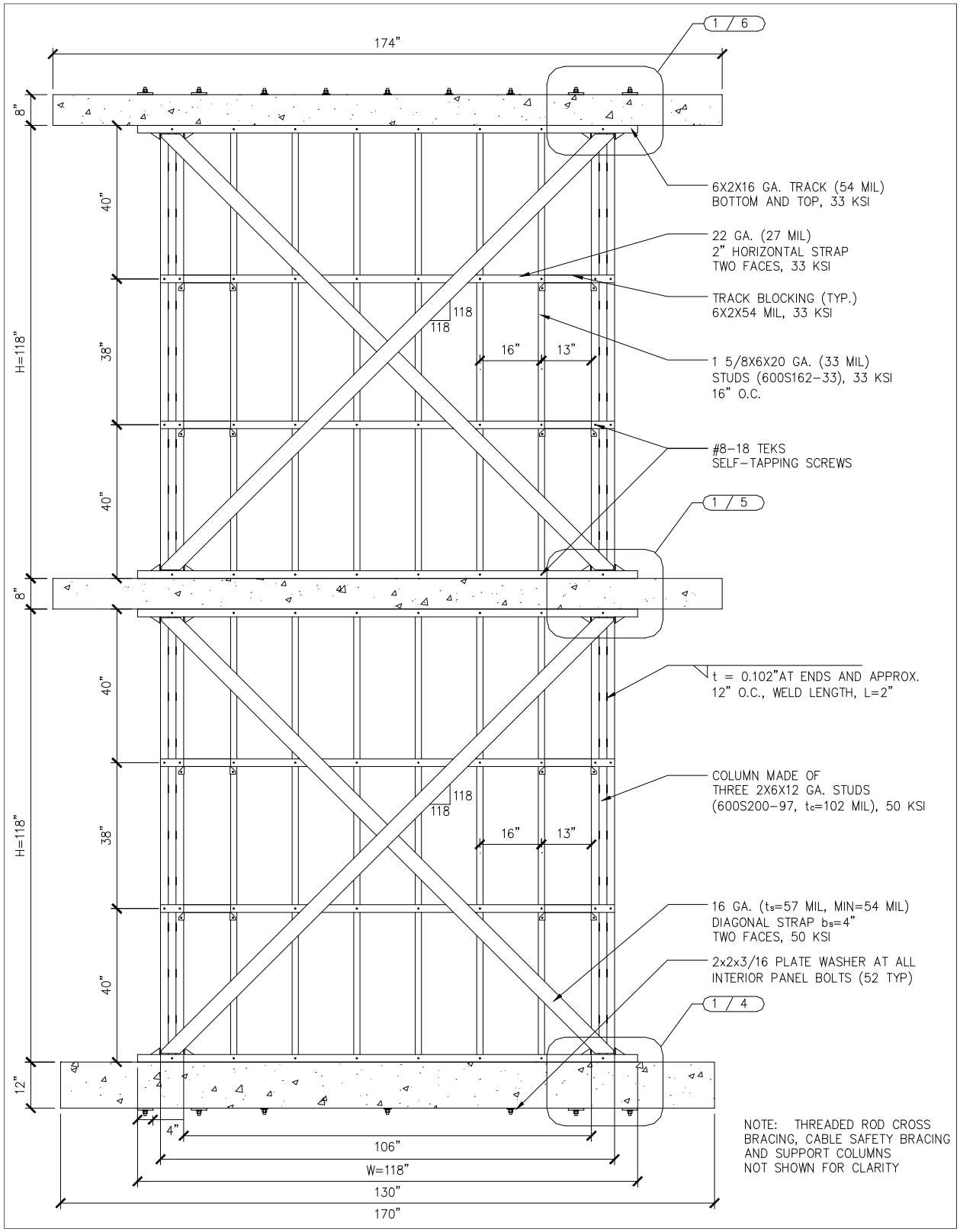

Figure 8-3. Out-of-plane elevation drawing of the verification model, showing weights.

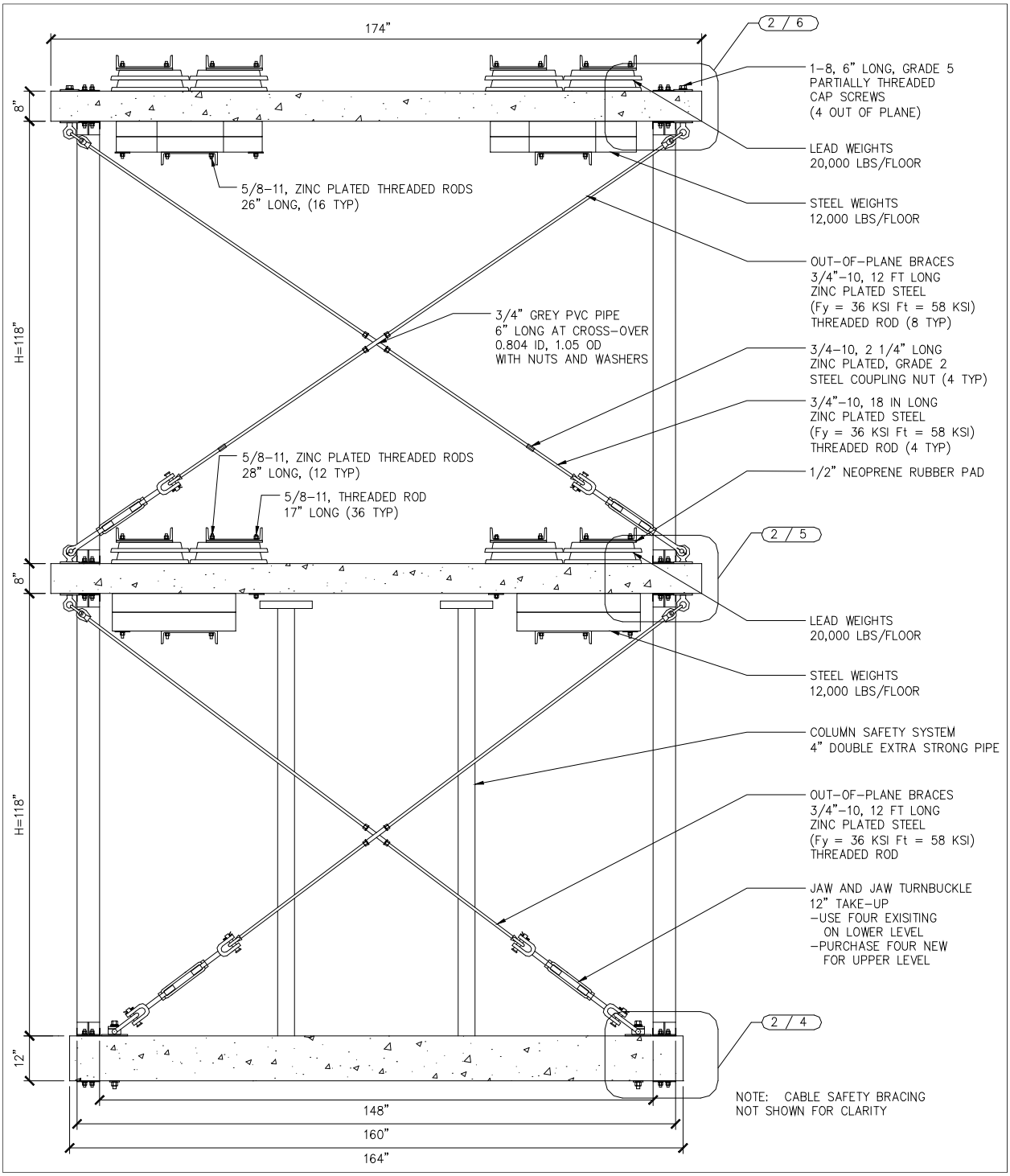

Figure 8-4. Plan view showing the steel plate weights below the first-story slab.

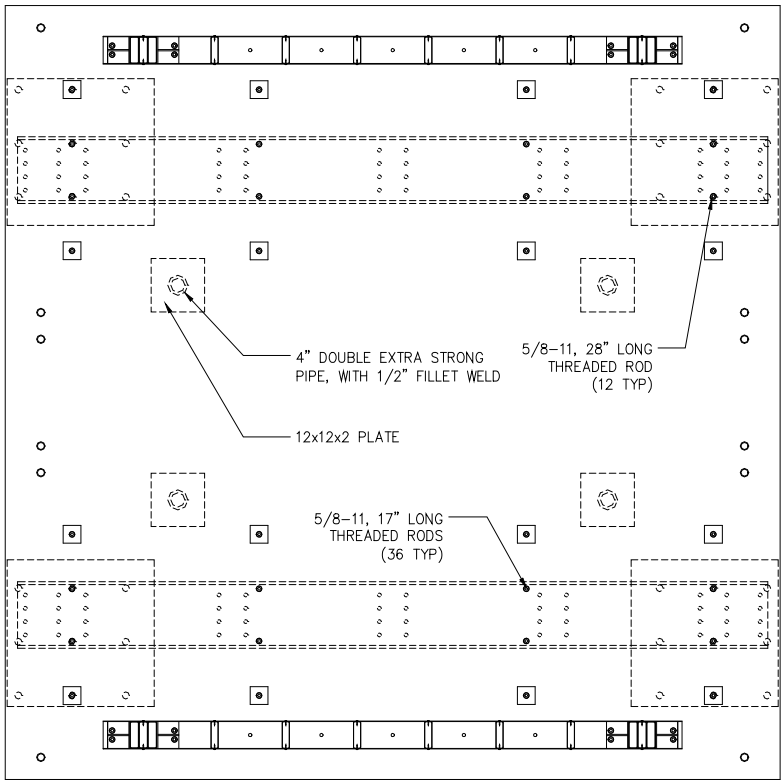

Figure 8-5. Plan view showing the lead weights above the first-story slab.

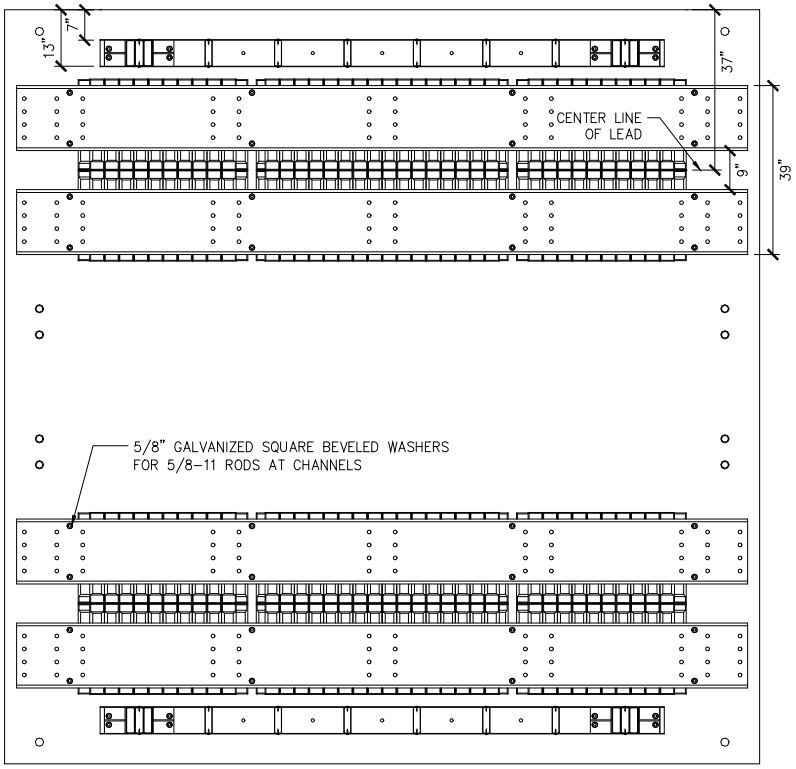

Figure 8-6. Plan view showing the steel plate weights below the second-story slab.

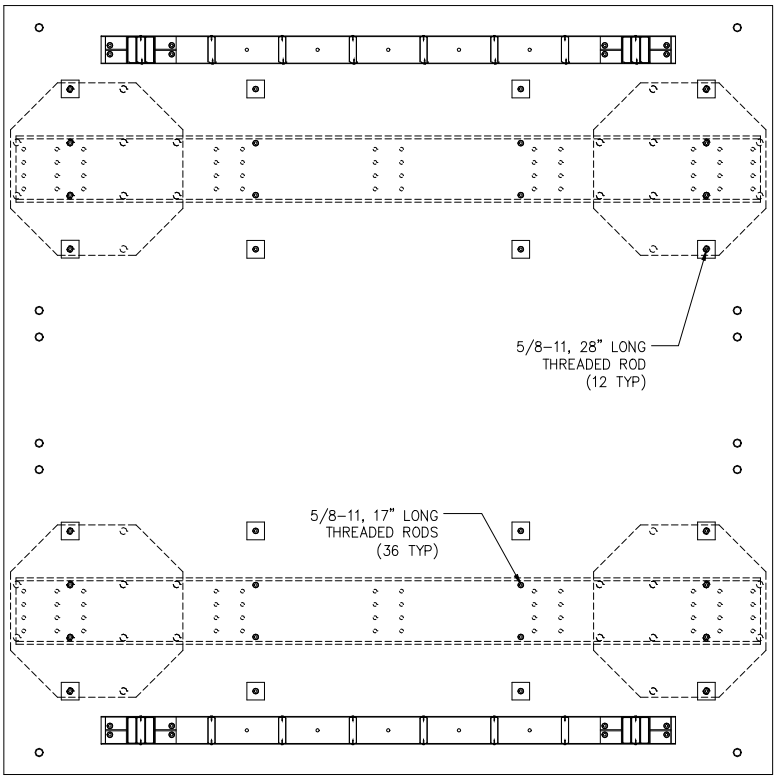

Figure 8-7. Plan view showing the lead weights above the second-story slab.

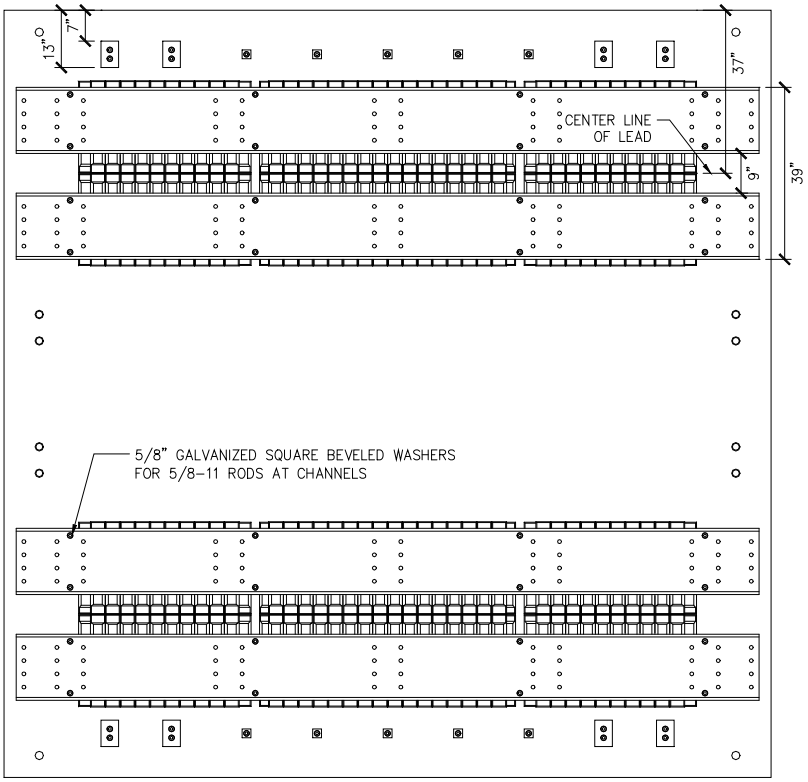

Figure 8-8. In-plane elevation view showing the floor slabs with safety cables (shear panels and weights not shown).

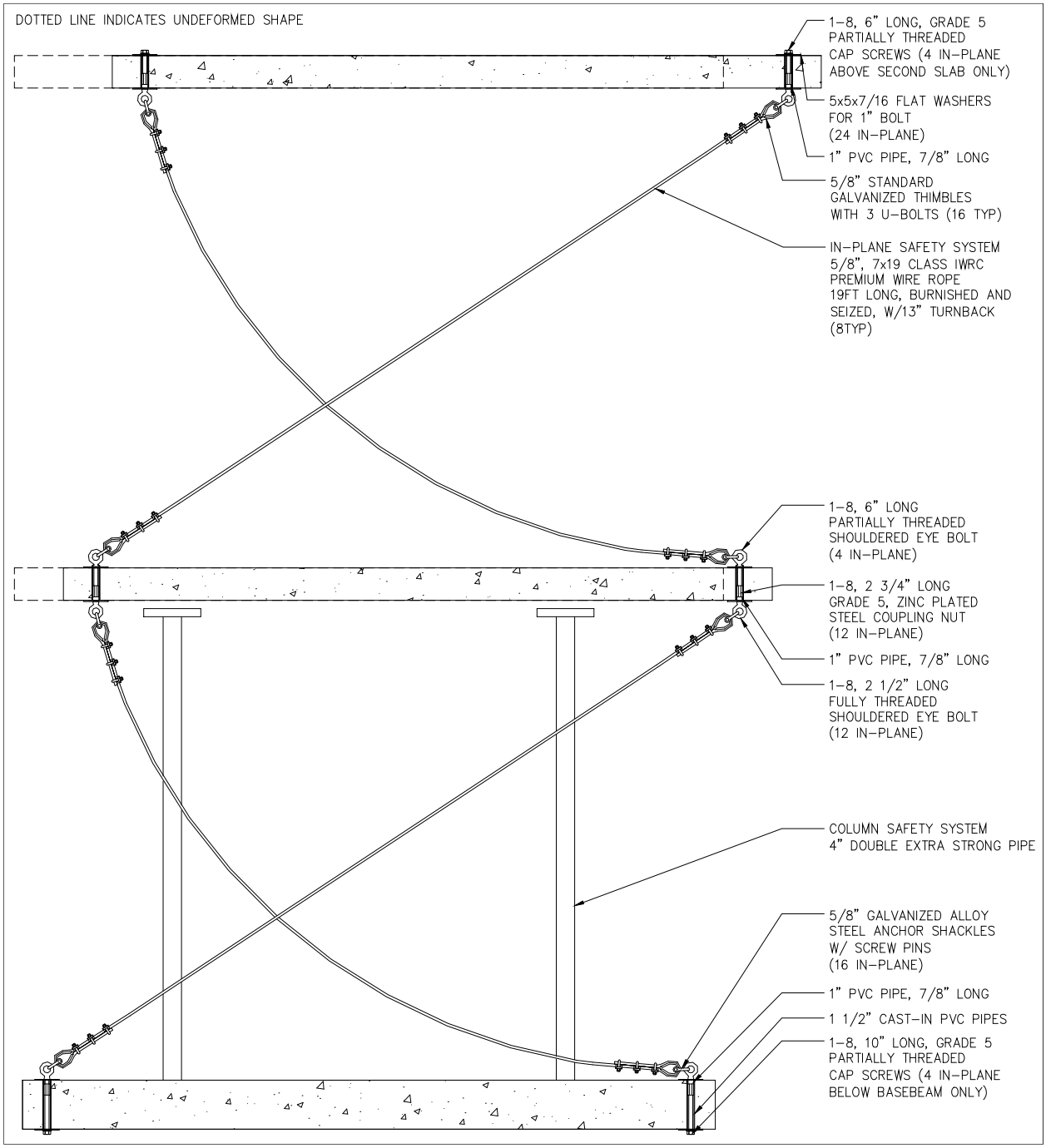

The weight estimates neglect the minimal additional weight of the hardware shown in Figure 8-3. The heavy slabs prevent flexural bending or in-plane rotation of the floor diaphragms, so that the single bay frame would provide similar frame response as a multiple bay building frame. The columns at the exterior edges of the frame were very stiff axially and had

moment connections to the slabs with through-bolts to the base beam below or slabs above.

Figure 8-3 shows that 0.75 in. threaded rod braces were installed out of plane to prevent unwanted out-of-plane model response. In the unlikely event that the panel diagonal straps were to fail in a brittle manner, loose cables were installed in the in-plane direction to "catch" the slabs. Two 5/8 in. diameter cables were installed in each direction at each floor level, and their lengths were such that they would become taut and carry load at 12 in. lateral deflection at each floor level. Figure 8-8 shows the floor slabs only (i.e., with shear panels and weights removed) at the 12 in. lateral deflection, when these cables would begin to restrain the slabs. In the very unlikely event that the model columns were to buckle and collapse, four 4 in. diameter double extra-strong pipe columns with 2 in. thick square plates welded to their tops and bottoms were installed below the first-floor slabs (see Figure 8-3 and Figure 8-8). The pipe column heights were such that the plates at the tops of the columns were 2 in. below the first-floor slab. Therefore this slab would need to drop 2 in. before making contact with these safety pipe columns. The safety columns were only installed at the first-floor level because the frames at the two levels are identical and the first-floor panel columns were loaded at almost twice the axial and bending loads as on the second floor.

8.2 Shake table model design

The shear panels installed in this model at both floor levels were full scale-wall panels designed for a base shear of 15.8 kips per panel, or 31.6 kips for both frames (see Table 8-1).

Table 8-1. Cold-formed steel diagonal strap design for shake table model.

Panel Level	Panel Width W (in)	Panel Height H (in)	Strap Faces n_s (#)	Strap Width b_s (in)	Strap Thickness (ga)	Strap Thickness t_s (in)	Strap Initial Lat Stiffness k_s (k/in)	Yield Stress of Strap F_{sy} (ksi)	Capacity at Strap Lat Yield Q_{sy} (k)	Design Shear Strength $\phi_t Q_{sy}$ (k)	Lat Defl at Strap Yielding δ_{sy} (in)	Applied Story Shear V_x (kips)	Elastic Lateral Defl δ_{xe} (in)	Defl Amp Factor C_d	Import Factor I	Design Story Drifts $\Delta = \delta_x$ (in)	Stability Coeff θ	Allow Story Drifts Δ_a (in)
2nd Fl	118	118	2	4	16	0.055	38	53.6	16.62	15.78	0.436	14.40	0.378	3.5	1.0	1.32	0.0100	2.36
1st Fl	118	118	2	4	16	0.055	38	53.6	16.62	15.78	0.436	21.58	0.567	3.5	1.0	1.98	0.0100	2.36

The diagonal straps were welded to the tops and bottoms of the columns as shown at the left sides of Figure 8-9 through Figure 8-11. These figures also show the column anchor details and out-of-plane details on their right sides. The connections and the columns themselves, plus the anchors to the base beam and floor slabs above, were all designed following the de-

sign recommendations presented in Chapter 11. However, these components were designed assuming the diagonal strap maximum strength was equal to the actual strength measured in coupon testing. They were also designed for the actual gravity load applied to the first-story panels (i.e., $Gl_{max} = GL_{min}$ = 115.1 kips/2 panels = 57.6 kips). The welded diagonal strap-to-column connections and the column anchors were then designed for the true loads applied to them based on the coupon material test results and actual gravity loads. These design assumptions provided an opportunity to evaluate actual shear panel performance under dynamic loading when critical components such as connections and anchors would be loaded the maximum that the design recommendations permit. They permit the evaluation of these potentially brittle components when the shear panels experience significant inelastic response. Section 8.4 presents tabular data on the shear panel design used to define the predicted lateral load-versus-deformation behavior.

The design recommendations in this Chapter 11 require the use of an R coefficient of 4. However, in order to test the nonlinear demand and capacity at large deformations, the cold-formed steel shear panels were undersized for the loads applied to them, based on an R coefficient of 4. Figure 8-12 shows one of the most severe synthetic records (SE32) used in the example analysis presented in Foutch and Wilcoski (unpublished). The model first mode of vibration was predicted to be just over 2 Hz. Figure 8-13 shows the SE32 record has a relatively level response-spectrum amplitude from 2.3 Hz down to 1 Hz. As the straps yield in the test, the effective natural frequency decreases so that the support motions below 2 Hz were expected to dominate the model response later in the test. The shake table model had to be tested in the shorter stroke direction of the TESS due to safety considerations. In this direction, the peak-to-peak stroke is limited to 5.5 in. The unfiltered record shown in Figure 8-12 has displacements that exceed the displacement limits of the TESS in this direction, so the record was high-pass filtered at 1.0 Hz to bring the maximum displacements down to within these limits. Figure 8-12 plots the 1.0 Hz high-pass filtered record with the unfiltered record, showing they match well. Figure 8-13 shows the response spectra for both the filtered and unfiltered records, showing the good fit above 1.0 Hz. Figure 8-14 shows the filtered and unfiltered acceleration records, zoomed in at the strong-motion portions between 16 and 40 seconds.

Figure 8-9. In-plane and out-of-plane connections and anchorage details at the second-story slab.

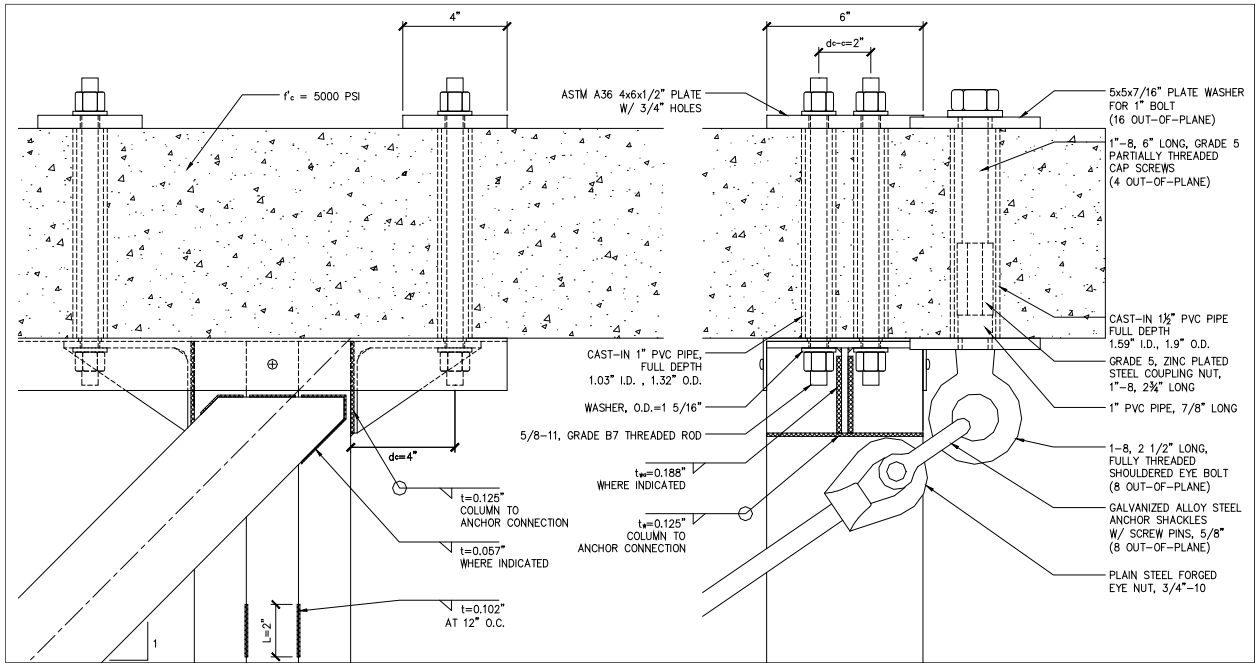

Figure 8-10. In-plane and out-of-plane connections and anchorage details at the first-story slab.

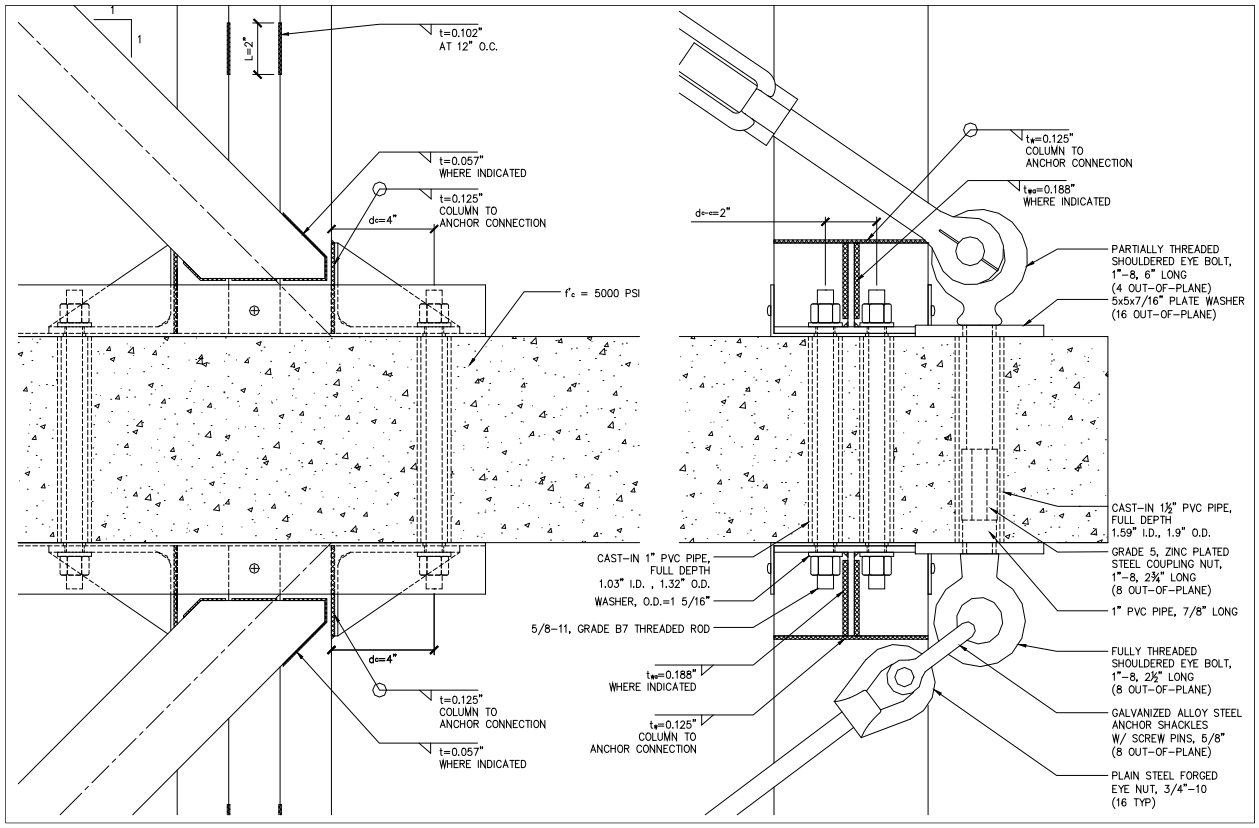

Figure 8-11. In-plane and out-of-plane connections and anchorage details at the base beam.

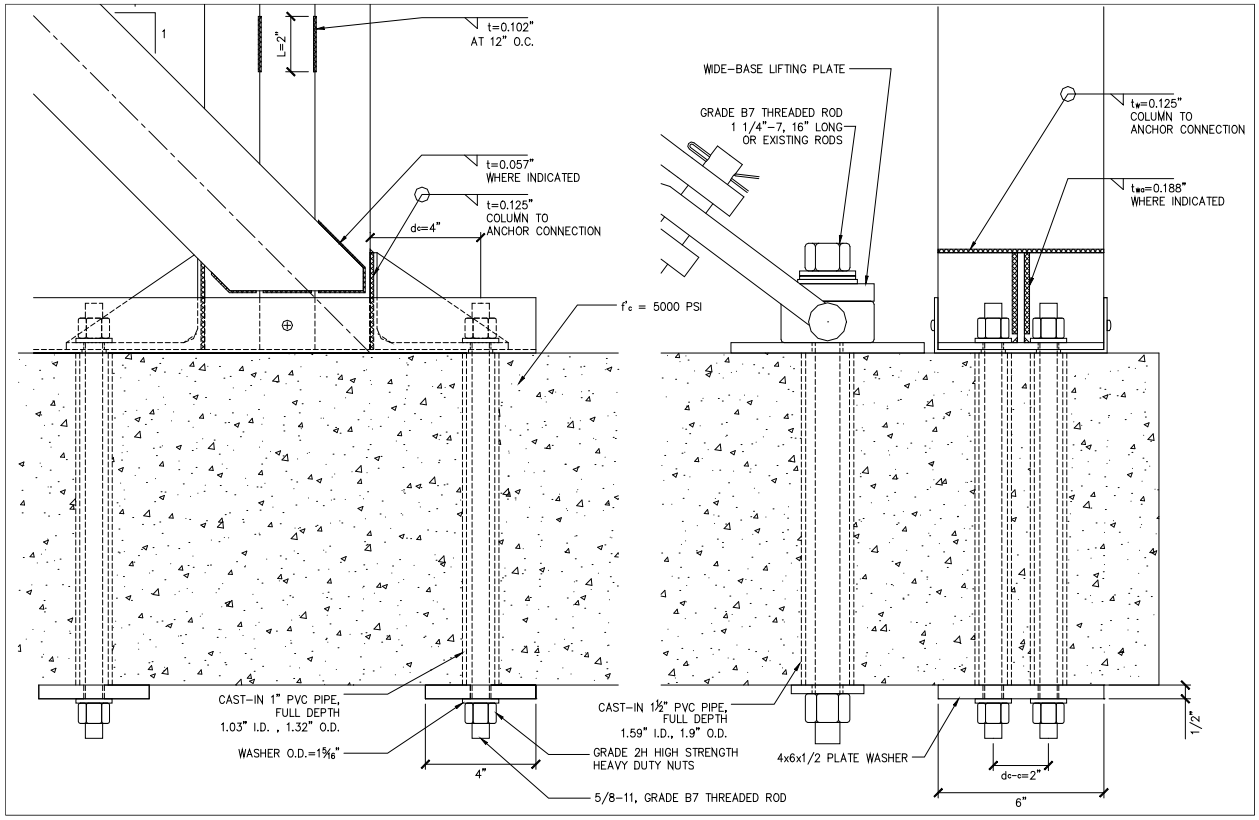

Figure 8-12. SE32 synthetic earthquake record and SE32 record filtered at 1.0 Hz.

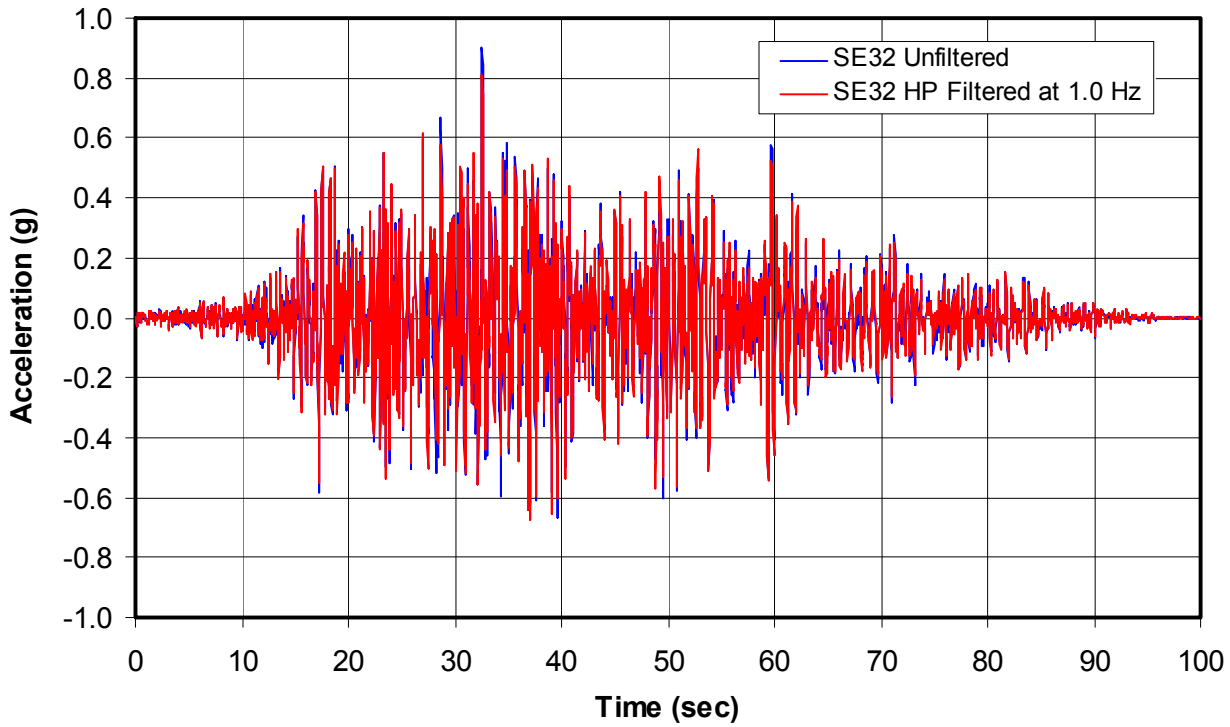

Figure 8-13. Response spectra plots of the SE32 unfiltered and filtered records.

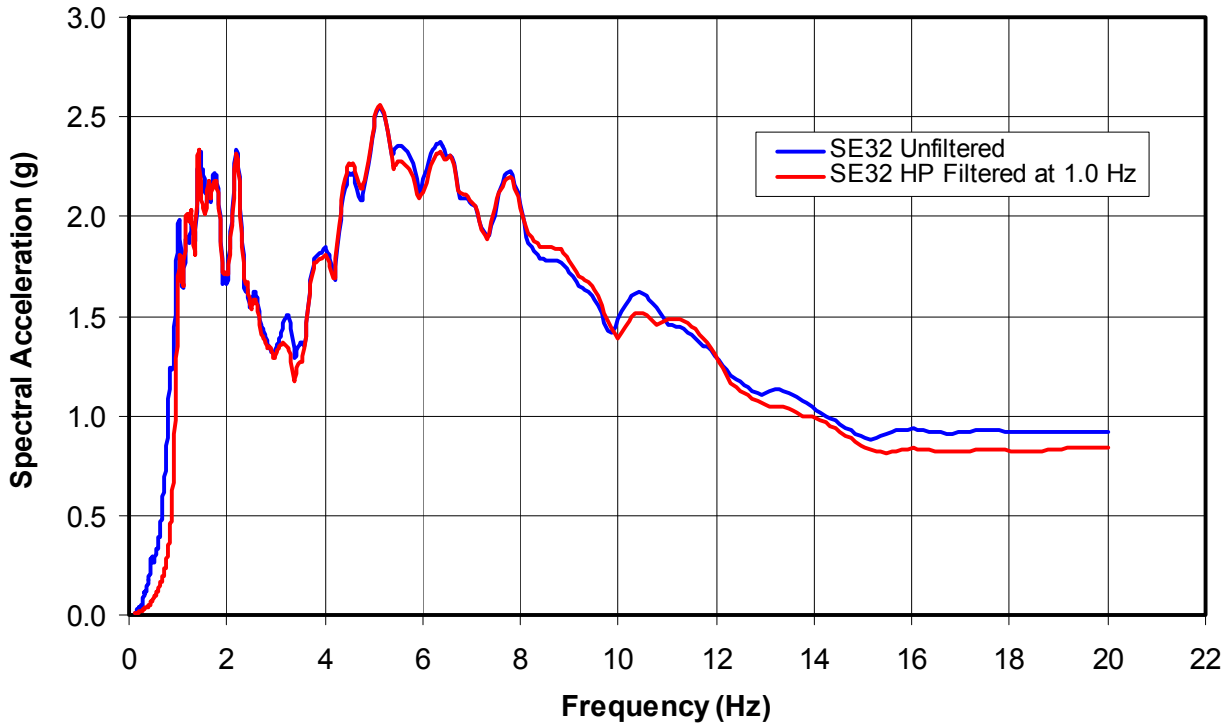

Figure 8-14. Strong motion portion of the SE32 unfiltered and filtered records.

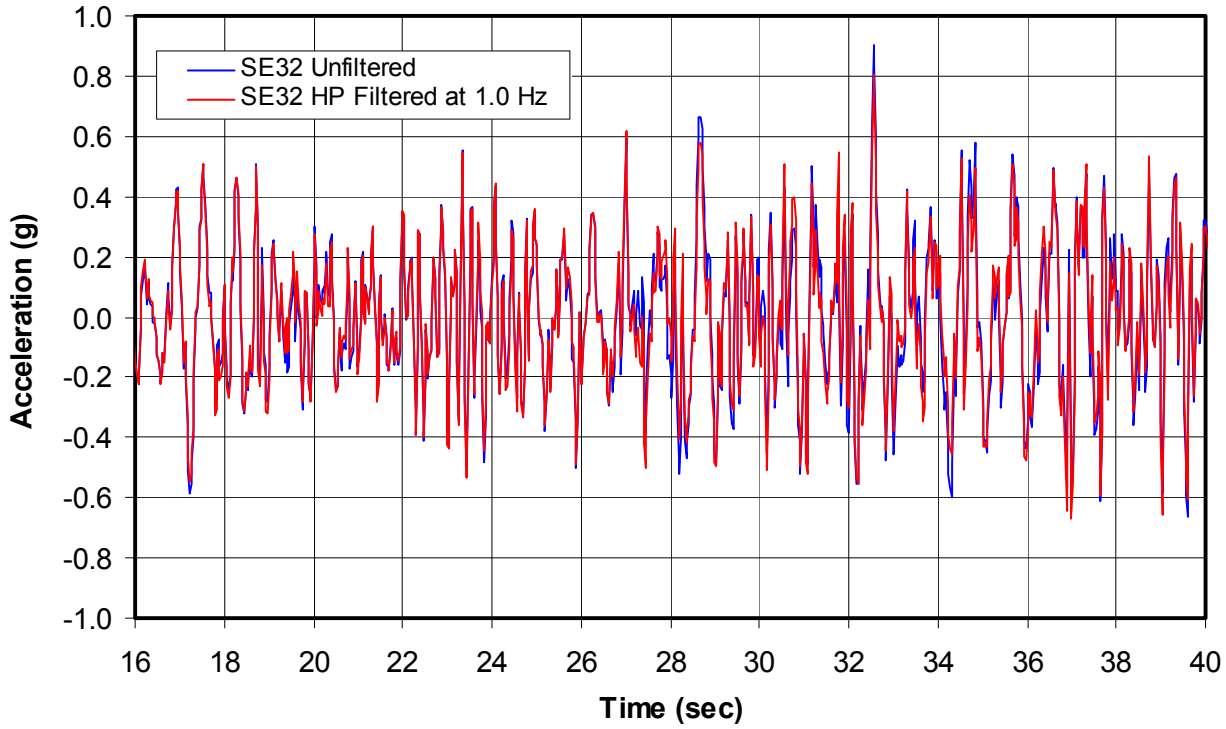

These records were double integrated to generate displacement time-history records. The strong-motion portions of these records are plotted in Figure 8-15 for both the filtered and unfiltered SE32 record, showing the large reduction of displacement amplitude in the filtered record.

Figure 8-15. Strong motion portion of the SE32 unfiltered and filtered displacement records.

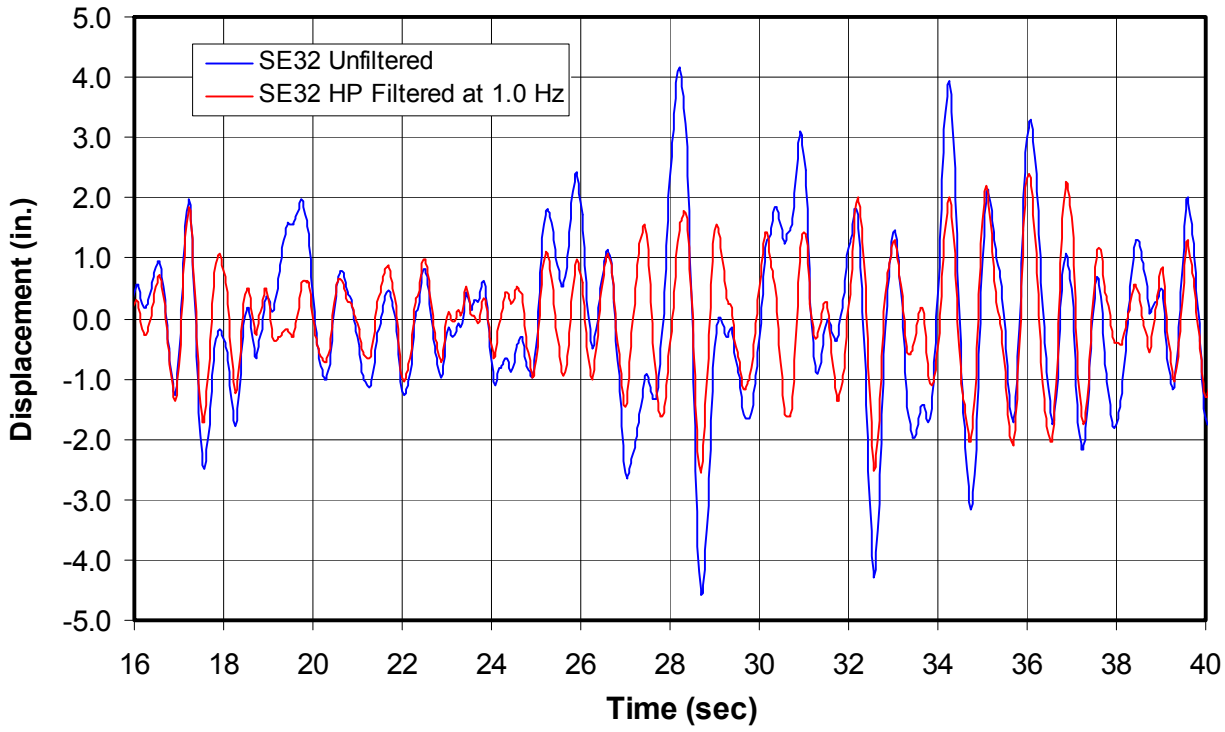

The unfiltered SE32 accelerometer waveform was developed to fit a design response spectrum that has a spectral response acceleration at short periods, S_{DS} of 1.5 g. Using the equivalent lateral force procedure, an R coefficient of 4, and an I of 1.0, the seismic base shear, V for this shake table model was estimated to be 21.6 kips per frame, or 43.2 kips for both frames ($V = S_{DS}I/R \times W$). Based on an R of 4, these first-story shear panels were significantly underdesigned. Table 8-2 summarizes these calculations based on the assumption that these frames are placed in the short direction of a building.

Table 8-2. Base shear and seismic story shears for shake table model.

Total Dead Load D_T= D+EW+IW (kips)	Total Floor Live Load L (kips)	Panel Level	Short Direction Total Weight W_S (k-mass)	Response Modification Factor R	Seismic Response Coefficient C_s (g)	Short Dir Base Shear V_S (kips)	Height at Floor Level h_{xS} or h_{xL} (ft)	Short Dir Vertical Distribution Factor C_{vxS}	Number Frames in Short Dir n_S	Short Dir Lateral Seismic Force/frame F_{xS} (kips)	Short Dir Seismic Story Shear V_{xS} (kips)
21	36.6	2nd	58				252	0.667	2	14.40	14.40
		Cumulative	58								14.40
21	36.5	1st	58				126	0.333	2	7.19	7.19
		Cumulative	115	4.00	0.375	43.2					21.58
			115	5.53	0.271	31.2					15.608

This applied load is 38% greater than the design capacity of the panels shown in Table 8-1. The last row in Table 8-2 shows that the R coefficient would need to be increased to 5.53 for the calculated first-story applied load to drop to the design capacity. The first-story shear panels were significantly undersized so they deform significantly, permitting the assessment of panel demand and capacity at very large drifts. This is needed to evaluate the ability to model nonlinear behavior at large drifts. The nonlinear analysis conducted using Drain 2DX predicts the panels will experience drifts of 5% of the story heights, which is almost 6 in. lateral drift in the first-story shear panels.

It must be noted that the purpose of the shake table test is to verify nonlinear analysis at large deformations, not to evaluate the performance of cold-formed steel shear panels. However, even though the cold-formed steel panels were significantly underdesigned for the loads that were be applied to them, the test should demonstrate very ductile behavior of this structural system, which is one of the benefits of cold-formed steel construction following the design recommendations presented in Chapter 11.

8.3 Model instrumentation

The shake table verification model was instrumented with accelerometers, displacement gages and strain gages. The instrument type and locations were selected to provide the model response measurements that could be compared directly with the calculated behavior from the DRAIN 2DX analysis.

8.3.1 Accelerometers

Table 8-3 gives the sensor names, locations, direction of measurement, full-scale range and resolution of measurement for each accelerometer.

Table 8-3. Shake table verification model accelerometers.

#	Sensor Name	Model Level	Sensor Coordinates* X (in.)	Y (in.)	Z (in.)	Sensor Direction	Full Scale (g)	Resolution (g)
0	ATx	TESS				Longitudinal (X)	4.0	0.00012
1	A1x	Basebeam	2	2	0	Longitudinal (X)	5.0	0.00015
2	A1y	Basebeam	2	2	0	Lateral (Y)	5.0	0.00015
3	A1z	Basebeam	2	2	0	Vertical (Z)	5.0	0.00015
4	A2x	Basebeam	168	2	0	Longitudinal (X)	5.0	0.00015
5	A2y	Basebeam	168	2	0	Lateral (Y)	5.0	0.00015
6	A2z	Basebeam	168	2	0	Vertical (Z)	5.0	0.00015
7	A3x	Basebeam	2	162	0	Longitudinal (X)	5.0	0.00015
8	A3y	Basebeam	2	162	0	Lateral (Y)	5.0	0.00015
9	A3z	Basebeam	2	162	0	Vertical (Z)	5.0	0.00015
10	A4z	Basebeam	168	162	0	Vertical (Z)	5.0	0.00015
11	A11x	1st Floor	2	2	126	Longitudinal (X)	5.0	0.00015
12	A11y	1st Floor	2	2	126	Lateral (Y)	5.0	0.00015
13	A11z	1st Floor	2	2	126	Vertical (Z)	5.0	0.00015
14	A12x	1st Floor	168	2	126	Longitudinal (X)	5.0	0.00015
15	A12y	1st Floor	168	2	126	Lateral (Y)	5.0	0.00015
16	A12z	1st Floor	168	2	126	Vertical (Z)	5.0	0.00015
17	A13x	1st Floor	2	162	126	Longitudinal (X)	5.0	0.00015
18	A13y	1st Floor	2	162	126	Lateral (Y)	5.0	0.00015
19	A13z	1st Floor	2	162	126	Vertical (Z)	5.0	0.00015
20	A14z	1st Floor	168	162	126	Vertical (Z)	5.0	0.00015
21	A21x	2nd Floor	2	2	252	Longitudinal (X)	5.0	0.00015
22	A21y	2nd Floor	2	2	252	Lateral (Y)	5.0	0.00015
23	A21z	2nd Floor	2	2	252	Vertical (Z)	5.0	0.00015
24	A22x	2nd Floor	168	2	252	Longitudinal (X)	5.0	0.00015
25	A22y	2nd Floor	168	2	252	Lateral (Y)	5.0	0.00015
26	A22z	2nd Floor	168	2	252	Vertical (Z)	5.0	0.00015
27	A23x	2nd Floor	2	162	252	Longitudinal (X)	5.0	0.00015
28	A23y	2nd Floor	2	162	252	Lateral (Y)	5.0	0.00015
29	A23z	2nd Floor	2	162	252	Vertical (Z)	5.0	0.00015
30	A24z	2nd Floor	168	162	252	Vertical (Z)	5.0	0.00015

*Accelerometer block base relative to the top northwest corner of the basebeam

The test was uniaxial, with the filtered SE32 synthetic earthquake motion (see Figure 8-12) in the longitudinal (X-direction) or in-plane direction with respect to the model drawings. Many accelerometers shown in Table 8-3 measured the desired longitudinal motions, including the input motion of shake table (ATX), base beam (A1x, A2x, and A3x), first floor (A11x, A12x, and A13x) and second floor (A21x, A22x, and A23x). Figure 8-16 through Figure 8-20 show all accelerometer locations. Table 8-3 and Figure 8-16 and Figure 8-17 show the second-floor accelerometers were located directly above the first-floor accelerometers, which are in turn directly above the base-beam accelerometers. The multiple accelerometers at each level were for measuring undesired torsional response (e.g., A21x and A23x on the second floor) and redundant measurement of the desired in-plane response (e.g., A21x and A22x, which were both on the west side (Y = 2 in.) of the second floor slab).

Figure 8-16. In-plane elevation drawing showing instrumentation.

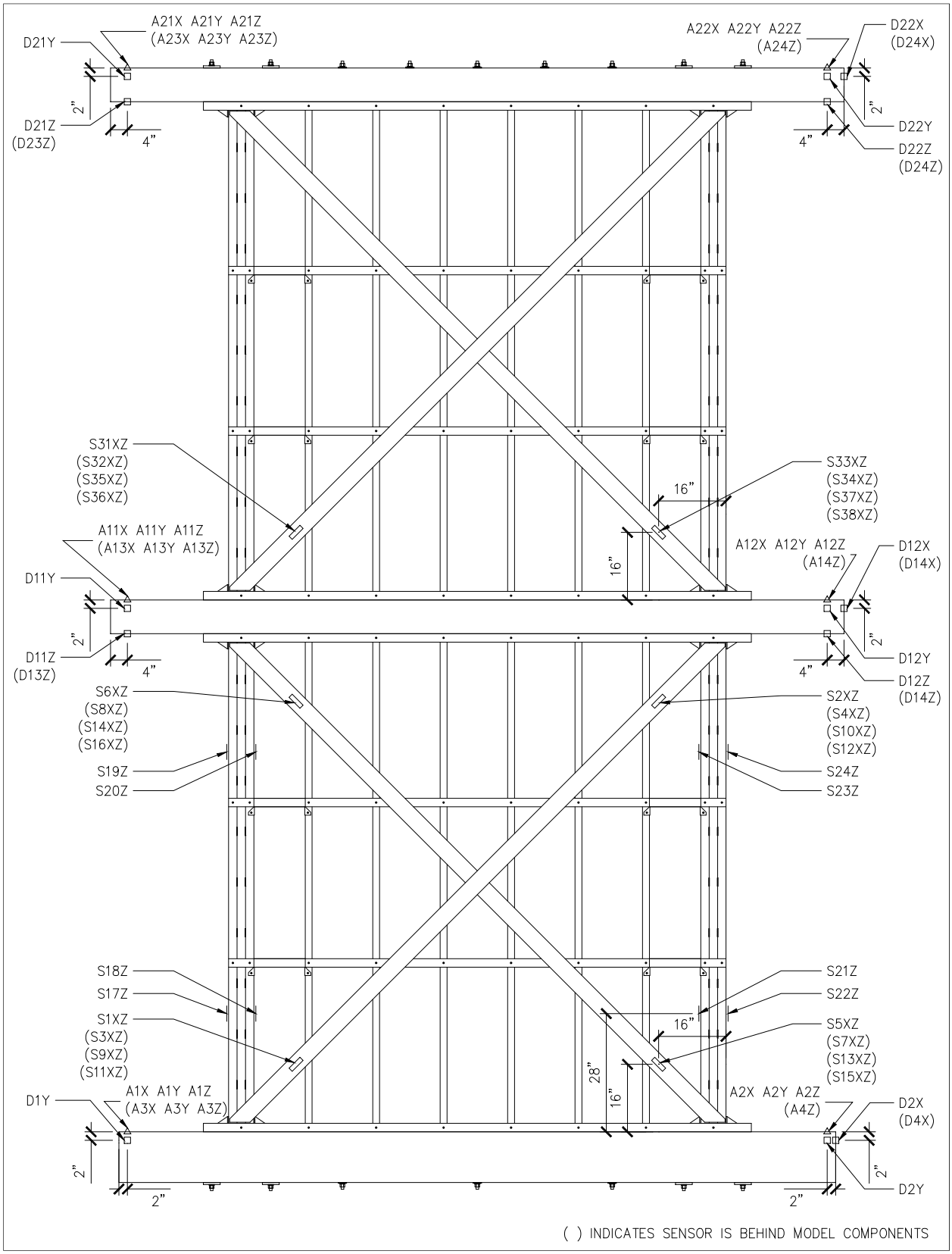

Figure 8-17. Out-of-plane elevation drawing showing instrumentation.

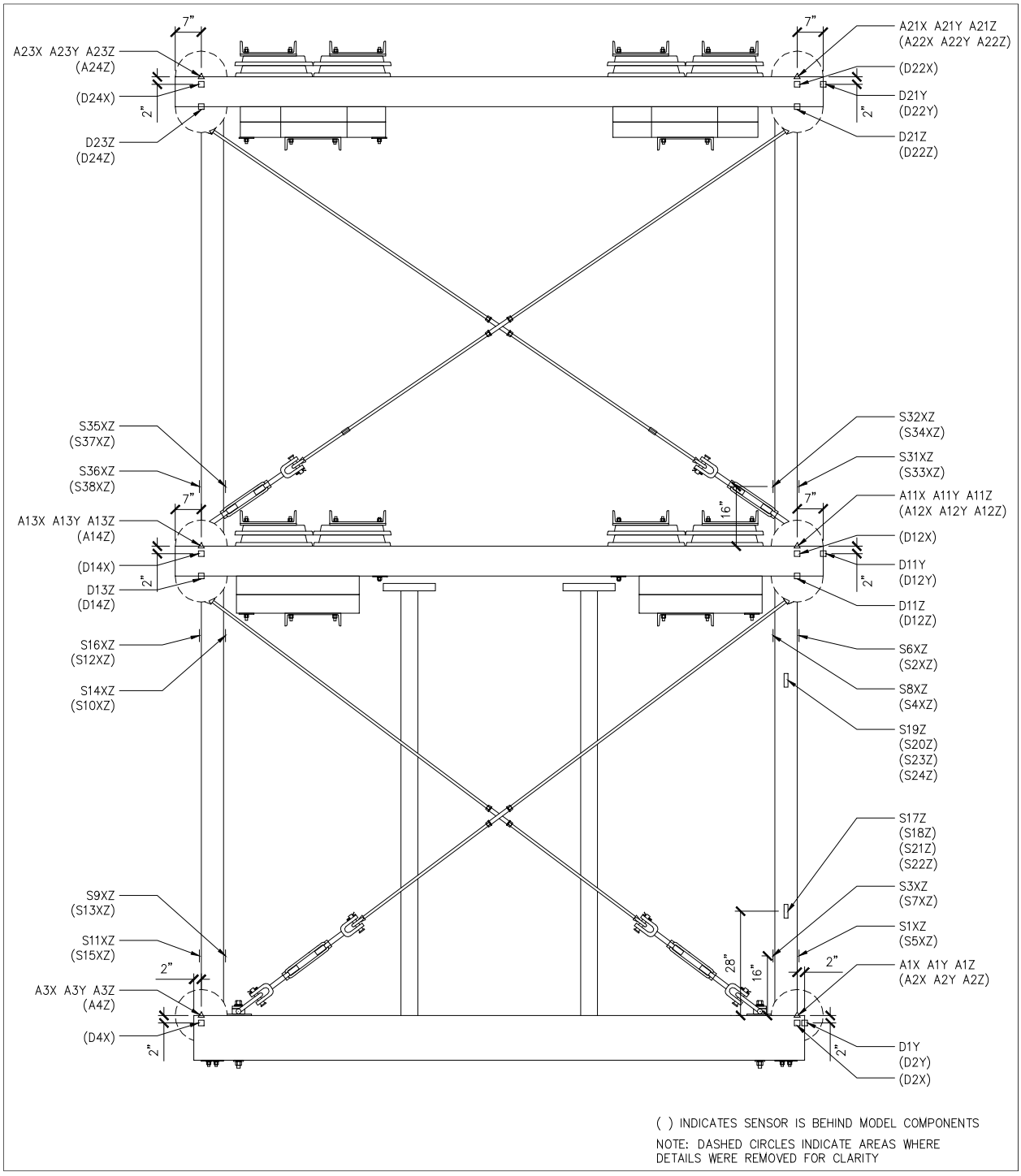

Figure 8-18. Plan view of the base beam showing instrumentation.

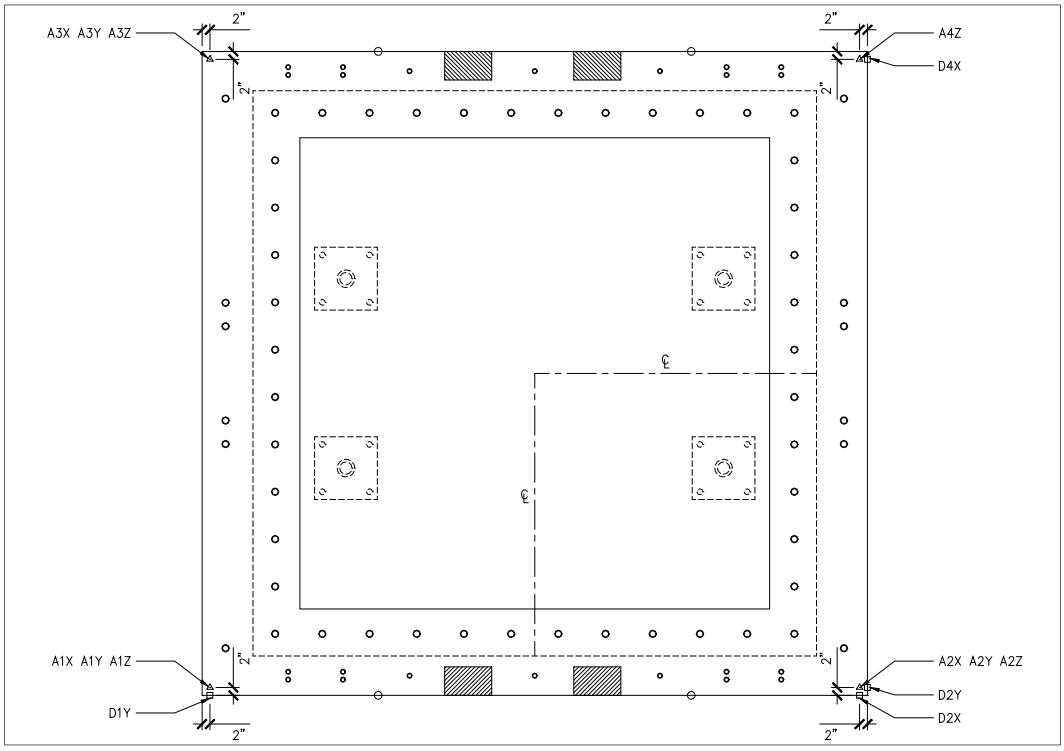

Figure 8-19. Plan view of the first-story slab showing instrumentation.

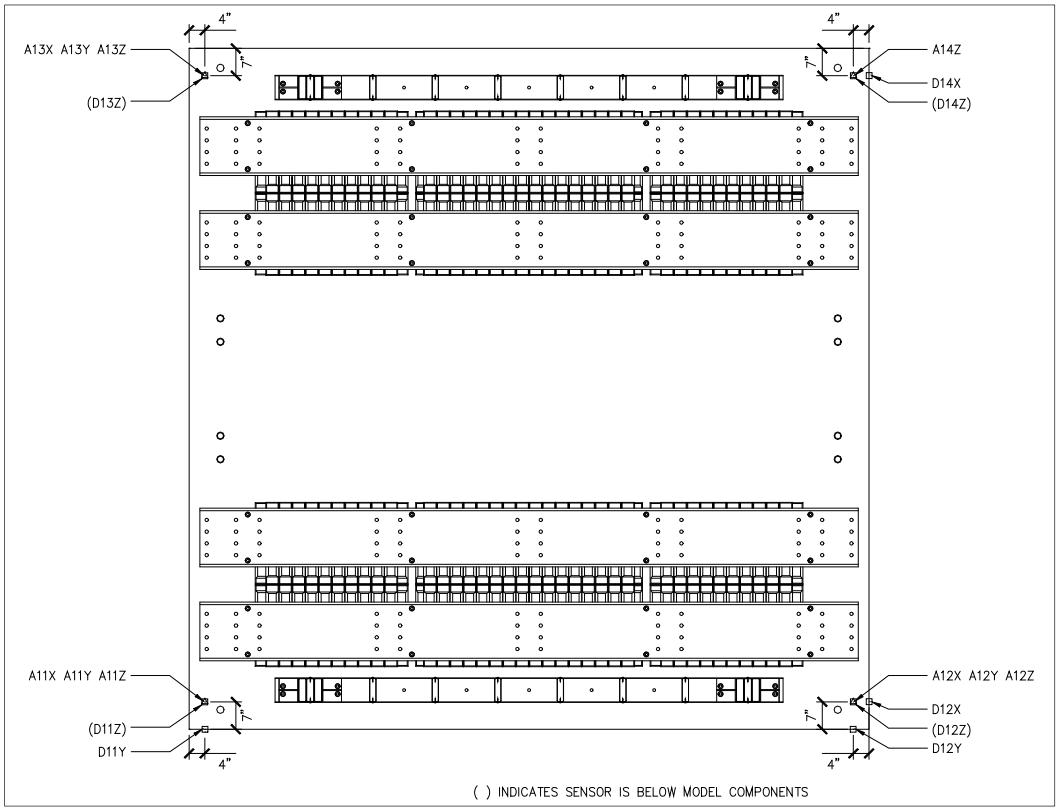

Figure 8-20. Plan view of the second-story slab showing instrumentation.

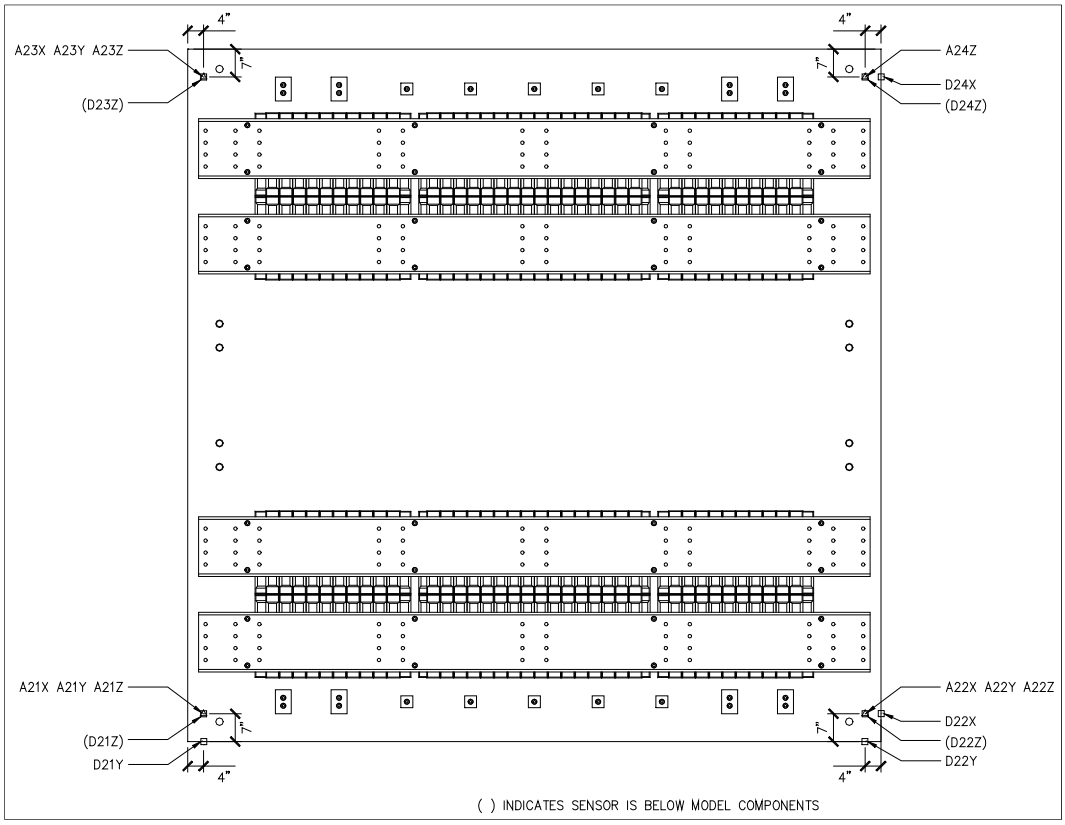

Other accelerometers were installed in the lateral (Y-direction) or out-of-plane direction to measure unwanted out-of-plane or torsional response. The model stiffness and mass distribution should have been very symmetric so that out-of-plane or torsional response would not be significantly induced. The out-of-plane threaded rods shown in Figure 8-3 were designed to restrain model response in this direction. The stiffness of this restraint was slightly less than the model stiffness in the in-plane direction. Therefore, the model was expected to have an out-of-plane mode of vibration with a frequency slightly less than the in-plane direction. This mode would be excited at low levels, but the levels of motion would be quite small because the mass and stiffness of the model were very symmetric and the model would not be excited out-of-plane. Still, the model would respond with relatively low levels of undesired rocking, torsion and out-of-plane motion. This motion was measured, so it could be accounted for when analyzing the response of the shake table model. The torsional and out-of-plane response should not be significant, and the rocking response can be accounted for in refined Drain 2DX analysis when comparing with predicted nonlinear response.

Some vertical response was expected of both the model and also the shake table surface itself. It was expected that the TESS surface would be driven somewhat by the very large overturning forces applied to it. The overturning motion of the TESS is unwanted but cannot be eliminated completely. The overturning flexibility of the TESS is due to the oil column and other flexibility associated with the vertical actuators. The TESS has tremendous overturning capacity and stiffness, with a total of nine 90 kip actuators, but the large overturning moment still causes unwanted vertical motions. The overturning moment applied to the TESS by testing to the filtered SE32 record is approximately 9900 k-in., calculated based on the seismic story shears per frame given in Table 8-2 (with an R of 4) times the two frames multiplied by the elevation of the floor slabs above the center of longitudinal actuators (12 in. below the TESS surface) (272 in. x 2 x 14.40 kip + 146 in. x 2 x 7.19 kip). The overturning capacity of the TESS is much greater at 25,920 k-in. (48 in. x 6 x 90 kips), showing that the TESS has more than adequate overturning capacity. However, due to the compressibility of the vertical actuator oil columns alone, the overturning stiffness, k_θ, can be roughly calculated to be 60,323,000 k-in. based on the oil column force per actuator, for a unit displacement times the number of actuators times the distance from the center of rocking divided by the rotation needed for a unit displacement (4 x 30 in^2 x 100 ksi /2.75 in. x 1 in. x 6 x 48 in./(1 in/48 in.)). If no compensation is made in the TESS control for oil compressibility, the overturning rotation may be approximately 0.000165 radians (9933 k-in./ 60,323,000 k-in.), which would result in 0.0097 in. (118 in./2 x 0.000166 radians) of unwanted vertical displacement, d_{VR}, at the exterior faces of the columns. This is a low estimate of vertical displacement because other sources of system flexibility increase displacements. However, these displacements are small relative to the large expected lateral deformation of the model. The polar moment of inertia of the model, J, was approximately 14,215 k-in.-sec^2 ($J = W/g \times r^2$ = (57.5 kip x (146 in.)^2 + 57.6 kip x (272 in)^2)/386 in./sec^2). From this, the rocking natural frequency, f_R, due to oil column compressibility alone was estimated to be 10 Hz ($f_R = 1/(2\pi) \times (k\theta/J)^{0.5} = 1/(2\pi) \times$ (60,323,000 k-in./14,215 k-in.-s2)$^{0.5}$). This was expected to be a high estimate of the overturning or rocking frequency of the system because of additional flexibility from the TESS system and the model itself. Still, this frequency was well above the model in-plane natural frequency, estimated to be 2 Hz. The vertical acceleration at the bottom of the model columns due to overturning, a_R, was estimated to be 0.107 g ($a_R = d_{VR}\omega^2$). The overturning-related lateral displacement, d_{Rx}, and acceleration, a_{Rx}, at the top of the model

were estimated to be 0.045 in. (272 in./(118 in./2) x 0.0097 in.) and 0.49 g (272 in./(118 in./2) x 0.107 g), respectively. However, because this estimated overturning frequency was much higher than the model frequency, the model could be isolated from the effects of this higher-frequency rocking. Still, the overturning response of the TESS was not well understood, and was measured with the vertical accelerometers shown in Table 8-3. The DRAIN 2DX analysis was repeated after the shake table test to adjust the predicted behavior in a way that accounts for TESS overturning. This correction was needed to facilitate valid comparisons. However, these approximations of expected overturning suggest the TESS overturning should not be large enough to interfere with the response of the model or the test verification purposes.

8.3.2 Displacement gages

Table 8-4 gives the sensor names, locations, direction of measurement, full-scale range and resolution for each displacement gage installed on the shake table model. The displacement gages, called cable-extension position transducers, use a wire under tension that coils into a box on one end and attaches to the model on the other. The longitudinal (X) and lateral (Y) displacement gages measured the model response relative to fixed references off the TESS surface. However, the vertical displacement gages measured the movement of the surface above to the level below (e.g., first-floor vertical displacement relative to the base beam below). These vertical displacements were expected to be very small relative to longitudinal displacements. Assuming no deformation in the cold-formed steel panel anchors, these measurements permit the calculation of the overall deformation history of individual panel diagonal straps, even at the largest nonlinear deformations. The strap deformation could not be easily measured directly with linear variable differential transducers (LVDTs) because of the extreme strap deformation in the first-story panels. Very small deformations were expected in the panel anchors relative to the panel straps, because of the direct load path between the straps, columns and anchors, and the linear response of the anchors and very large nonlinear response of the straps. The displacement gages also provided independent measurement of the overall model response relative to the accelerometers. Figure 8-16 through Figure 8-20, above, show the locations of all displacement gages.

Table 8-4. Shake table verification model displacement gages.

#	Sensor Name	Model Level	Sensor Coordinates* X (in.)	Y (in.)	Z (in.)	Sensor Direction	Full Scale (in.)	Resolution (g)
1	D1y	Basebeam	2	0	-2	Lateral (Y)	10.0	0.00031
2	D2x	Basebeam	168	0	-2	Longitudinal (X)	10.0	0.00031
3	D2y	Basebeam	170	2	-2	Lateral (Y)	10.0	0.00031
4	D4x	Basebeam	170	162	-2	Longitudinal (X)	10.0	0.00031
5	D11z	1st Floor	2	2	118	Vertical (Z)	10.0	0.00031
6	D12z	1st Floor	168	2	118	Vertical (Z)	10.0	0.00031
7	D13z	1st Floor	2	162	118	Vertical (Z)	10.0	0.00031
8	D14z	1st Floor	168	162	118	Vertical (Z)	5.0	0.00015
9	D11y	1st Floor	2	-5	124	Lateral (Y)	10.0	0.00031
10	D12x	1st Floor	172	2	124	Longitudinal (X)	10.0	0.00031
11	D12y	1st Floor	168	-5	124	Lateral (Y)	10.0	0.00031
12	D14x	1st Floor	172	162	124	Longitudinal (X)	10.0	0.00031
13	D21z**	2nd Floor	2	2	244	Vertical (Z)	5.0	0.00015
14	D22z**	2nd Floor	168	2	244	Vertical (Z)	5.0	0.00015
15	D23z**	2nd Floor	2	162	244	Vertical (Z)	5.0	0.00015
16	D24z**	2nd Floor	168	162	244	Vertical (Z)	5.0	0.00015
17	D21y	2nd Floor	2	-5	250	Lateral (Y)	10.0	0.00031
18	D22x	2nd Floor	172	2	250	Longitudinal (X)	10.0	0.00031
19	D22y	2nd Floor	168	-5	250	Lateral (Y)	10.0	0.00031
20	D24x	2nd Floor	172	162	250	Longitudinal (X)	10.0	0.00031

*Displacement (yo-yo) gage block base relative to top northwest corner of base beam.

**2nd floor vertical displacement gages run between the 1st and 2nd floor.

8.3.3 Strain gages

Table 8-5 presents the sensor names, locations, direction of measurement, full-scale range, and resolution for each strain gage installed on the shake table model. These sensors were installed on the cold-formed steel panel diagonal straps and columns. The shear panels were the same height and width, both dimensions being 118 in. An extension of the strap center lines extend through the exterior edge of the columns where they intersect the top and bottom of the panels at the concrete slab or base beam, as shown in Figure 8-9 through Figure 8-11. The center locations of all strain gages were 16 in. vertically and horizontally from this intersection, which placed them at the center of the strap cross-sections (see Figure 8-16). They were located this distance from the welded connection to the columns so that the stress and strains would be fairly uniform through the strap cross-sections. Near the welded connection these would not be uniform due to slight deformations of the anchors and columns and concentrations of stress and strain at the welds. The straps would also have some residual strains from the cold forming process and cutting to their 4 in. width. These residual strains may be quite different near the strap edges,

but should be fairly uniform along the length of the strap. The diagonal strap strain gages were primarily intended to measure the linear strains. As is explained later in the detailed test steps, these strain measurements were used to guide test levels for the linear shake table testing.

Table 8-5. Shake table verification model strain gages.

#	Sensor Name	Model Level	Sensor Coordinates* X (in.)	Y (in.)	Z (in.)	Sensor Direction	Full Scale** (mico in/in)	Resolution (mico in/in)
1	S1xz	1st Floor Straps	42	2	16	Long/Vert (XZ)	50000	1.53
2	S2xz	1st Floor Straps	128	2	102	Long/Vert (XZ)	50000	1.53
3	S3xz	1st Floor Straps	42	8	16	Long/Vert (XZ)	50000	1.53
4	S4xz	1st Floor Straps	128	8	102	Long/Vert (XZ)	50000	1.53
5	S5xz	1st Floor Straps	128	2	16	Long/Vert (-XZ)	50000	1.53
6	S6xz	1st Floor Straps	42	2	102	Long/Vert (-XZ)	50000	1.53
7	S7xz	1st Floor Straps	128	8	16	Long/Vert (-XZ)	50000	1.53
8	S8xz	1st Floor Straps	42	8	102	Long/Vert (-XZ)	50000	1.53
9	S9xz	1st Floor Straps	42	156	16	Long/Vert (XZ)	50000	1.53
10	S10xz	1st Floor Straps	128	156	102	Long/Vert (XZ)	50000	1.53
11	S11xz	1st Floor Straps	42	162	16	Long/Vert (XZ)	50000	1.53
12	S12xz	1st Floor Straps	128	162	102	Long/Vert (XZ)	50000	1.53
13	S13xz	1st Floor Straps	128	156	16	Long/Vert (-XZ)	50000	1.53
14	S14xz	1st Floor Straps	42	156	102	Long/Vert (-XZ)	50000	1.53
15	S15xz	1st Floor Straps	128	162	16	Long/Vert (-XZ)	50000	1.53
16	S16xz	1st Floor Straps	42	162	102	Long/Vert (-XZ)	50000	1.53
17	S17z	1st Floor West Columns	26	5	28	Vertical (Z)	5000	0.15
18	S18z	1st Floor West Columns	32	5	28	Vertical (Z)	5000	0.15
19	S19z	1st Floor West Columns	26	5	90	Vertical (Z)	5000	0.15
20	S20z	1st Floor West Columns	32	5	90	Vertical (Z)	5000	0.15
21	S21z	1st Floor West Columns	138	5	28	Vertical (Z)	5000	0.15
22	S22z	1st Floor West Columns	144	5	28	Vertical (Z)	5000	0.15
23	S23z	1st Floor West Columns	138	5	90	Vertical (Z)	5000	0.15
24	S24z	1st Floor West Columns	144	5	90	Vertical (Z)	5000	0.15
25	S31xz	2nd Floor Straps	42	2	142	Long/Vert (XZ)	50000	1.53
26	S32xz	2nd Floor Straps	42	8	142	Long/Vert (XZ)	50000	1.53
27	S33xz	2nd Floor Straps	128	2	142	Long/Vert (-XZ)	50000	1.53
28	S34xz	2nd Floor Straps	128	8	142	Long/Vert (-XZ)	50000	1.53
29	S35xz	2nd Floor Straps	42	156	142	Long/Vert (XZ)	50000	1.53
30	S36xz	2nd Floor Straps	42	162	142	Long/Vert (XZ)	50000	1.53
31	S37xz	2nd Floor Straps	128	156	142	Long/Vert (-XZ)	50000	1.53
32	S38xz	2nd Floor Straps	128	162	142	Long/Vert (-XZ)	50000	1.53

*Center of strain gage relative to the top northwest corner of the basebeam.
**The maximum strain measurement may be limited by bond failure of the brittle cement.

Pairs of strain gages were also installed near the top and bottom of the first-story west shear panel columns. For example, the lower-left corner of Figure 8-16 shows that one gage (S17z) was installed on the in-plane outside face and one (S18z) on the inside face, both 28 in. above the bottom of the column. A similar pair (S19z and S20z) was installed 28 in. below the

top of this same column. Similarly, the right side of Figure 8-16 shows that pairs of strain gages were installed near the bottom (S21z and S22z) and top (S23z and S24z) of the other column of this west shear panel. These pairs of sensors were used to measure the shear in the columns. The column shears should be uniform throughout their heights, so that the column moment near the column anchors can be estimated. These gages are placed far enough away from the column tops and bottoms, so that the strains should remain linear. These measurements were to be used to estimate when the columns yield.

8.4 Shear panel design details and predicted lateral load versus deflection

The model presented in Chapter 5 is also used here to predict the lateral load versus deflection of the shear panels used in the shake table model. Material tests were conducted on the steel used in the diagonal straps, columns, and column anchors by testing five coupons of each of these panel components. Figure 8-21 plots the stress-versus-strain results from a typical coupon test for each of these components. Each plot shown in Figure 8-21 is for a coupon that best represents the average of all five coupons tested for each component (straps, columns, and anchors).

Figure 8-21. Stress-versus-strain plots for shake table model shear panel materials.

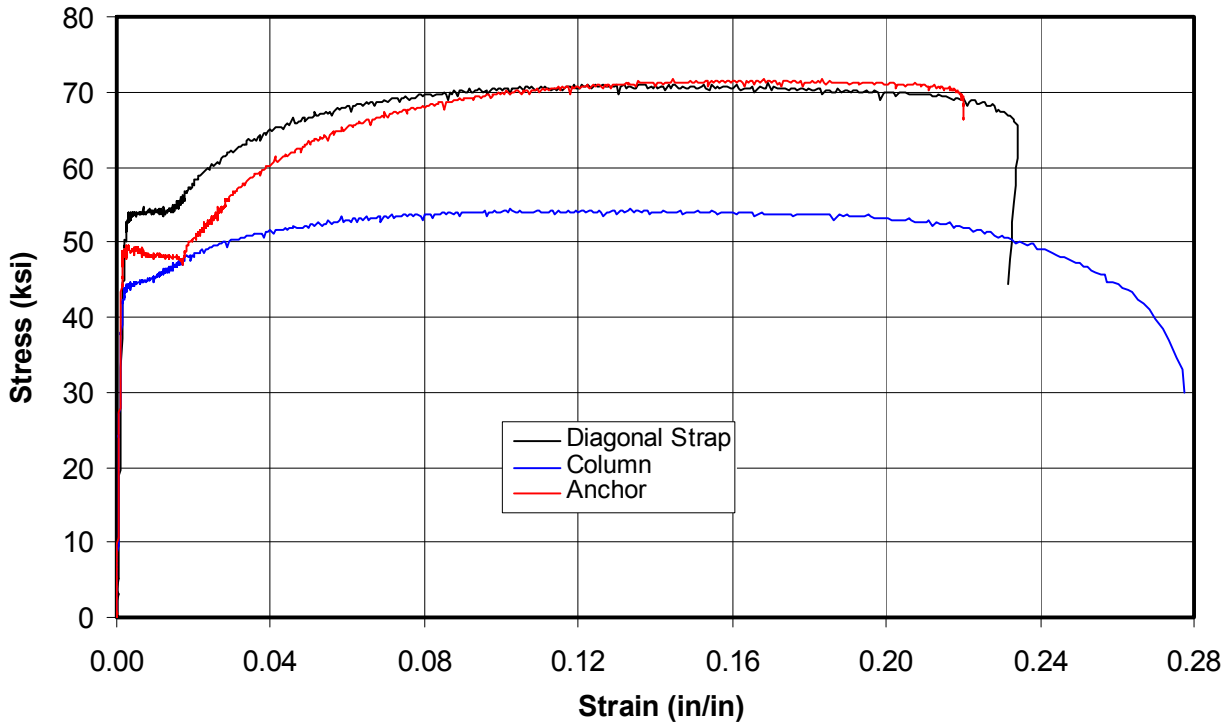

Figure 8-21 and Table 8-6 show that the material in the diagonal straps easily meets the required 1.08 ratio of ultimate over yield strength and the 10% elongation (0.10 in./in. strain) for ASTM A 1003/A 1003M high-ductility material (ASTM 2013b). Table 8-6 shows the material thickness, yield strain, yield stress, F_y, ultimate stress, F_u, ratio of ultimate over yield stress and elongation within 2 in. coupon gage length for the materials used in each component of the cold-formed steel shear panels. The thickness, yield stress, ultimate stress, ratio of ultimate over yield stress and elongation are average values from all five coupons tested for each panel component (diagonal straps, column studs and anchor angles). The yield stress was the average stress for all five coupons, at which a line drawn parallel to and offset 0.2% strain (0.002 in./in.) to the elastic region crosses the stress-versus-strain measured data. The yield strain in this table is the strain at which the representative coupon stress reached this average yield stress for the particular component. The elongation given in Table 8-6 is the average percentage of elongation over the 2 in. gage range at which the coupon ruptured for each material.

Table 8-6. Coupon test results for materials used in shake table model shear panels.

Material	Thickness (in.)	Yield Strain (in/in)	Yield Stress (ksi)	Ultimate Stress (ksi)	Ultimate / Yield Stress	Elongation in 2 in.
Diagonal Straps	0.055	0.0029	53.6	71.0	1.32	22.6%
Column Studs	0.116	0.0026	44.9	54.5	1.21	26.1%
Anchor Angle	0.257	0.0015	48.0	71.0	1.48	22.6%

Figure 8-22 plots the same material test data, but zooms in on the region of smaller strains that are still well beyond the greatest strains expected in the shake table test. The diagonal strap plot shows they begin to yield at a stress of 50 ksi. A yield strength, F_{sy}, of 53.6 ksi (design was 50 ksi) was used to calculate the panel capacity as shown in Table 8-7 (a repeat of Table 8-1 for convenience). The strain when the straps first begin to yield, ε_{sy}, should be 0.0017 in./in. (ε_s = 50 ksi/E). The straps initially yield at some unknown location that would most likely not be within the length of the strain gages. As strap yielding progressed locally, they would begin to strain harden at a strain of about 0.015 in./in. (see Figure 8-22). This would cause strap yielding throughout the length of strap between the columns. The first-story straps should be fairly uniformly yielded at the 0.015 in./in. strain when the first-story panel reaches about 3.2 in. drift (δ = 0.015 in./in. x ((106 in)^2 + (106 in)^2) / 106 in.).

Figure 8-22. Stress versus strain plots for shear panel materials, at small strains.

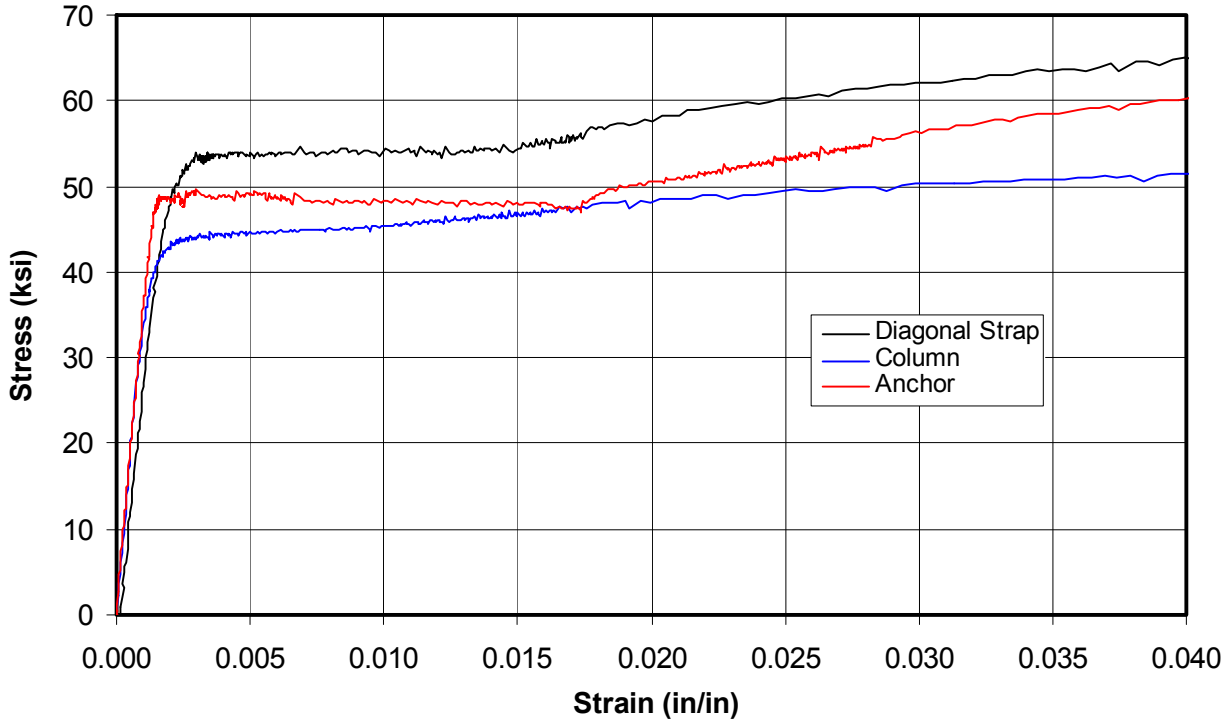

Table 8-7. Diagonal strap design for shake table model shear panels.

Panel Level	Panel Width W (in)	Panel Height H (in)	Strap Faces n_s (#)	Strap Width b_s (in)	Strap Thickness (ga)	Strap Thickness t_s (in)	Strap Initial Lat Stiffness k_s (k/in)	Yield Stress of Strap F_{sy} (ksi)	Capacity at Strap Lat Yield Q_{sy} (k)	Design Shear Strength $\phi_t Q_{sy}$ (k)	Lat Defl at Strap Yielding δ_{sy} (in)	Applied Story Shear V_x (kips)	Elastic Lateral Defl δ_{xe} (in)	Defl Amp Factor C_d	Import Factor I	Design Story Drifts $\Delta = \delta_x$ (in)	Stability Coeff θ	Allow Story Drifts Δ_a (in)
2nd Fl	118	118	2	4	16	0.055	38	53.6	16.62	15.78	0.436	14.40	0.378	3.5	1.0	1.32	0.0100	2.36
1st Fl	118	118	2	4	16	0.055	38	53.6	16.62	15.78	0.436	21.58	0.567	3.5	1.0	1.98	0.0100	2.36

This section presents the shake table model shear panel design details based on the panel configuration and details shown in Figure 8-2 and Figure 8-9 through Figure 8-11, and material properties shown in Table 8-7. Table 8-7 through Table 8-15 present the design details for both the first- and second-floor shear panels. The purpose of showing these details is that it shows the design demand and capacities for each of the panel components for both the first and second-story shear panels. These details will facilitate later discussion on panel performance observations and the adequacy of the design recommendations upon which these tables are based. Table 8-7 repeats the panel diagonal strap design details shown in Table 8-1. The first- and second-floor shear panels are identical, so their lateral deflection at strap yields, δ_{sy}, are both 0.436 in. in Table 8-7. Table 8-7 shows that design applied story shear V_x (21.58 kips) is much greater than the capacity at strap lateral yield, Q_{sy} (16.62 kips). This underdesign of the

shear panels was intentional so that significant nonlinear response would occur. As was mentioned earlier, the first-floor shear panels were designed as if an R coefficient of 5.53 were used.

Table 8-8 shows the diagonal strap ultimate strength, F_{su} and the maximum strap ultimate strength, F_{sumax}, equal each other, because they are the values measured in the coupon tests. Table 8-8 also shows the maximum gravity load per shear panel, GL_{max}, which is the total weight applied to each shear panels at both the first and second stories of the model. From these values the total compressive load applied to the columns, P_{vumax}, is shown. Table 8-8 shows the measured column yield and compressive strength, and thickness along with the other column properties. Table 8-9 shows the calculated column capacity, P, that exceeds the applied load, P_{vumax}. The left side of Table 8-10 summarizes the calculations used to determine the maximum intermittent weld spacing that will cause the column studs work together as a composite section. The intermittent weld length, L, is 2 in. and the maximum calculated spacing, s_{max}, is 11.7 in. and Figure 8-9 through Figure 8-11 show they were spaced slightly greater at 12 in. on center.

Table 8-8. Column design for shake table model shear panels.

Panel Level	Diagonal Strap Ult Stress F_{su} (ksi)	Max Ult Strap Stress F_{sumax} (ksi)	Max Gravity Load/ Panel GL_{max} = (kips)	Column Axial load at Strap Ult P_{vumax} (k)	Column Yield Stress F_{cy} (ksi)	Column Ultimate Stress F_{cu} (ksi)	Column Thickness (ga)	Column Thickness t_c (in)	Number of Studs /Column n	Panel Thickness /Column b_c (in)	Col Stud Flange Width b_f (in)	Column Depth h_c (in)
2nd Fl	71	71	28.8	36.4	44.90	54.50	12	0.116	3	6.0	2.0	6.0
1st Fl	71	71	57.6	50.8	44.90	54.50	12	0.116	3	6.0	2.0	6.0

Table 8-9. Column capacity calculations for shake table model shear panels.

Panel Level	Nominal Column Area A_c (in^2)	Distance to Extreme Fiber c (in)	In-Plane Mom of Inertia I_x (in^4)	In-Plane Radius of Gyration r_y (in)	Out-of-Plane Mom of Inertia I_y (in^4)	Out-of-Plane Radius of Gyration r_x (in)	Eff Length Factor K	Elastic Flexural Stress F_e (ksi)	λ_c	Nominal Axial Stress F_n (ksi)	Knockout hole dia d_h (in)	Flat Width w (in)	Slenderness factor λ	Eff Width b (in)	Eff Column Area A_e (in^2)	Column Design Strength P (kips)
2nd Fl	3.49	3.21	16.34	2.17	17.64	2.25	0.5	385	0.34	42.8	1.5	5.54	0.962	3.19	2.67	97.0
1st Fl	3.49	3.21	16.34	2.17	17.64	2.25	0.5	385	0.34	42.8	1.5	5.54	0.962	3.19	2.67	97.0

Table 8-10. Column intermittent weld design and combined axial and moment capacity.

Panel Level	Max Column Shear V_{cm} (kips)	Area on 1 Side of Crit Weld A (in^2)	Distance to Neutral Axis y (in)	Mom of Column Area Q (in^3)	Weld Shear/ Length q (k/in)	Intermittent Weld Length L (in)	Max o.c. Spacing s_{max} (in)	Strap Max Yield Stress F_{symax} (ksi)	Max Est Lat Defl at Strap Yield δ_{symax} (in)	Applied Moment @ δ_{symax} M_a (k-in)	Column Nominal Moment M_{nx} (k-in)	Column Interaction I
2nd Fl	3.9	2.32	1.62	3.8	0.9	2.0	11.7	53.6	0.436	105	263	0.631
1st Fl	3.9	2.32	1.62	3.8	0.9	2.0	11.7	53.6	0.436	111	263	0.747

The right side of Table 8-10 shows that the combination of axial load and moment on both columns, expressed in terms of an interaction expression, is well below 1.0. Table 8-11 summarizes the design of the welded diagonal strap connection to the columns. This shows that the maximum strap force, P_{su}, based on the measured ultimate strength of the straps is slightly greater than the welded connection capacity based on the measured ultimate strength of the thinner material welded (straps in this case). Figure 8-9 through Figure 8-11 show the weld capacity could have been increased by lengthening the weld along the longitudinal side of the straps. This was not done in order that the ability of these welds to perform without failure at their design limit could be tested, verifying the welded connection recommendations in the process.

Table 8-11. Welded connection design.

Panel Level	Max Est Ult Strap Force P_{su} (kips)	Fillet Weld Thickness t (in)	Longitudinal Weld Length L (in)	Longitudinal Weld Design Strength P_L (kips)	Long/Trans Weld Length L	Long/Trans Weld Design Strength P_{LT} (kips)	Welded Conn Total Capacity $(P_L+P_{LT})n_s$ (kips)
2nd Fl	31.1	0.055	3.25	5.2	5.16	10.1	30.7
1st Fl	31.1	0.055	3.25	5.2	5.16	10.1	30.7

The applied shear at the base of the columns, P_{humax}, is shown in Table 8-12. The total shear strength, V_T, far exceeds this applied load. In fact, the column shear capacity alone, V_C, without the anchor contribution to shear, exceeds this applied load. Therefore, the shear strength of the column and anchors were not close to being tested.

Table 8-12. Column and anchor shear design.

Panel Level	Column Shear Strength V_C (kips)	Strap Lat Ult Capacity $P_{humax}=A_0Q_E$ (kips)	Yield Stress of Angle F_{yA} (ksi)	Angle Thickness t_A (in)	Anchor Shear Strength V_A (kips)	Total Shear Strength V_T (kips)
2nd Fl	37.6	22.0	48	0.257	44.4	126.4
1st Fl	37.6	22.0	48	0.257	44.4	126.4

The panel anchors are most heavily loaded when the minimum gravity load is applied. For the shake table model, the gravity load does not change so that the minimum gravity load per shear panel, GL_{min}, equals the maximum gravity load per shear panel, GL_{max}. Table 8-13 shows that the height of the angles, H_A used in the anchors (3.5 in.) was sized so that the angle total weld strength, P_A, would barely exceed the maximum applied tensile force per anchor angle ($P_{vymax}/2 + P_M$) at the first-floor panel anchors. The shake table test then provided a good test of the design recommendations for the design of the welded connection between the columns and anchors.

Table 8-13. Shear panel anchor angle and plate design.

Panel Level	Min Gravity Load/ Panel GL_{min} (kips)	Anchor Uplift @ max Strap Yield P_{vymax} (kips)	Remaining Column Bending Cap M_{rem} (k-in)	Tensile Force Avail/angle P_M (kips)	Tensile Force/ Angle $P_{vymax}/2+P_M$ (kips)	Angle Horiz Weld Strength P_T (kips)	Col/Anchor Weld Thickness t_w (in)	Yield Stress F_{yA} (ksi)	Anchor Angle Size				Angle Vert Weld Strength P_G (kips)	Angle Tot Weld Strength P_A (kips)
										H_A (in.)		W_A (in.)	t_A (in.)	
2nd Fl	28.8	2.2	259.4	43.24	44.35	22.80	1/8	48	L	3.5	x	5.0	x 0.257	18.29	41.08
1st Fl	57.6	-12.2	283.6	47.27	41.19	22.80	1/8	48	L	3.5	x	5.0	x 0.257	18.29	41.08

Four, n_{AB} 5/8 in. diameter bolts were installed at each column anchor connection. Table 8-14 shows that bolt shear strength, P_v, far exceeded the applied shear per bolt, P_{hAB}. This table also shows the maximum tensile force per bolt, P_{tAB}, without prying action, and the bolt tensile design strength, P_t. Table 8-15 presents the total force per bolt when the effects of angle prying action are added, showing that this total force is still significantly less than the bolt tensile capacity. The significant difference in these values means that bolt strength in either shear or tension is not tested in the shake table test.

Table 8-14. Anchor moment and anchor bolt shear design.

Panel Level	# Anchor Bolts/col n_{AB} (in)	Anchor Bolt Dia d_{AB} (in)	Applied Shear/ Bolt P_{hAB} (kips)	Bolt Nom Shear Strength F_v (ksi)	Bolt Shear Design Strength P_v (kips)	Strap Max Yield Strength P_{symax} (kips)	Conn C/L Vert Dist from Base s_V (in)	Moment Arm of Dia Strap L_s (in)	Anchor Bolts to Column Face Spacing d_c (in)	Tensile Force/ Bolt $P_{tAB} = r_{ut}$ (kips)	Bolt Nom Tensile Strength F_t (ksi)	Bolt Design Strength $P_t = \phi r_n$ (kips)
2nd Fl	4	5/8	5.50	60	13.81	23.50	0.00	7.78	4.0	10.90	90	20.71
1st Fl	4	5/8	5.50	60	13.81	23.50	0.00	7.78	4.0	7.87	90	20.71

Table 8-15. Anchor bolt design with prying action.

Panel Level	Angle/stiff Weld Thickness t_{wA} (in)	Stiffener Plate Thickness t_S (in)	Washer Diameter OD (in)	Out-of-plane Space btw Bolts d_{c-c} (in)	a (in)	b (in)	a' (in)	b' (in)	ρ	β	δ	α'	Required Angle Thickness t_{req} (in)	No Prying Thickness t_c (in)	α	Factore Prying Force q_u (kips)	Force /bolt w/prying $r_{ut}+q_u$ (kips)
2nd Fl	3/16	1/4	1 5/16	2.00	1.09	0.88	1.41	0.56	0.40	2.25	0.87	1.00	0.285	0.537	1.491	2.46	13.36
1st Fl	3/16	1/4	1 5/16	2.00	1.09	0.88	1.41	0.56	0.40	4.08	0.87	1.00	0.242	0.537	0.757	1.25	9.12

The concrete slab was designed to be very stiff and strong, and also to provide significant weight for the model. The bolts are through-bolts, not anchor bolts, so the cone failure strength or edge distance capacity was not tested in the shake table model test. Because the concrete slab was quite heavy and well reinforced, the bending and shear modes of failure of this diaphragm were not tested in this model.

8.5 Predicted model behavior

The same model used in Chapter 5 to predict panel lateral load versus deflection capacity is used to predict the shake table model shear panel behavior. Table 8-7 through Table 8-15 summarize these calculated capacities based on the shear panel configurations and details shown in Figures 8-2, 8-9, 8-10, and 8-11, and material properties shown in Table 8-6. The lateral capacity shown in Table 8-7 is based on only the diagonal strap capacity. Since the column anchors are moment connections, the columns will act somewhat as a moment frame. If the columns were fully fixed at both top and bottom, the additional lateral capacity would increase significantly. Equation 3-7 in Chapter 3 gives an expression for lateral capacity of a shear panel at strap yield when the columns are fully fixed. The second and third columns of Table 8-16 show the lateral deflection at strap yielding, δ_{sy}, and the combined lateral capacity at strap yielding, Q_{Tsy}. This capacity is still less than the designed applied story shear, so significant nonlinear response was expected in the first-story panels. Figure 8-23 plots the shear panel predicted lateral capacity versus lateral deflection for both the first- and second-story shear panels. This plot assumes the columns

were fully fixed. Figure 8-23 plots lateral capacity with the diagonal strap only, Q_{sy} (first point on plot), and with the columns acting as a moment frame, Q_{Tsy} (second point), both with respect to the lateral deflection at strap yielding, δ_{sy}. The difference between Q_{Tsy} and Q_{sy} is the contribution of the moment frame, and since both capacities are based on the measured coupon strengths of the straps and columns, these plots can be used to compare with the measured panel response in the shake table test to evaluate the panel behavior and actual contribution of the columns acting as a moment frame.

Table 8-16. Lateral load versus deflection predictions for shake table model panels.

Panel Level	Lat Defl at Strap Yielding δ_{sy} (in)	Capacity at Strap Lat Yield Q_{scy} (k)	Lat Defl at Col Yielding δ_{cy} (in)	Column Lat Cap @Yield Q_{cy} (k)	Total Lat Cap @CYield Q_{Tcy} (k)	Col Axial Stress @ Strap Yield f_{ca} (ksi)	Col Bend Stress @ Col Yield f_{cb} (ksi)	Col Comb Stress @ Col Yield f_{cr} (ksi)
2nd Fl	0.436	19.64	0.861	5.96	22.58	6.51	38.39	44.90
1st Fl	0.436	19.64	0.723	5.00	21.62	10.64	34.27	44.90

Figure 8-23. Predicted lateral load versus deflection for shake table model shear panels.

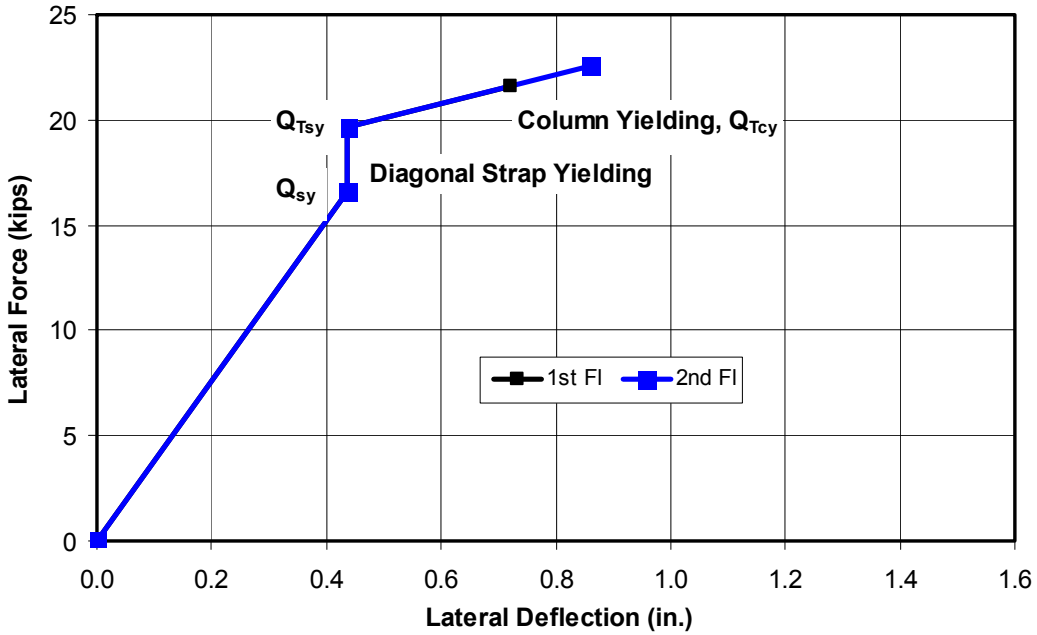

The second portion of Table 8-16 shows the calculation of the total panel lateral capacity at column yielding, Q_{Tcy}, defined in Equation 5-1, for both the first- and second-floor panels. Figure 8-23 plots these predicted capacities with respect to the panel lateral displacement at column yielding, δ_{cy}.

The predicted displacement at column yielding assumes the columns are fully fixed at both their top and bottoms. The columns will be less than fully fixed, so that actual column yielding will take place at larger displacements if at all. The panel capacity at column yielding should be less than those shown in Table 8-16 and Figure 8-23, because the increased deflection will increase moments due to P-delta effects, which would reduce the capacity available to resist lateral forces. Actual column behavior in the shake table model can be assessed based on the column strain gage measurements.

8.6 Test plan

Preliminary DRAIN 2DX analysis of the shake table model using the filtered SE32 record indicated the straps at the first-story panel would yield at only 11% of this record. This conservatively assumed strap yield strength of 47 ksi, which as shown in Figure 8-22, is the point where the strap coupon test results show the material first begins to yield. The column anchors were assumed fully fixed at their connection to the base beam and slab above. If the columns were not fully fixed, the straps could yield at even lower motion levels. Yielding of these straps should be the first nonlinear response of the model. At higher amplitudes, the columns should also yield. Figure 8-23 provided an estimate of predicted first-story panel capacity with respect to lateral deflection (drift). The model has two shear panels, and therefore it should have approximately twice the capacity shown in Figure 8-23.

Several shake table tests were planned prior to the full filtered SE32 test. The model was firmly bolted down to the TESS before testing. Rubber pads were taped to the intermediate studs, where the diagonal straps cross and between the crossing points of the opposing diagonal straps. These pads should not influence the panel behavior, but would reduce the distracting banging noise of the straps when they cycle between buckling and snapping in tension. All the instrumentation was installed prior to testing. The SE32 record used a time step of 0.025 sec, or a sampling rate of 40 Hz. The filtered SE32 record used to drive the shake table applied a smaller time step of 0.0125 sec (80 Hz sampling rate), by inserting interpolated acceleration levels, so that model behavior could be obtained at higher frequencies. Data were recorded with a time step of 0.008 sec (125 Hz sampling rate). The following steps summarize the planned tests:

1. Conduct uniaxial random vibration tests in each of the three translational directions (X, Y, and Z) and each of the three rotations (yaw, pitch, and roll). The amplitude of these motions was planned to begin at 0.02 g and then increase to about 0.05 g. The frequency range was to be 0.2 to 25 Hz, to ensure measuring any modes of vibration that may contribute to the response of this model. Transfer functions between the first- and second-floor slabs and base beam were to be used to determine the first and second modes of vibration in the X and Y direction. Transfer functions were to be used between the TESS accelerometers and the first and second slabs to determine the pitch, roll and yaw modes of vibration. For each mode of vibration, the damping was to be estimated based on the width of the transfer functions. Random testing might be repeated at higher levels as needed to achieve improved resolution. Understanding these modes may be important to understanding the desired response in the in-plane longitudinal direction. Lateral frequency should be slightly less than the in the longitudinal direction, because the out-of-plane stiffness provided by the threaded rods would be less than the shear panel stiffness.
2. First test at 2% of the filtered SE32 motions. This level may be large enough to provide very low measurements in all of the sensors. All data channels would be checked to confirm they were properly recording.
3. Test at 5% of the filtered SE32 motion. Check selected channels to confirm they were recording properly. Check overturning response of the model to confirm that it was within acceptable levels. Review more closely the strains in the first-story shear panels. They should be below 50% of their yield strain compared to the coupon strain data shown in Figure 8-22 (i.e., 0.0008 in./in.). The strains may be somewhat less because the straps are slightly slack when the model is not deformed, so the model has to rack over slightly to begin to strain them (e.g., 0.2 in.). This may cause a slight snapping effect, before yielding the straps. The strap strain levels should increase linearly with respect to test level, beyond the initial level needed to tighten them.
4. Test at 8% of the filtered SE32 record (i.e., 73% of the level estimated to cause yield). Review all the first-story strap strain data and predict the test level that should cause the average peak strain of all straps to reach 80% or the maximum of all straps to reach 90% of yield.
5. Test at the level of the filtered SE32 record that will cause all first-story straps to reach an average of 80% of yield, or the highest-strained strap reach 90% of yield. Review the achieved response levels for all data

channels. Compare these levels with predictions based on the DRAIN 2DX analysis results.

6. After reviewing step 5 data and comparing measured data with DRAIN 2DX analysis (this review was expected to take a day or two), test with the full filtered SE32 record. This test was expected to result in very large longitudinal displacements in the first-floor shear panel, estimated to be up to 6 in. This would cause significant yielding in the straps along their entire length and yielding of the columns near the anchors. The columns were expected to yield first at their compression face and possibly at their tensile face. No nonlinear response was expected in the second-story shear panels.
7. If the first-story shear panels did not experience significant nonlinear response and very large drifts that would permit the examination of P-delta effects, they were to be tested again using sinusoidal motions near the natural frequency of the model. This frequency would be much lower than the frequency of the undamaged model. This frequency would be estimated based on either uniaxial random tests or through transfer functions from the model response in the previous test. At low levels of random motion, the model would act as a very flexible moment frame, where only the columns contribute to the model lateral stiffness. At much greater levels of excitation, the model response becomes very nonlinear because the diagonal straps would become taut and then make the model much stiffer than with the columns alone. This increase stiffness though is only very temporary, creating an impact-loading effect. Therefore, further sinusoidal tests would be needed at the natural frequency of the model based on the low-level random motions, where only the columns contribute to the model stiffness and the frequency would be very low. The amplitude of these sinusoidal tests would start small and gradually increase. Safety considerations might limit these tests. The model was designed so that safety cables would "catch" the floor slabs once the first-floor drift reaches 12 in.

8.7 Modal test results

Shake table tests were conducted according to the above plan on 5 – 7 June 2002. Random tests (step 1) were initially conducted with a root-mean-squared (RMS) amplitude of 0.02 g. To achieve better resolution RMS amplitude was increased to 0.1 g for vertical, longitudinal (in-plane), and yaw (torsional) motions. The random motion levels were also increased to 0.05 g for lateral (out-of-plane), while pitch (in-plane rocking) and roll (out-of-plane rocking) were not increased beyond 0.02 g. Table

8-17 provides both the DRAIN2DX analysis predicted along with the measured frequencies and damping from these modal tests. One prediction model assumed a fixed base and another assumed that the foundation of the model was on a rotational spring, representing the pitch stiffness of the TESS. This rocking spring was represented in DRAIN2DX using vertical springs with a stiffness of 225 k/in. under each of the two columns. The vertical stiffness of the springs was defined such that the calculated frequency would match the measured first-mode measured frequency. Table 8-17 shows fixed-base frequency was greater (2.16 Hz) than the measured (1.65 Hz), while the pitch spring case matches the measured. Table 8-17 also shows that the measured out-of-plane (lateral) frequency was less than the in-plane, as was expected because of the relatively flexible threaded rods bracing the model in this direction. The calculated in-plane second mode frequency was greater than measured for both the fixed-base model and with the rocking spring, but the rocking spring value was closer. The lower-frequency measurements are most likely due to the fact that the shake table did pitch significantly, and the earlier DRAIN2DX model assumed a rigid base.

Table 8-17. Predicted and measured model frequencies and damping.

Mode of Vibration	Fixed Base		TESS Pitch Spring		Measured Frequency (Hz)	Measured Damping (% critical)
	Predicted Frequency (Hz)	Assumed Damping (% critical)	Predicted Frequency (Hz)	Assumed Damping (% critical)		
first Out-of-Plane					1.22	6.7
first In-Plane	2.12	4.0	1.64	6.0	1.65	7.2
first Torsion					2.02	4.0
second In-Plane	5.71	4.0	5.6	6.0	5.25	1.6

8.8 Linear seismic tests

Low-level shake table tests were then conducted at 2, 5, and 8% of the filtered SE32 record. Several data channels were checked to ensure data were being properly recorded. The measured strains from the 8% test showed that average strain measured in the first-story diagonal straps was 1,281 microstrain (75% of yield) and the peak value was 1,396 microstrain (82% of yield). These values were somewhat below the levels indicated in step 5 of the test plan (80% and 90%), but the linear tests ended at this level, because some of the strain measurements showed a slight offset during testing (maximum of 40 microstrain), suggesting that slight yielding of

the straps might have occurred. If yielding at this level took place across the entire length of a strap between the columns, it would only result in 0.006 in. strap elongation and a first-story lateral deflection of only 0.0085 in. This should have a very minor influence on later nonlinear testing.

8.8.1 Measured acceleration response

The acceleration and displacement data were examined to determine which data or combinations of them best represented the response of the model. The acceleration measured in the in-plane direction at A23x (top left corner in Figure 8-20) was much greater than measured at other locations on the second floor slab (at A21x and A22x). The out-of-plane accelerometers (A21y, A22y and A23y) or displacement gages (D21y and D22y) showed very little out-of-plane or torsional response. The in-plane displacements measured at the second floor (D22x and D24x) were very consistent with each other, confirming little torsional response. The acceleration recorded on the second floor were double integrated and corrected for any offsets, to provide displacement records that could be compared with the recorded displacement. The records from the A21x and A22x accelerometers were much less than the displacements measured by D22x and D24x. The displacement record from the A23x integrated record agreed very well with D22x and D24x. Therefore, the A23x acceleration measurements were the most representative of the second-floor acceleration.

The location of the A13x accelerometer on the first-floor slab is directly below A23x. The acceleration measured at this location was very similar to A12x, but significantly greater than at A11x (Figure 8-19 shows the location of all first-floor accelerometers). Similar to the second floor, the first-floor acceleration records were integrated to provide displacement records. The recorded displacements from the integrated A11x record were much lower than the recorded displacements at D12x and D14x, while those from both A12x and A13x agreed very well. Therefore, the A13x acceleration measurements were the most representative of the first-floor acceleration.

Figure 8-24 plots the measured acceleration at the TESS shake table (filtered ATx), first-story slab (A13x) and second-story slab (A23x). The ATx motions are an average of the longitudinal accelerometers inside the TESS. This plot shows the base motions (measured at the TESS) amplified significantly at the first-story slab, but slightly less at the second story. Figure 8-25 shows the same acceleration records, zoomed in on the 13–18 second

region. Figure 8-24 shows the model responded with slightly greater amplitudes between 50 and 51 seconds, but Figure 8-25 focuses on the 13–18 second region because the response is almost as great, plus the response in this region can be compared later to the nonlinear behavior, in the next test, during the same time region as the model begins to yield. Figure 8-24 and Figure 8-25 show the second-story slab (measured by the A23x accelerometer) responds at only slightly greater amplitudes than the first-story slab (A13x). Table 8-3 shows that the A13x and A23x accelerometers are directly above or below one another, located on the first- and second-floor slabs, respectively. Both the first- and second-floor accelerometers show the model responds in both the first (1.65 Hz) and second (5.25 Hz) modes of vibration of the model. The second-floor response is much more dominated by the first mode, while the first floor is influenced almost as much by the second mode, explaining why the first-floor acceleration is almost as great as the second floor.

Figure 8-24. Measured accelerations at the TESS, first-story, and second story in the 8% SE32 test.

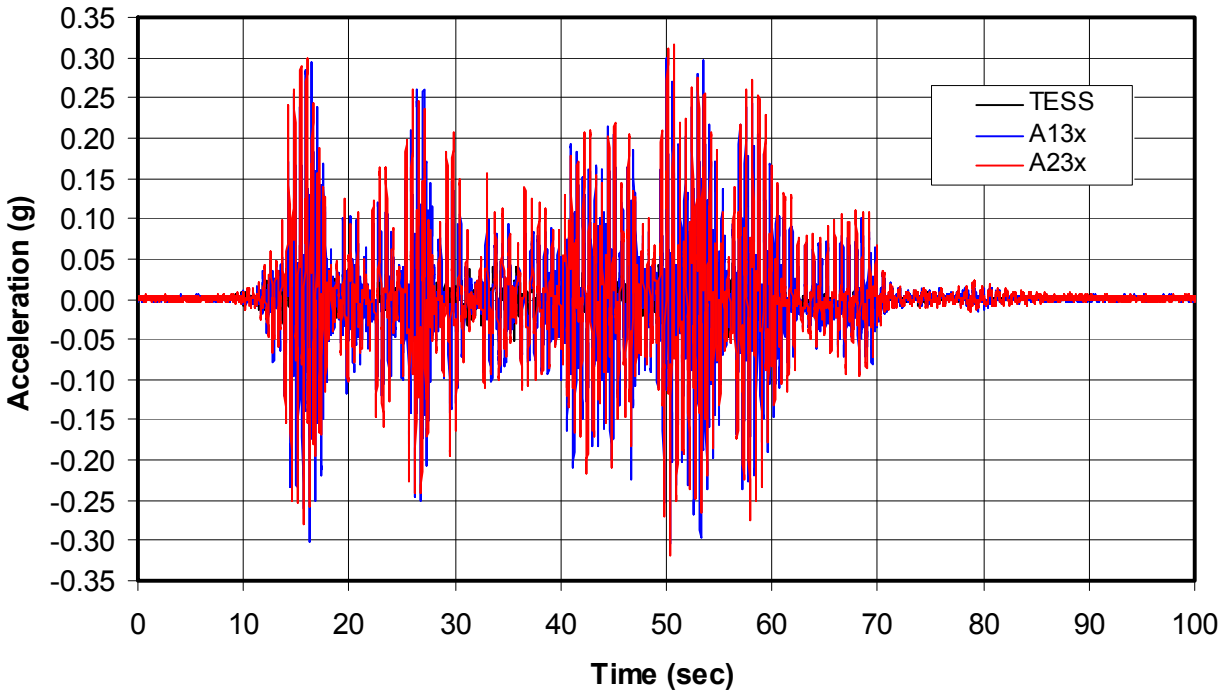

Figure 8-25. Accelerations at the TESS, first-story, and second story for 13–18 sec.

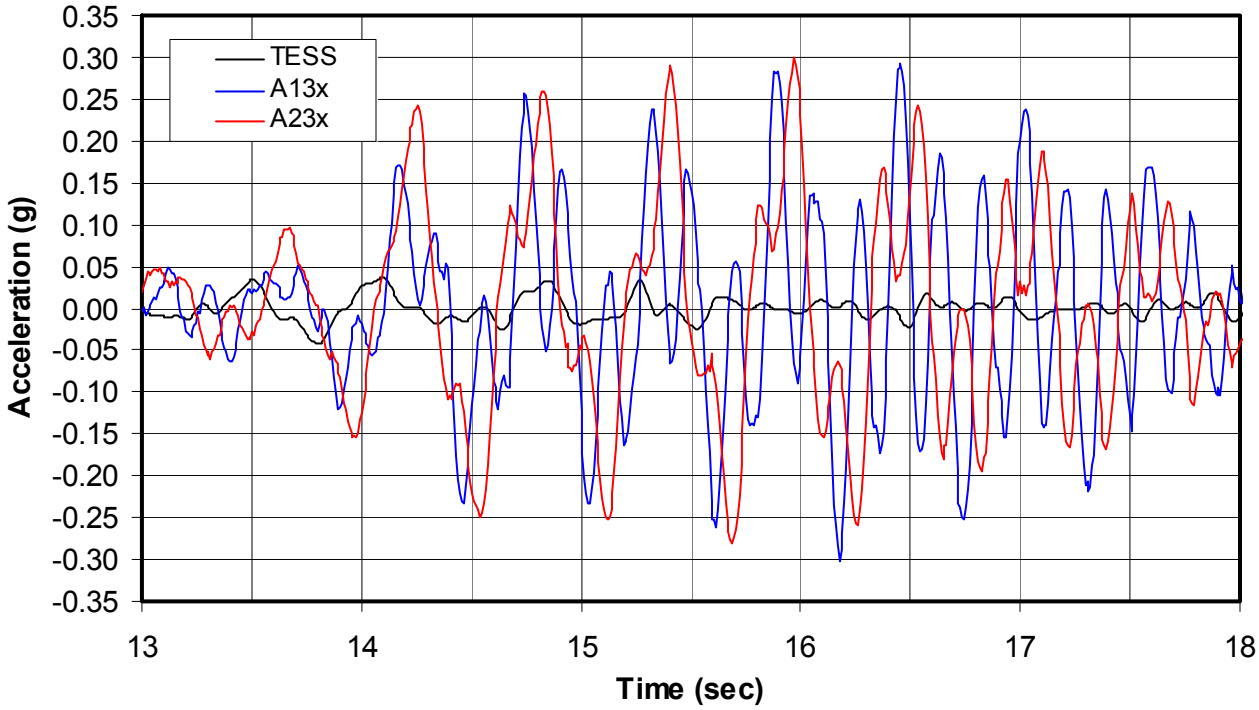

8.8.2 Measured displacement response

Figure 8-26 shows the displacements for the entire 8% SE32 test, measured at the base beam, first-floor level, and second-floor level. The displacement measurements define the behavior of the model better than the acceleration data because both displacement sensors on the same floor level provide measurements that are more consistent with each other than the accelerations. The base-beam displacements are the average of D2x and D4x (see Table 8-4 and Figure 8-16 and Figure 8-18); the first-floor displacements are the average of D12x and D14x; and the second-floor displacements are the average of D22x and D24x. Figure 8-26 also plots the pitch displacement, which is the in-plane rocking motion of the TESS. Figure 8-27 plots these displacements in the 13–18 second region of the 8% SE32 test.

Figure 8-26. Measured displacements at the base beam, first story and second story.

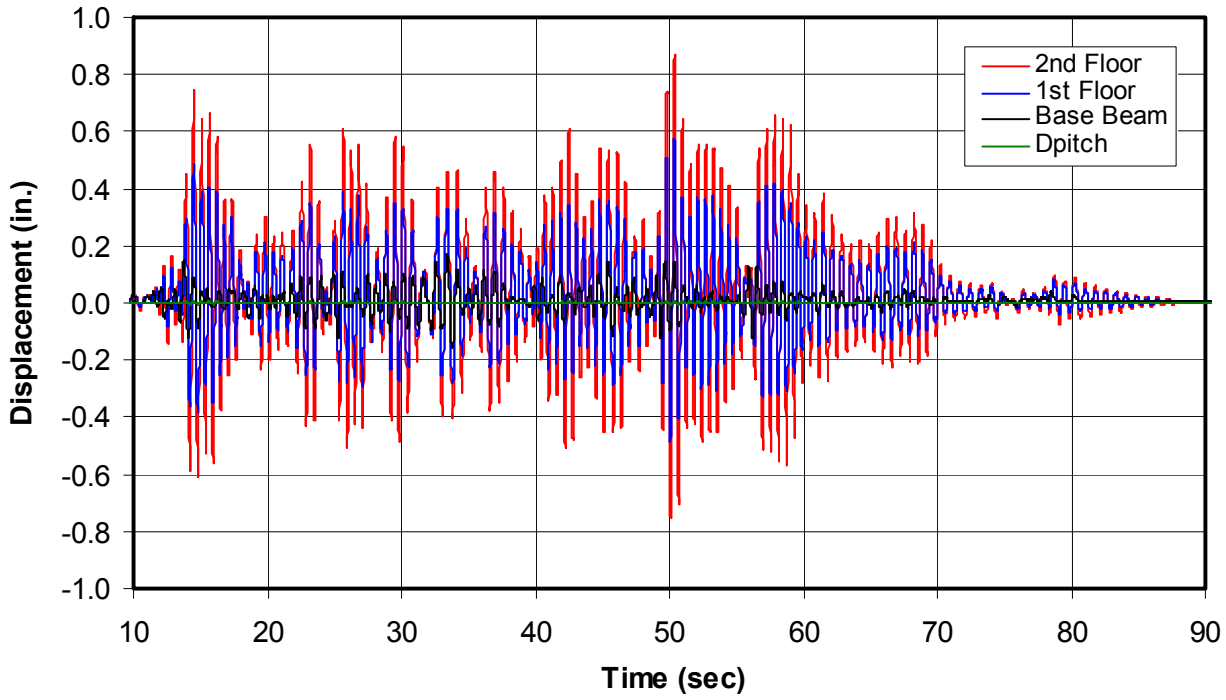

Figure 8-27. Displacements at the base beam, first story and second story, 13 through 18 seconds.

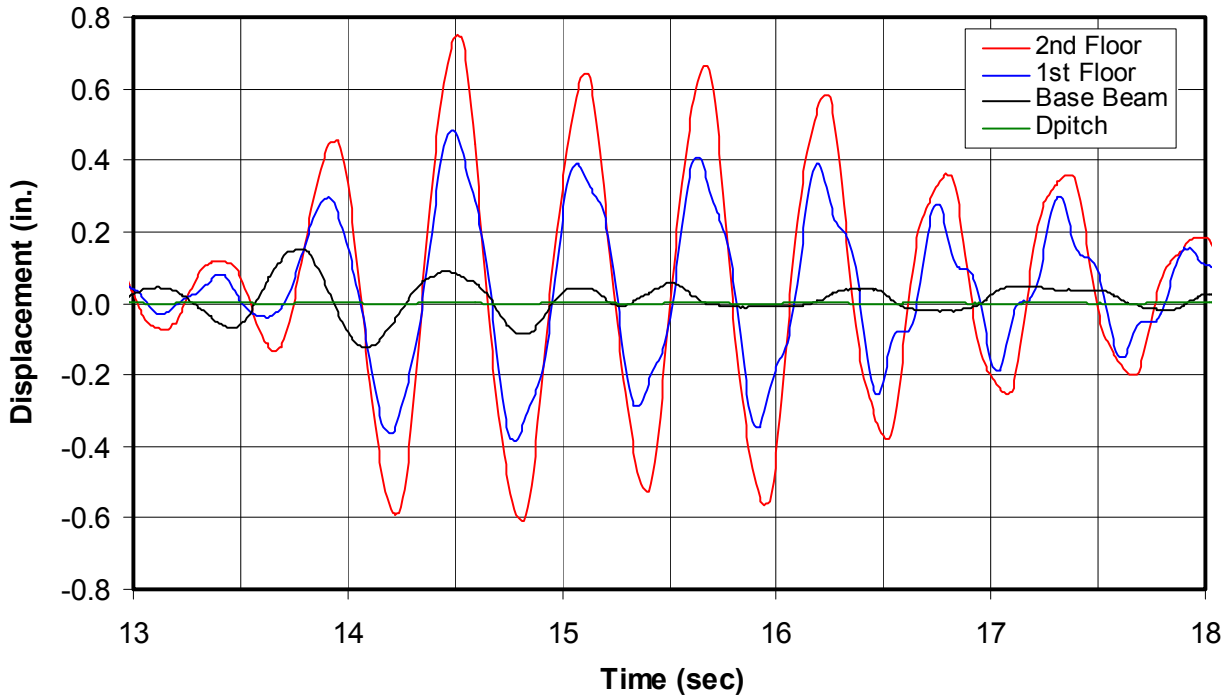

The pitch displacements were quite small in this test, but they do have a small influence on the measured displacements at the first- and second-story levels of the model. The first-floor lateral displacement relative to the base beam after correcting for the pitch motion of the TESS can be calculated as follows:

$$1stStoryDrift = 1stFlRel = 1stFloor - BaseBeam - (124" + 2")\frac{D_{pitch}}{48"} \quad \text{(Eq 8-1)}$$

As indicated in Equation 8-1, the first-story drift is identical to the first-floor relative displacement. D_{pitch} is the measured pitch displacement of the TESS. Vertical displacement of the TESS is measured with linear variable differential transducers (LVDTs) in each of the vertical actuators. There are a total of nine vertical actuators in a symmetric 3 x 3 pattern, spaced 48 in. both directions. The pitch displacement is the average vertical displacement on the three north actuators minus the average of the three south actuators divided by two. This pitch displacement is divided by 48 in. in Equation 8-1 to calculate the pitch rotation. This rotation is multiplied by the vertical distance between the base-beam displacement gages (Z = -2 in.) and first-floor displacement gages (Z = 124 in.). Similarly, the second-floor lateral displacement relative to the base beam can be calculated as follows:

$$2ndFlRel = 2ndFloor - BaseBeam - (250" + 2")\frac{D_{pitch}}{48"} \quad \text{(Eq 8-2)}$$

The second-story drift is the difference between the second-floor relative lateral displacement and first-floor relative lateral displacement, expressed as follows:

$$2ndStoryDrift = 2ndFlRel - 1stFlRel \quad \text{(Eq 8-3)}$$

Figure 8-28 plots the first floor (first-floor drift) and second-floor relative displacements for the portion of the test that caused significant model deformation. This plot shows that the largest model deformations take place between 13 and 18 seconds, and between 49 and 54 seconds. Figure 8-29 plots the story drifts for both the first and second stories calculated from the measured data according to Equations 8-1 and 8-3. This plot zooms into the 13–18 second region, and Figure 8-30 zooms into the 49–54 second region. Both plots in Figure 8-29 and Figure 8-30 show that the first-story drift is consistently greater than the second story.

Figure 8-28. Relative displacements and first-story drift.

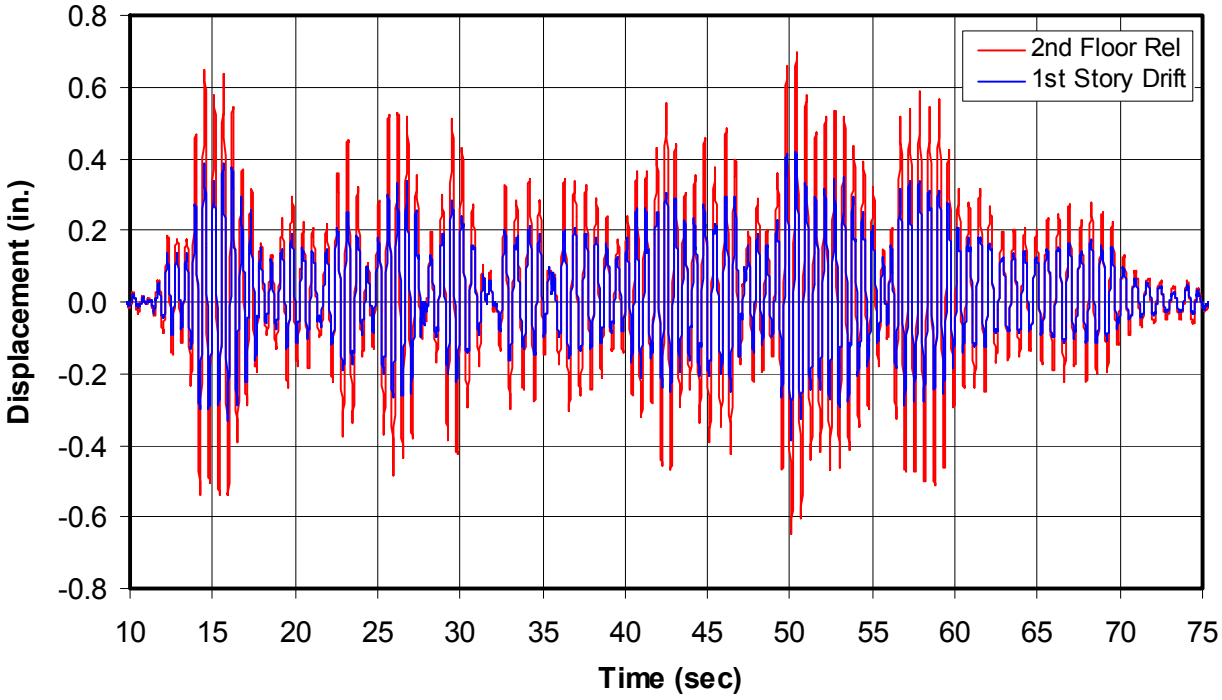

Figure 8-29. First- and second-story drifts, 13–18 seconds.

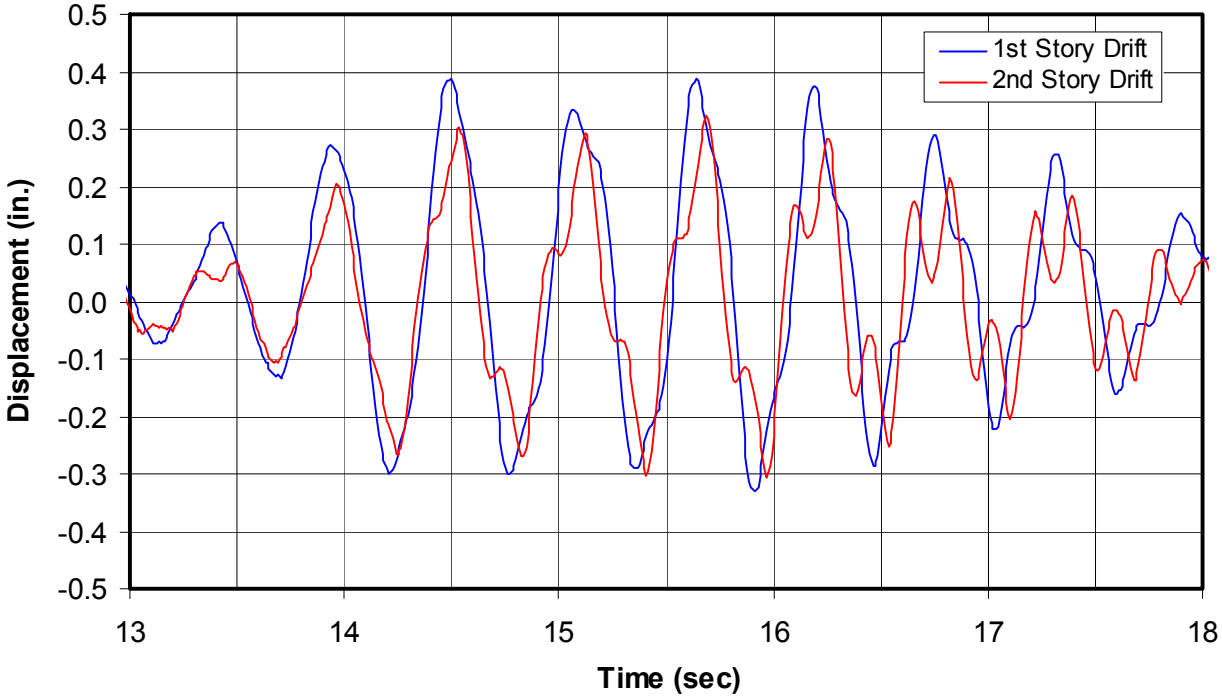

Figure 8-30. First- and second-story drifts, 49–54 seconds.

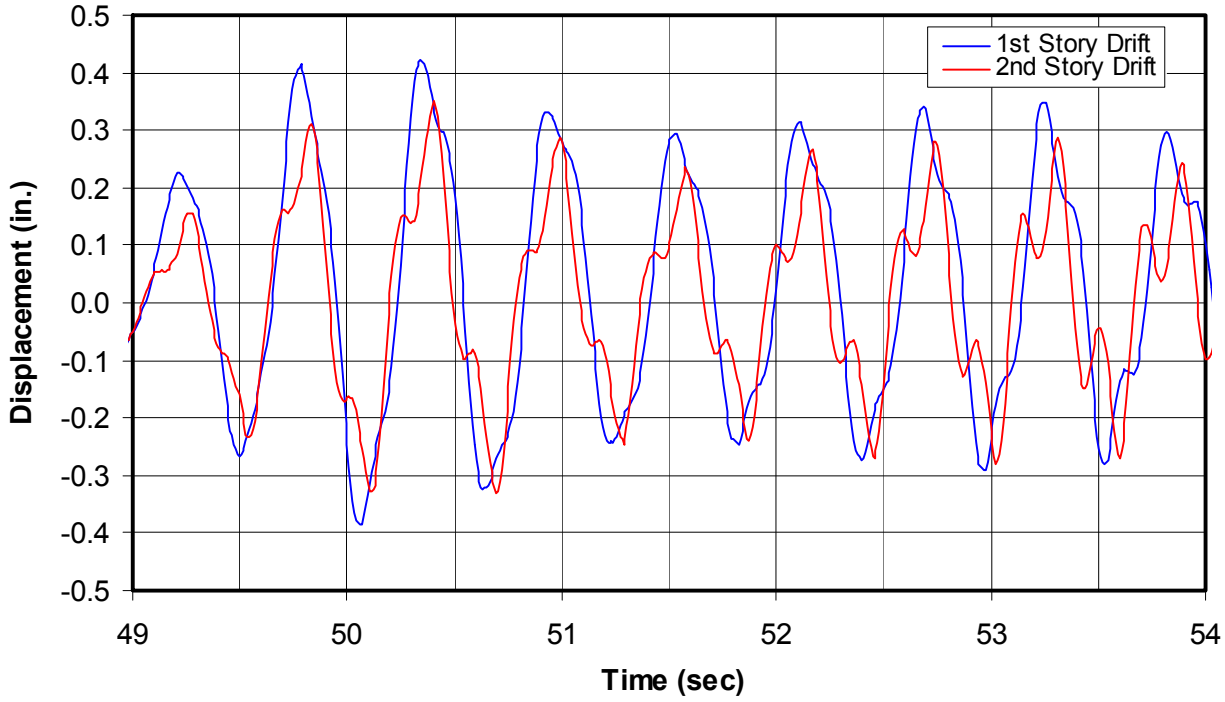

The drifts are somewhat greater in Figure 8-30, reaching peak amplitudes of 0.42 in. and 0.35 in. at the first and second stories, respectively, at 50.4 seconds. The greatest first-story drift (0.387 in.) measured during the first time region plotted in Figure 8-29 occurred at 14.496 seconds. This drift is the most critical deflection parameter defining the behavior of the model, and the amplitude at this time is almost as great as at 50.4 seconds. The deformed model shape is plotted at 14.496 seconds in Figure 8-31, because the model shape at this time can be compared with the behavior of the model at the same time region during the nonlinear test, documented later in this report. Figure 8-31 shows the absolute measured displacements, base beam, D_{pitch}, first floor, and second floor that were plotted in Figure 8-27, at 14.496 seconds, graphically showing the model displacement at that instant in time. Figure 8-31 also shows the relative displacements and drifts, illustrating the deformed shape of the model at this time of close to the greatest first-story drift. Table 8-7 showed that the calculated lateral deflection at strap yielding was 0.436 in., indicating that the first-story panels may have been on the verge of yielding in this test.

Figure 8-31. Model displacement and deformation in the 8% SE32 test at 14.496 seconds.

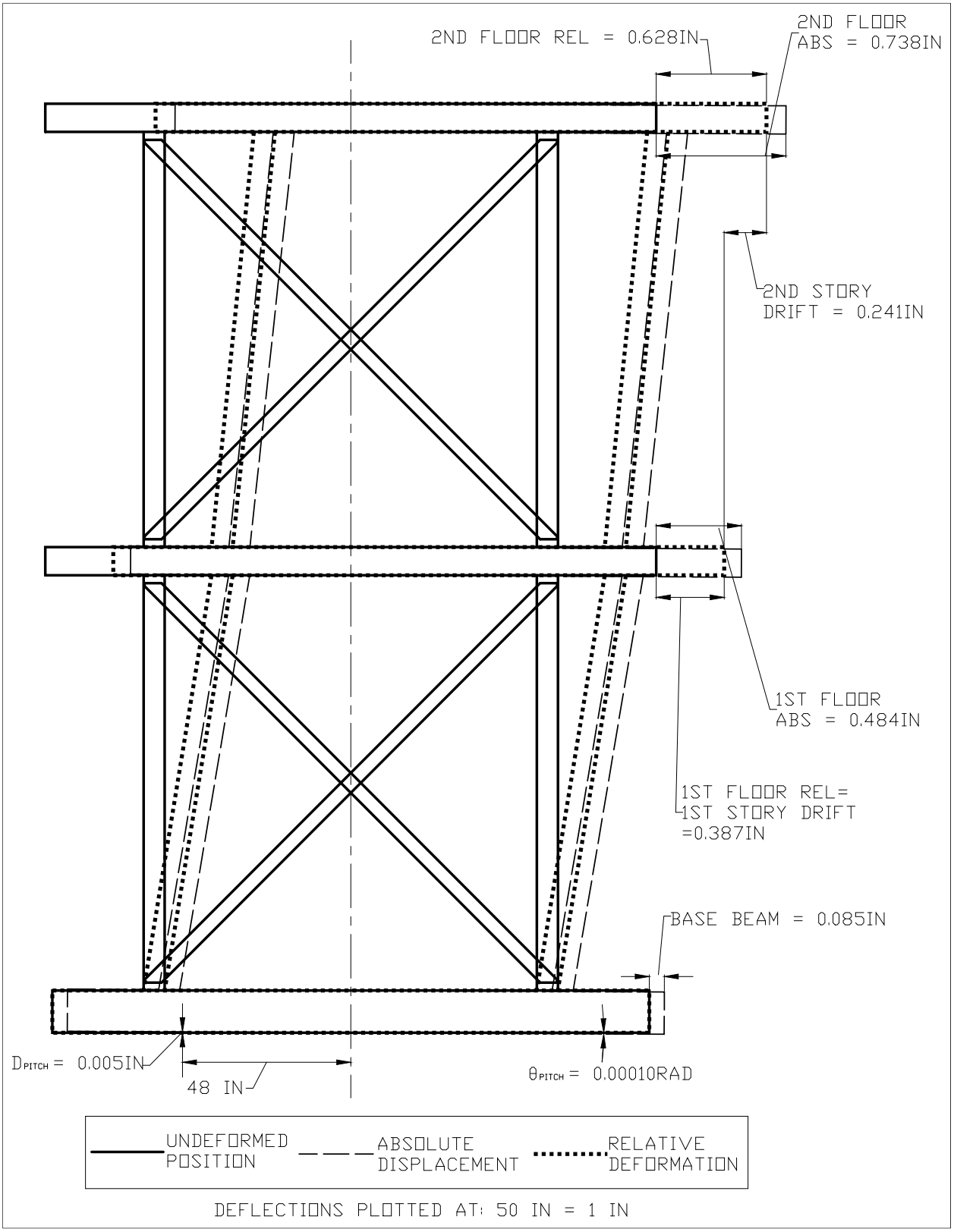

Since the mass of the model is well understood (57,500 lb at first floor and 57,600 lb at second floor, defined in section 8.1), inertia forces can be calculated based on the measured acceleration data presented in Figure 8-24 and Figure 8-25. These inertia forces can be used to estimate the applied lateral forces at both story levels, and they are used to develop plots of story shear versus story drift. These inertia forces are used to calculate the first-story shear per panel as follows:

$$1stStoryShear = \frac{57{,}500lb}{2} A13x + \frac{57{,}600lb}{2} A23x \qquad \text{(Eq 8-4)}$$

Similarly, the second-story shear per panel is calculated as follows:

$$2ndStoryShear = \frac{57{,}600lb}{2} A23x \qquad \text{(Eq 8-5)}$$

Figure 8-32 plots the first-story shear per panel with respect to the first-story drift. This figure also plots the shear versus drift for the second story, showing that both the story shear and drift were greater at the first story. These have been plotted along with the predicted lateral load versus deflection (see Figure 8-23). The portion of the predicted plot is only up to the point where the diagonal strap yields, and does not include any moment frame capacity contribution from the columns. The plots show that the shear panels on both levels have the same slope or lateral stiffness, because the panels were identical. Figure 8-33 shows the same story shear versus drift data, but for only the time region of 14.368–14.96 seconds, which includes the peak first-story drift that occurs at 14.496 seconds illustrated in Figure 8-31. The plots indicate essentially elastic behavior that agrees well with the predicted behavior, and it forms a basis for later comparison with the nonlinear behavior seen in the next test.

Figure 8-32. Story shear versus story drift
for both stories for the 8% SE32 test.

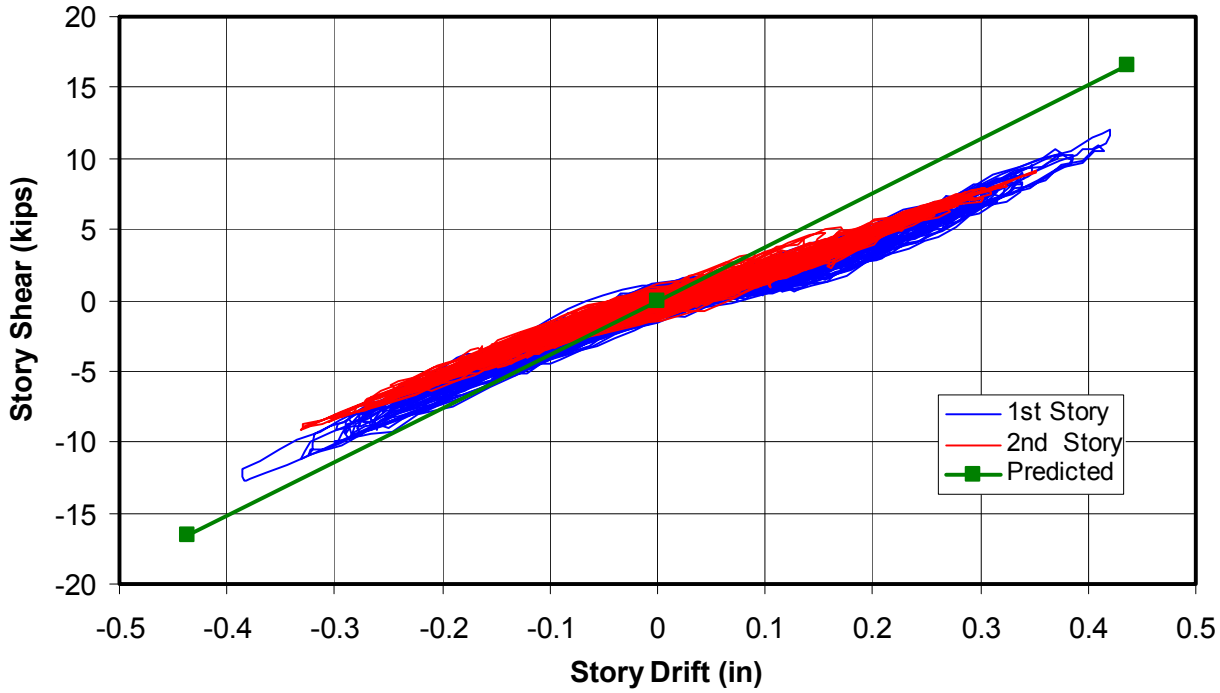

Figure 8-33. Story shear versus story drift
for 8% SE32 test, for 14.4–15 seconds.

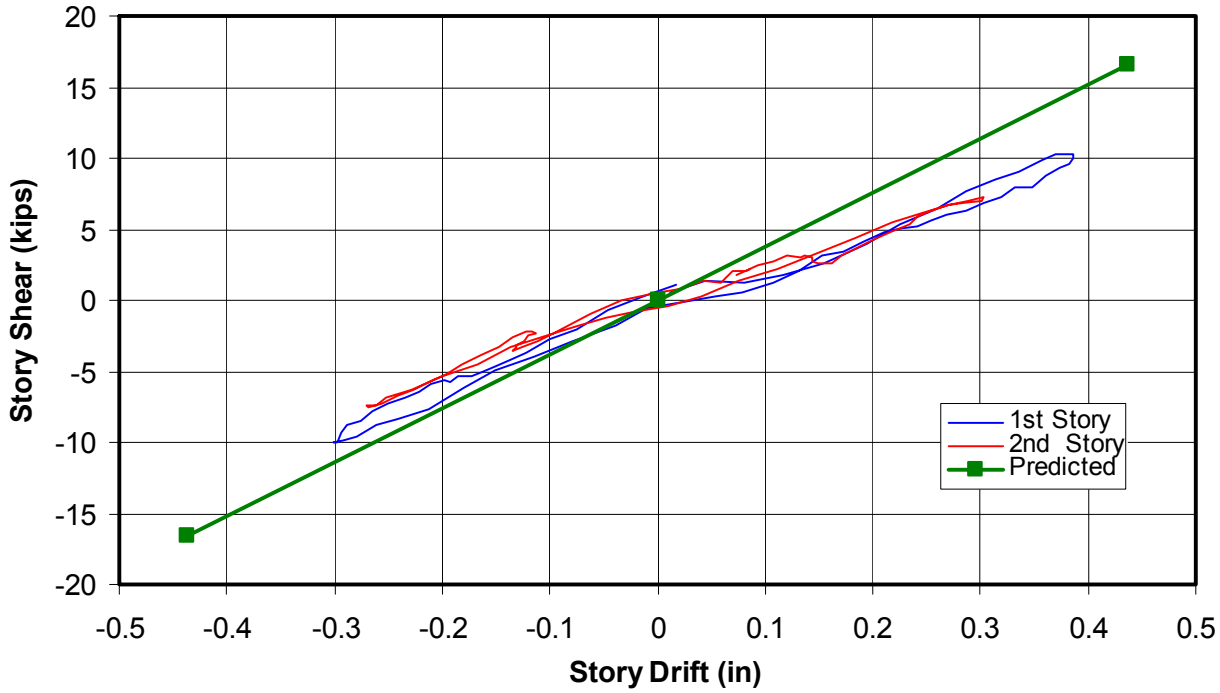

8.8.3 Measured strains

Figure 8-34 shows strains measured in one of the diagonal straps on the first-story shear panel (S13xz) and one on the second story (S36xz). These strain gages were selected because they have the greatest strains for their story level and yet their amplitudes are close to those values measured in other straps at their floors. Figure 8-16 showed that the S13xz gage was located at the lower south corner of the west face of the east shear panel, while the S36xz gage was located at the lower north corner of the east face of the east shear panel. The peak strain measured at the S13xz first-story strap was 1400 microinches/in., while the peak strain at the S36xz second-story strap was 997 microinches/in. Close inspection of the coupon data in Figure 8-22 showed that the straps began to yield at strains of 1700 microinches/in., indicating both first- and second-floor diagonal straps were significantly stressed but not about to yield.

Figure 8-34. Strains measured at first-story and second-story diagonal straps.

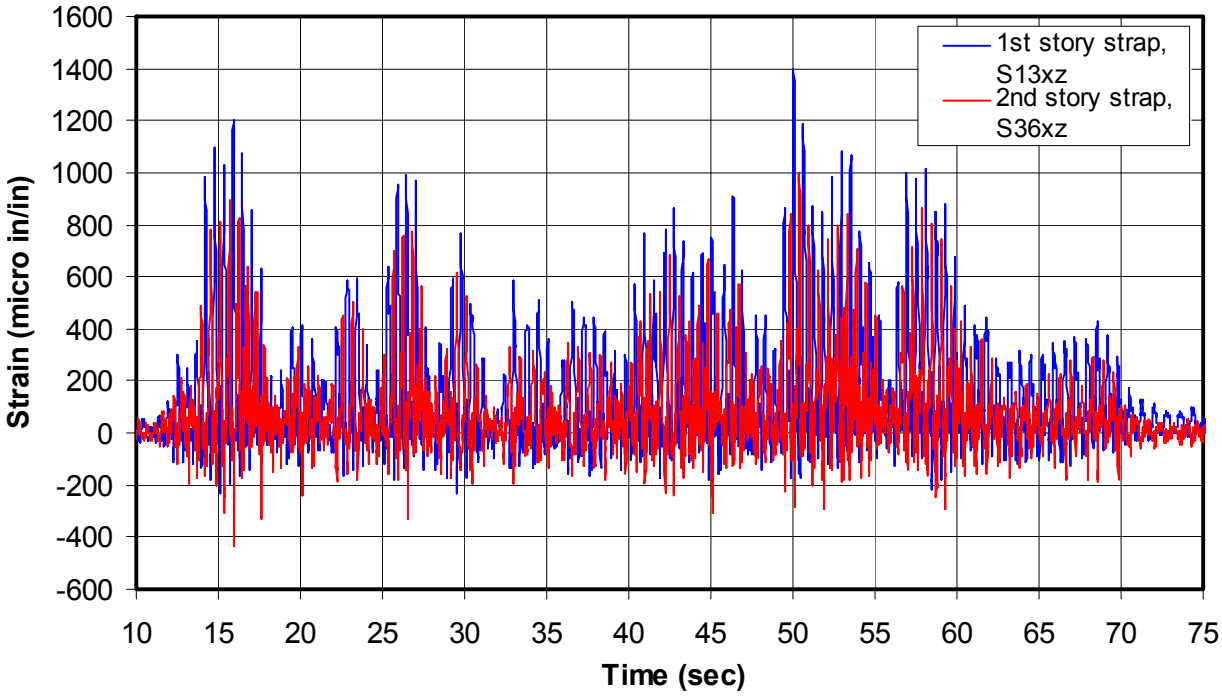

The straps were tension only, so the positive strains shown in Figure 8-34 were much greater than the small negative compressive strains, developed as the straps buckle. Figure 8-35 shows these strain measurements for the 13–18 second region. The maximum strain measured at the first-story strap, within the 13–18 second region (1201 microinches/in.), was significantly less than the maximum measured at 50 seconds. The strains for all

but one first-story diagonal strap remained below 90% in this region, relative to the peak strains measured near 50 seconds. For the second-story straps, the strains in this region generally reach 95% of the peak measured near 50 seconds.

Figure 8-35. Strains at the first-story and second-story straps, 13–18 seconds.

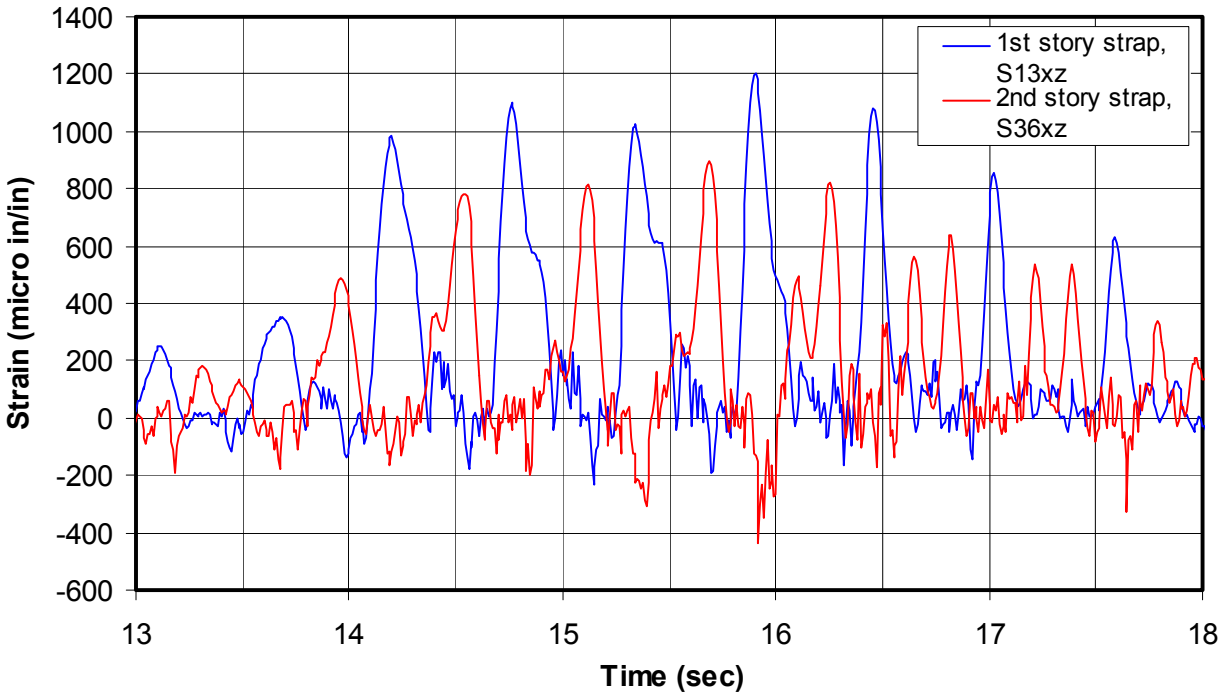

Figure 8-36 shows strains measured on the northwest column that have been reduced by 256 microinches/in. to account for an estimate of the strain in the columns due to gravity loading on the model. The reason for plotting an estimate of the true column strains, which have been offset by the effects of gravity, is to see if these strains overcome gravity and produce actual tensile strains and stresses in the columns at the locations of these gages. Inspection of all the column strain data for the 8% SE32 test shows that the effects of gravity are never overcome at the location of the gages, but projecting the decrease in compressive strains to the ends of the columns indicates small tensile strains and stresses occurred at the column tops and bottom. This strain correction assumes the columns equally distribute the load throughout their cross-section, and the intermediate studs carry a portion of the gravity load proportional to half their area relative to the columns (5.83 kips per panel). The much thinner intermediate studs (33 mil) were open C-sections and were therefore much more vul-

nerable to local buckling than the columns. Some intermediate studs did buckle during the placement of weights on the model before the test.

Figure 8-36. Strain measurements on the first-story northwest column.

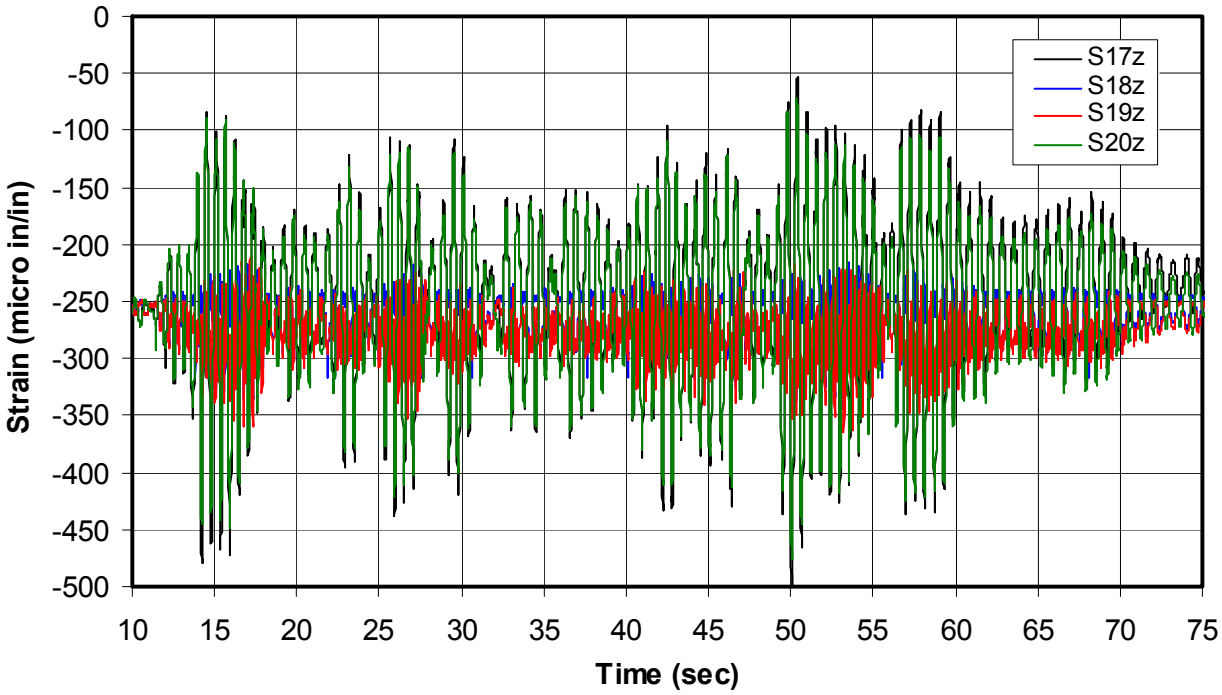

Figure 8-16 showed the S17z and S18z strain gages were 28 in. above the column bottom, at the outside and inside face of the column respectively, while S19z and S20z were at similar locations 28 in. below the column top. Figure 8-37 plots the same corrected strain measurements, zoomed in on the 13 through 18 second region of these records. Close inspection of the column coupon data plotted in Figure 8-22 indicates the columns begin to yield at strains of 1,300 microinches/in. This is much greater than the maximum compressive strains of 500 microinches/in. measured in the columns in the 8% SE32 test (Figure 8-36), indicating that the columns were far from yielding.

Figure 8-37. Strains on the first-story northwest column, for 13 to 18 seconds.

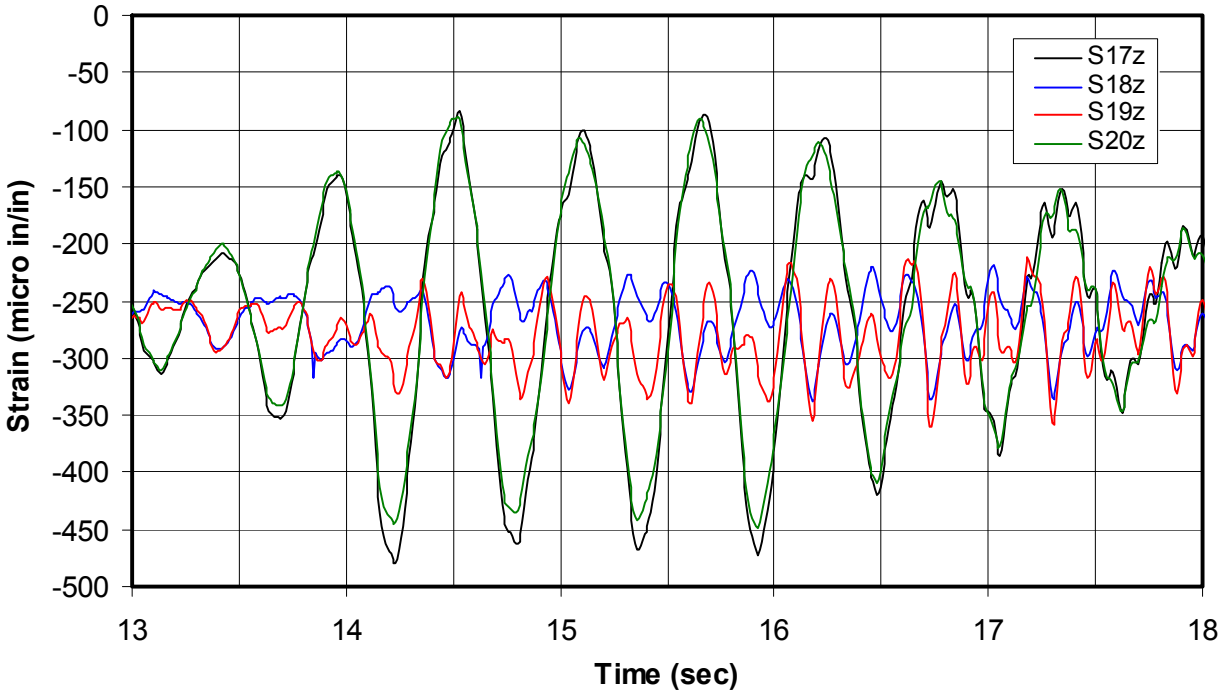

The strains measured near the bottom of the column (S17z and S18z) are out of phase with each other at the beginning of each cycle, because as the model racks in one direction, one strain gage measures an increase in strain while the other measures a decrease. When the model racks to the right (positive deflection), the deformed shape of the column, fixed at both its top and bottom, causes the strains at the bottom left face (S17z) to increase (reduction in compressive strains) while the strains at the right face (S18z) decrease further (e.g., 14.4 seconds in Figure 8-37). Figure 8-37 shows that when the model is racked to the right (e.g., at 14.4 seconds), the strains near the top, on the south face of this column (S20z), increase similar in phase and amplitude to S17z. The strains at the top-north face of this column (S19z) decease similar in phase and amplitude with S18z. These strains reflect the expected deformation of a column that is deformed laterally, while restrained from rotation at both top and bottom. When the model is racked to the right, the diagonal straps that connect the bottoms of the north (left) columns to the tops of the south columns are in tension. This loads the right columns with additional compressive load. At the same time the left column experiences a net increase in tensile strain because it is resisting the tensile load developed in the diagonal strap in the story above, plus it is resisting overall model overturning. This is consistent with the overall average increase in tensile strain in the left column

(S17z, S18z, S19z, and S20z), when the model is racked to the right (14.5 seconds in Figure 8-37). Close inspection of Figure 8-37 shows that the strains at S18z near the column bottom initially decrease out-of-phase with S17z as explained above, but then at 14.5 seconds the strain at S18z begins to increase due to the net tensile force applied to this column. The strain gages at both S17z and S18z experience a similar pattern of an initial strain change out of phase with the opposite side of the column due to column flexural deformation, followed by a change in strain that is in-phase with the opposite side of the column due to column overall axial deformation.

When the model racks to the left (e.g., at 14.7 seconds in Figure 8-37), the strains measured near the bottom of the column (S17z and Z18z) are again initially out of phase with each other, but with S17 experiencing a large decrease in strain (compressive strain) due to both the flexural deformation of the column and the net compressive axial load applied to the left (north) column, because the diagonal strap attached to its top is in tension. At 14.7 seconds the strain at S18z initially increases, out of phase with S17z, and then at 14.8 seconds begins to decrease, because of the overall increase in compressive load in this column. Similar response can be seen near the top of the column where S20z decreases in phase and amplitude with S17z, and S19z agrees with S18z. In general the strain at S18z appears to be more influenced by flexural deformation while S19z appears more influenced by axial deformation, though they are both similarly influence by the both deformations and are in phase with each other. Figure 8-38 provides similar column strain data for the southwest column (see Figure 8-16 for sensor locations) for the 13–18 second region. The strain measurements are greater on this column, and the strains near the bottom of the column are greater than on top. As expected, they do oscillate in a mirror image of those at the northwest column.

Figure 8-38. Strains on the first-story southwest column for 13–18 seconds.

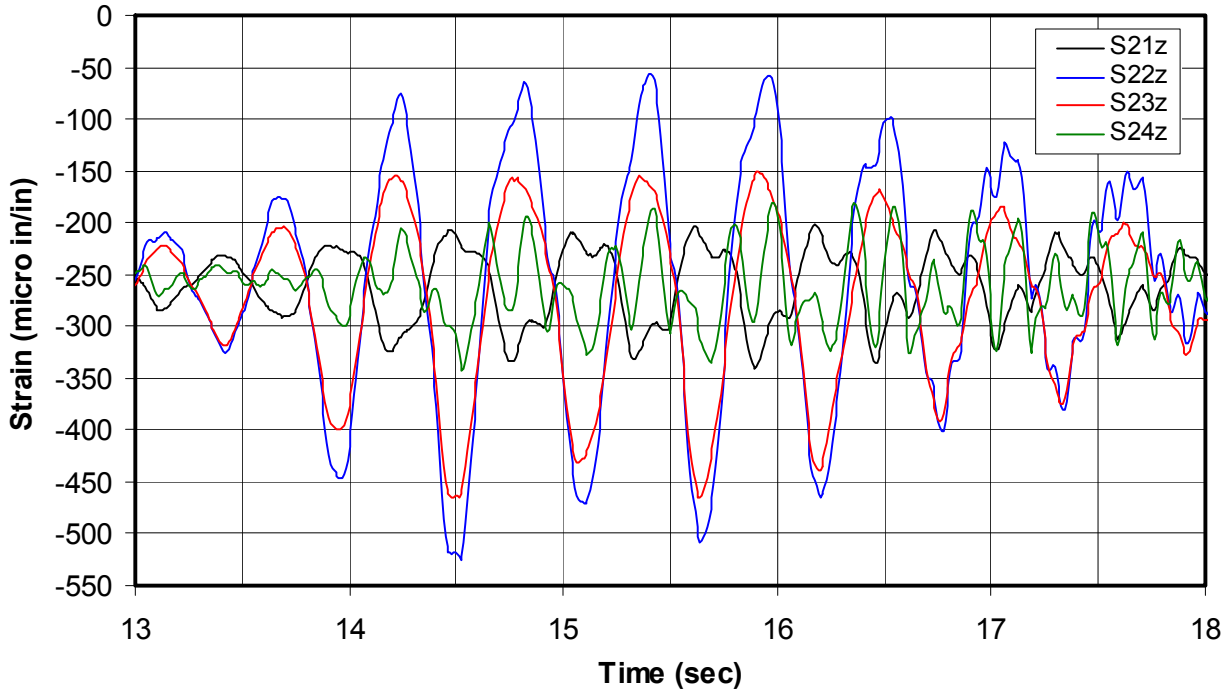

8.8.4 Column axial load, moments, and shears

These column strains can be used to estimate the column axial load, load carried in shear by the columns, and column moments at their tops and bottoms. Only the columns of the west shear panel on the first story were instrumented. The model experienced little torsional response, so the west side shear panel behavior should be representative of both sides. The first-story shear panels were more heavily loaded both laterally and vertically, so this panel is of greater interest. The axial load applied to the northwest (left) column, P_{aNW} is defined as follows:

$$P_{aNW} = \frac{(S17z+S18z+S19z+S20z)}{4} EA_c \qquad \text{(Eq 8-6)}$$

where

S17z, S18z, S19z and S20z are strains measured on the northwest column (see Figure 8-16), which have been corrected for the effects of gravity by decreasing their measurements by 256 microinches/in., and are plotted in Figures 8-36 and 8-37

E = modulus of elasticity of steel, which is 29,000 ksi

A_c = the column nominal area, which equals 3.49 sq in., as shown in Table 8-9.

The axial load applied to the southwest (right) column, P_{aSW}, is calculated in the same way using the strain gage data measured at S21z, S22z, S23z, and S24z (see Figure 8-38). Figure 8-39 and Figure 8-40 plot the applied axial load for both the north and south columns of the first-story west shear panel. Figure 8-40 shows the overall decrease in compressive load on the northwest column at 14.4 seconds, when the model is racked to the right. The increase in compressive load can also be seen in this figure when the model is racked to the left at 14.7 seconds.

Figure 8-39. Applied axial load for first-story west shear panel columns in the 8% SE32 test.

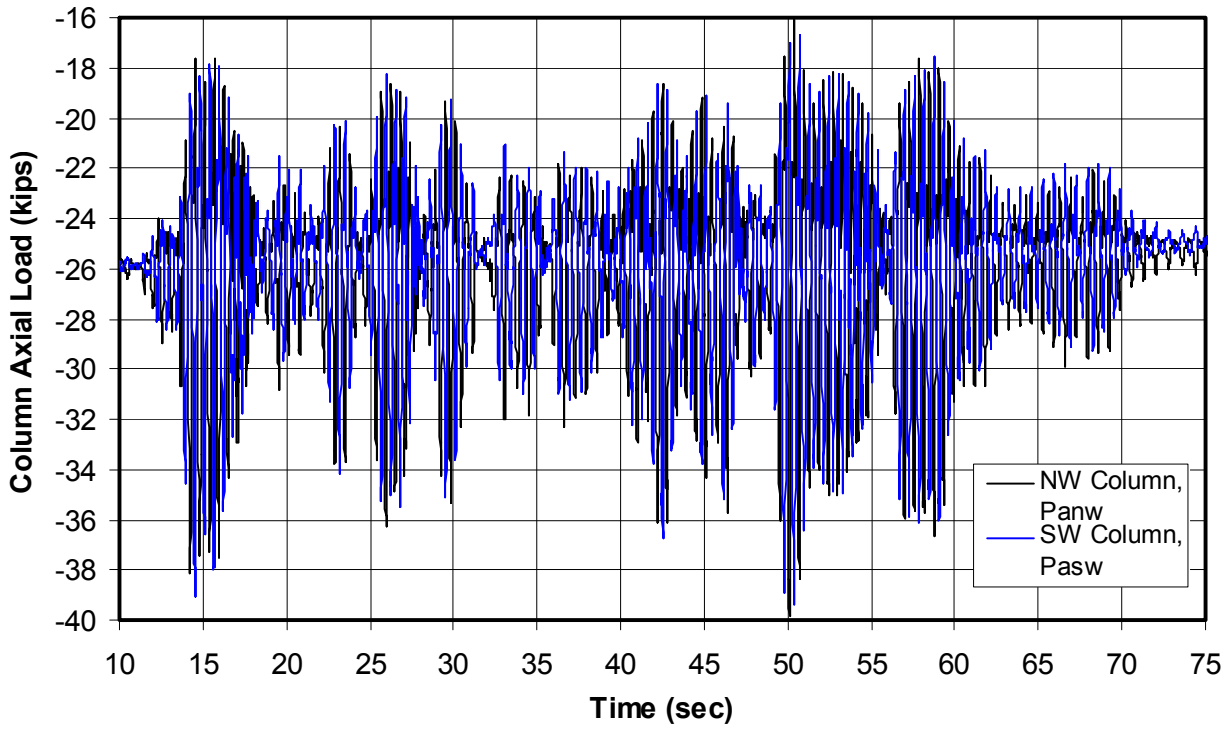

Figure 8-40. Axial load for first-story west panel columns, 8% SE32, 13–18 seconds.

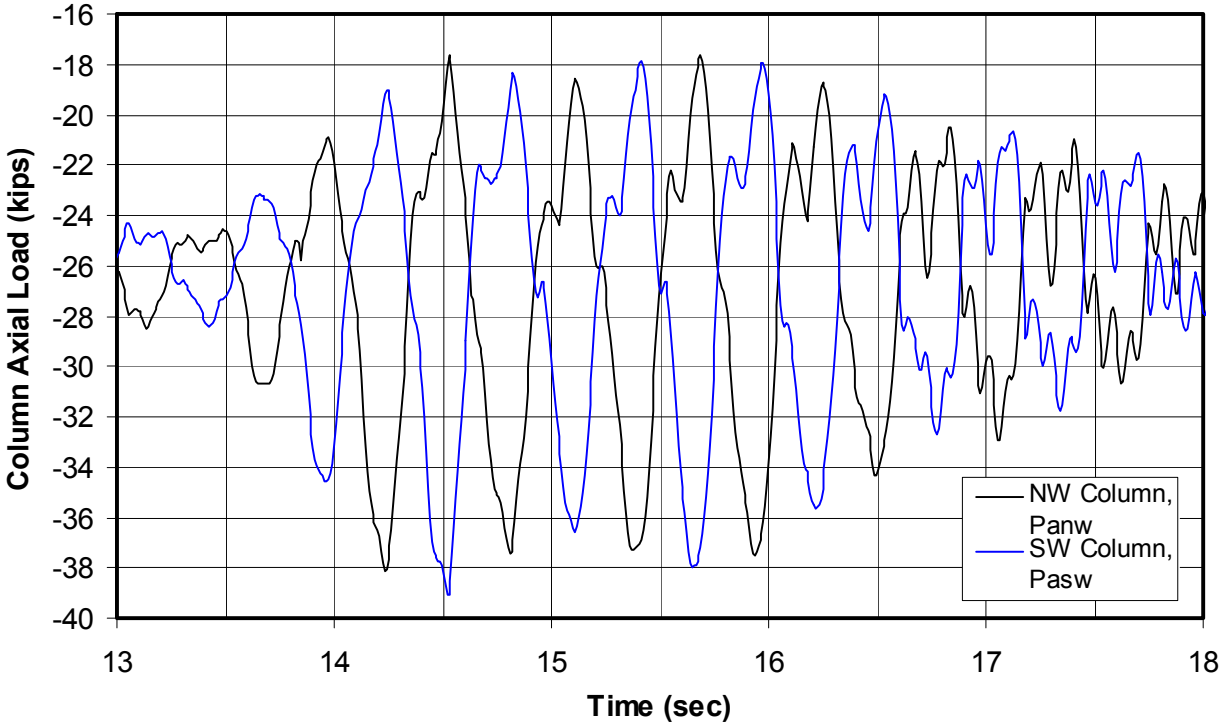

The diagonal strap connections to the columns and the column anchors are identical at their tops and bottoms. Figure 8-36, Figure 8-37, and Figure 8-38 show that the strains measured 28 in. above the bottom of the columns and 28 in. below their tops are similar. The overturning moment at the bottom of the columns is greater, so the difference in strains on opposite faces of the column should be greater near the bottom of the columns. Greater strains are more clearly seen on the bottom of the southwest column (S22z in Figure 8-38) than on the northwest column (S17z in Figure 8-37). The difference in strains measured near the ends of the columns can be linearly factored up to estimate the moment at the ends of the columns. The applied moment at the bottom of the northwest column, M_{anwb}, based on the strain data measured 28 in. above the bottom of the column, can be calculated as follows:

$$M_{anwb} = \frac{(S17z - S18z)}{2} ES_x \left[\frac{H}{H - 2(28in.)}\right] \quad \text{(Eq 8-7)}$$

where

S_x = the section modulus of the column, equal to 5.09 cu in., which equals Ix/c = 16.34 in.^{4}/3.21 in. as defined in Table 8-9.

H = the panel height, equal to 118 in.

Similarly, the applied moment at the top of the northwest column, M_{anwt}, based on the strain data measured 28 in. below the top of the column can be calculated as follows:

$$M_{anwt} = \frac{(S20z - S19z)}{2} ES_x \left[\frac{H}{H-2(28in.)}\right] \quad \text{(Eq 8-8)}$$

The moment applied to top and bottom of the south (right) column, M_{aswt} and M_{aswb}, are calculated in the same way using the strain gage data measured at S21z, S22z, S23z, and S24z. Figure 8-41 and Figure 8-42 plot the moments applied to the top and bottom of both the north and south columns of the first-story west shear panel. The sign convention in these plots use the right hand rule so that the applied moment at both the top and bottom of the columns are positive when the model is deformed to the right (south). This results in the moments always being in phase with each other, facilitating comparison of their relative amplitudes.

Figure 8-41. Applied moment for first-story west shear panel columns in the 8% SE32 test.

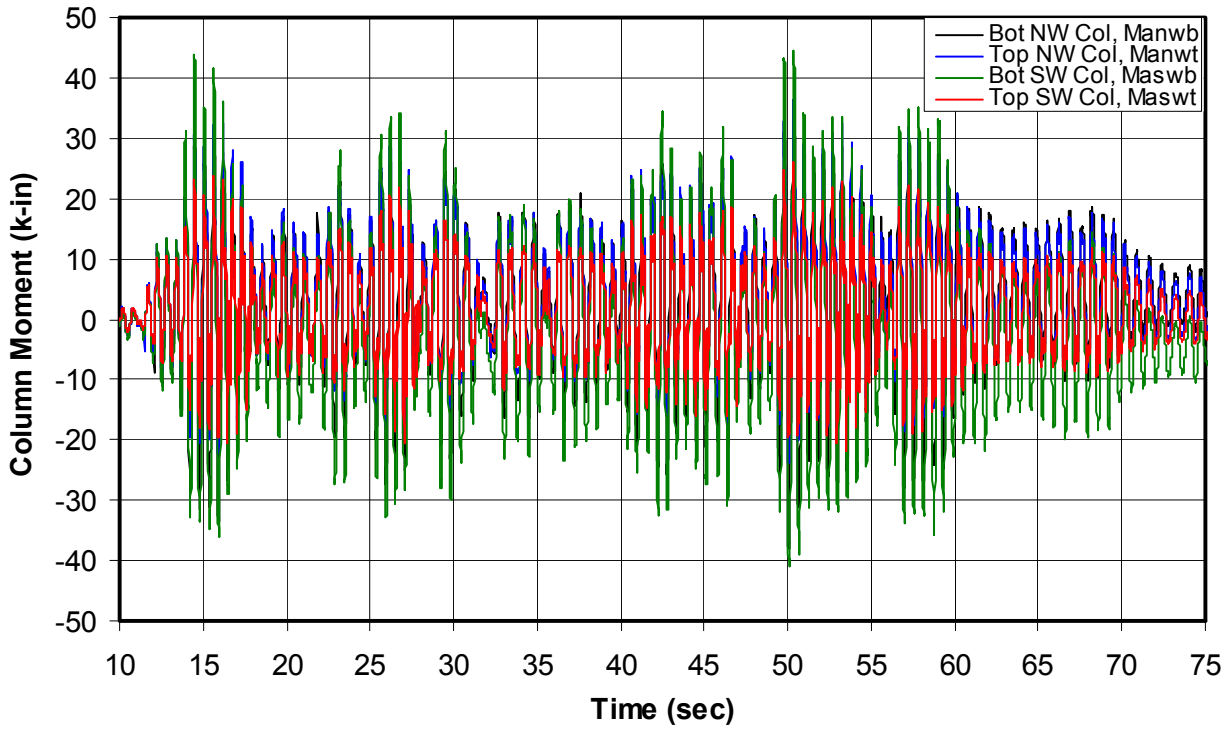

Figure 8-42. Moment for first-story west panel columns, 8% SE32, 13 through 18 seconds.

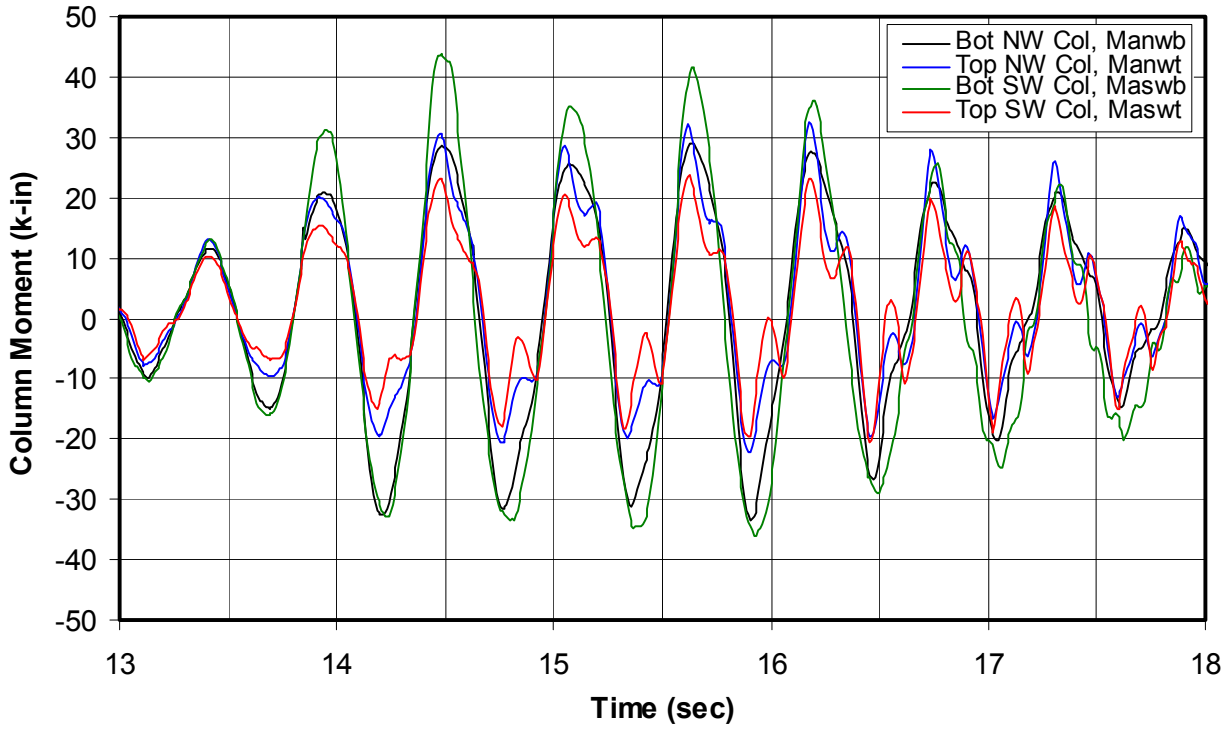

Normally the sign of at the bottom of the columns would be reversed. This shows the moments in the southwest column are consistently greater at the bottom than at the top. However, for the northwest column, when the model deforms to the right, the moments are greater at the column top.

The applied shear at the north column, V_{anw}, can be calculated as follows:

$$V_{anw} = \frac{(S17z - S18Z - S19Z + S20Z)}{2}\left[\frac{ES_x}{H - 2(28\ in)}\right] \qquad \text{(Eq 8-9)}$$

The shear applied to the south (right) column, V_{asw}, is calculated in the same way using the strain gage data measured at S21z, S22z, S23z, and S24z. Figure 8-43 and Figure 8-44 plot the applied shear at both the north and south columns of the first-story west shear panel. Figure 8-32 and Figure 8-33 (above) plotted the story shear per shear panel based on the inertia forces defined by the model acceleration and weight. This story shear at the first story carried by the columns is the total of the northwest and southwest column shear in Figure 8-43 and Figure 8-44, and the portion carried by the diagonal straps is the amount in Figure 8-32 and Figure 8-33 minus the total of the northwest and southwest columns.

Figure 8-43. Applied shear for first-story
west shear panel columns in the 8% SE32 test.

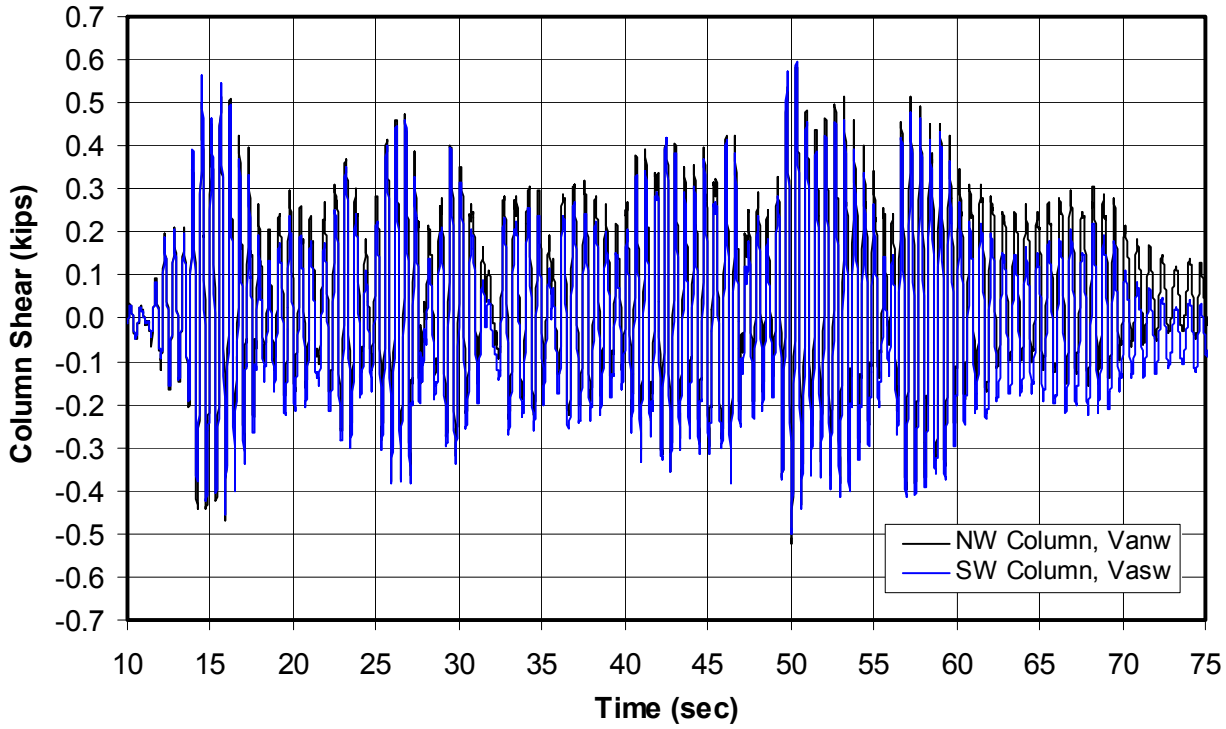

Figure 8-44. Shear for first-story
west panel columns, 8% SE32, 13–18 seconds.

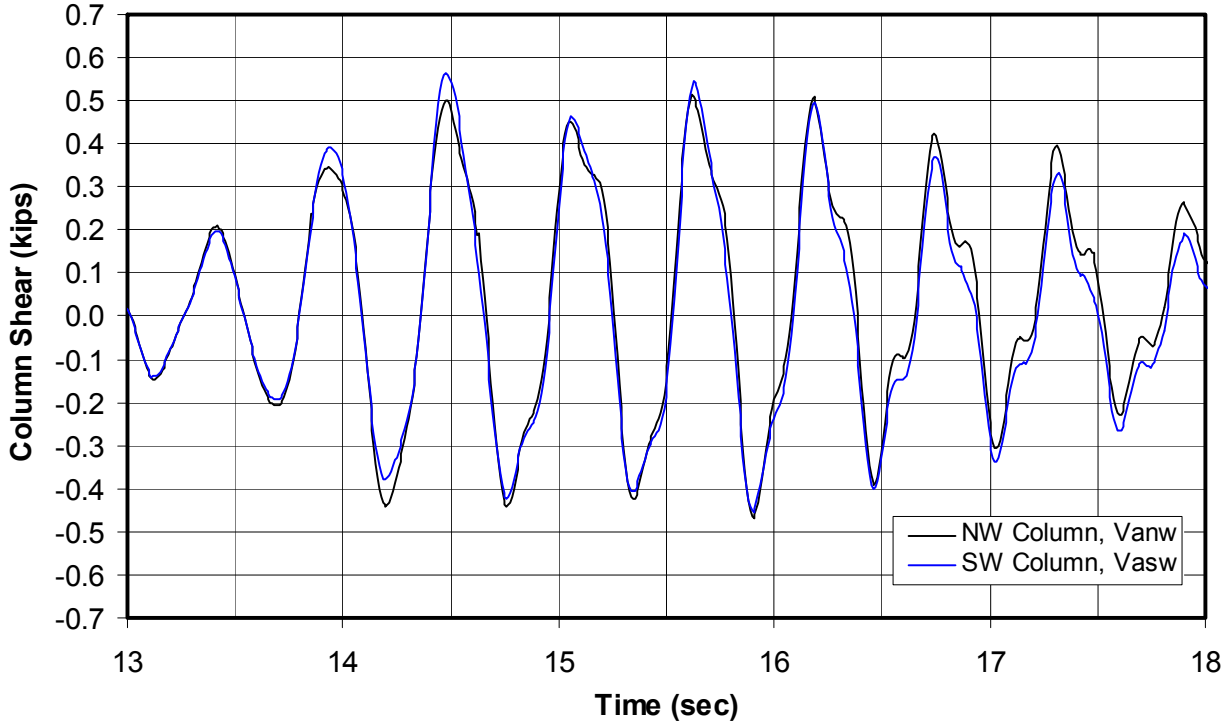

For the cycle between 14.4 and 15 seconds, the total positive column shear is 1.07 kips (Figure 8-44), which is 10% of the panel story shear of 10.28 kips (Figure 8-33). In the negative direction, the total column shear is 0.87 kips, which is 9% of the panel story shear of 10.02 kips. Table 8-16 predicted a total shear panel lateral capacity at strap yield (the model in this test is below yield) of 19.64 kips, and a lateral capacity of the strap alone of 16.62 kips, indicating a total column capacity at strap yield of 3.02 kips, which is 15% of the total. Since the measured data indicate 10% of the capacity was carried by the columns and the predicted analysis is based on assuming the columns are fully fixed, one estimate is that the columns have a fixity of 60 to 65%. These data could also be used to define a rotational spring that could be used to represent the column fixity in an analytical model.

8.9 Nonlinear seismic test

Following the 8% SE32 test, the model was tested with the full filtered SE32 record. This test was expected to cause significant nonlinear response in the shear panels. The test would provide a basis for evaluating if the cold-formed steel design recommendations developed in this program do in fact lead to ductile shear panel performance. The test should result in significant yielding of the diagonal straps and columns, and perhaps minor yielding of the anchors, but not in damage that could lead to brittle failure, such as joint or anchor failures. (Section 8.2 described the various modes of failure that would be tested in this shake table test.)

8.9.1 Measured acceleration response

The acceleration and displacement data were again examined during the linear portion of the 100% SE 32 test, to confirm that the same data channels best represented the response of the model. The acceleration measured at A23x was still much greater than at the other two second-floor slab accelerometers (A21x and A22x). The out-of-plane and torsional response was again very small. The in-plane displacements measured at the second floor (D22x and D24x) were consistent with each other, confirming little torsional response. The accelerations recorded on the first floor were double integrated and corrected for offsets, to provide displacement records that could be compared with recorded displacements. The displacements integrated from the A21x and A22x accelerometers were much less than the measured displacements at D22x and D24x. The displacements from the A23x accelerometer agreed very well with the measured displace-

ments, so the A23x record was taken as most representative of the second-floor acceleration. The first-floor acceleration measured at the A13x accelerometer, directly below A23x, agreed well with the acceleration measured at A12x and with the displacement data. Therefore, as in the linear test (8% SE32) the A13x and A23x acceleration data were determined to be most representative of the model response in this nonlinear test.

Figure 8-45 plots the measured acceleration at the TESS, first-story slab (A13x), and second-story slab (A23x). Very small out-of-plane or torsional response was seen in either the 8% or 100% SE32 tests. Some high-frequency, high-acceleration spikes were seen in the accelerometer data for the first- and second-floor levels, but the displacement data do not contain these spikes, indicating the high accelerations were due to snapping of the out-of-plane threaded rods. Figure 8-46 and Figure 8-47 zoom in on the same motions at 9–13 seconds and 13–18 seconds, respectively.

Figure 8-45. Accelerations at the TESS, first story, and second story in the 100% SE32 test.

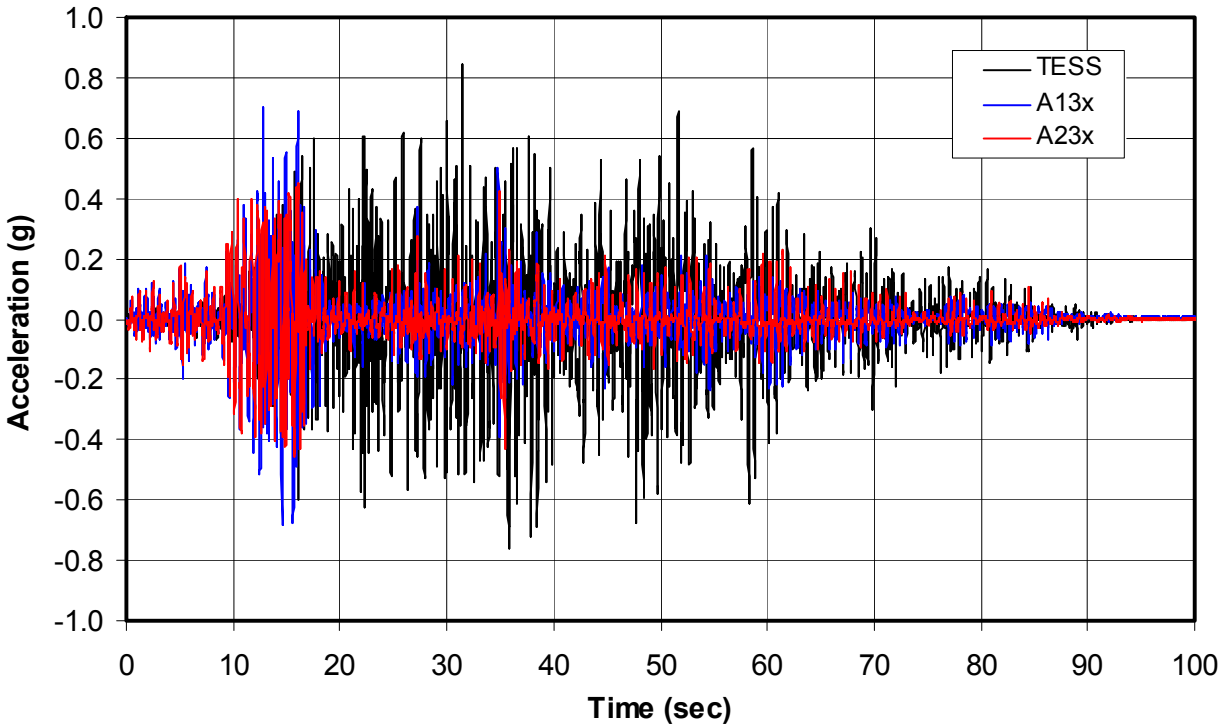

Figure 8-46. Accelerations at the TESS, first story, and second story in SE32 test, 9–13 sec.

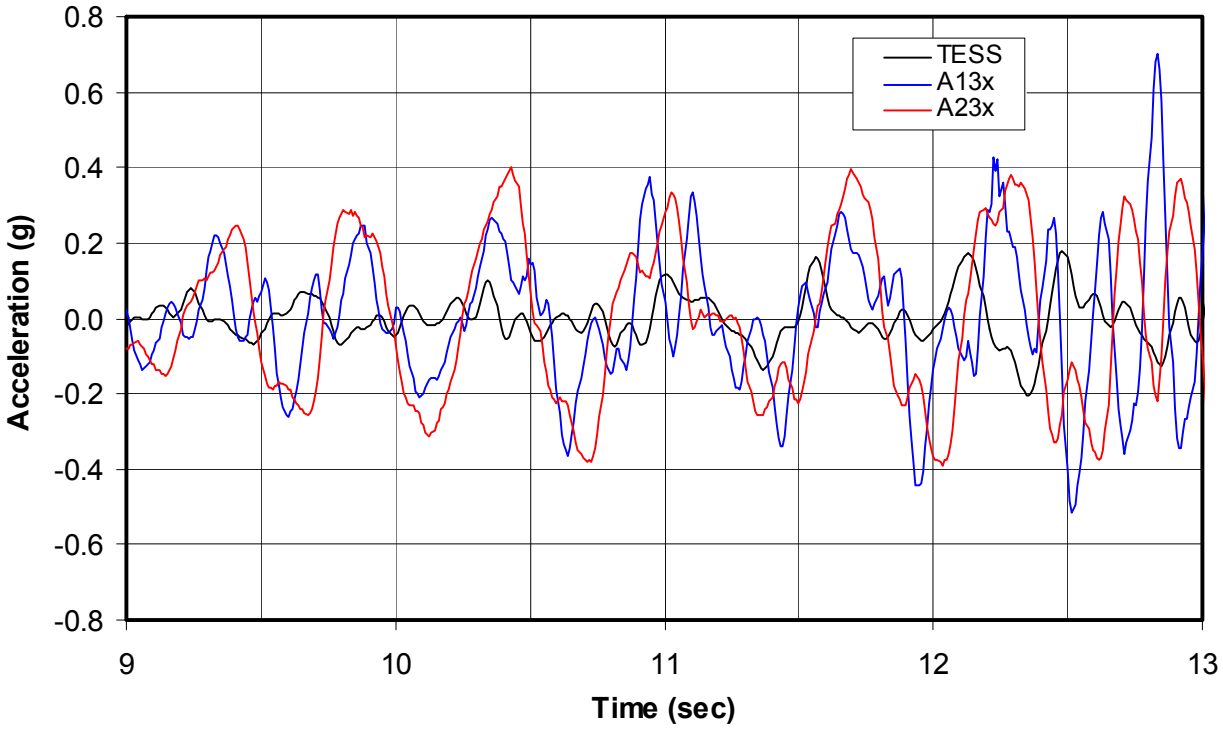

Figure 8-47. Accelerations at the TESS, first story, and second story in SE32 test, 13–18 sec.

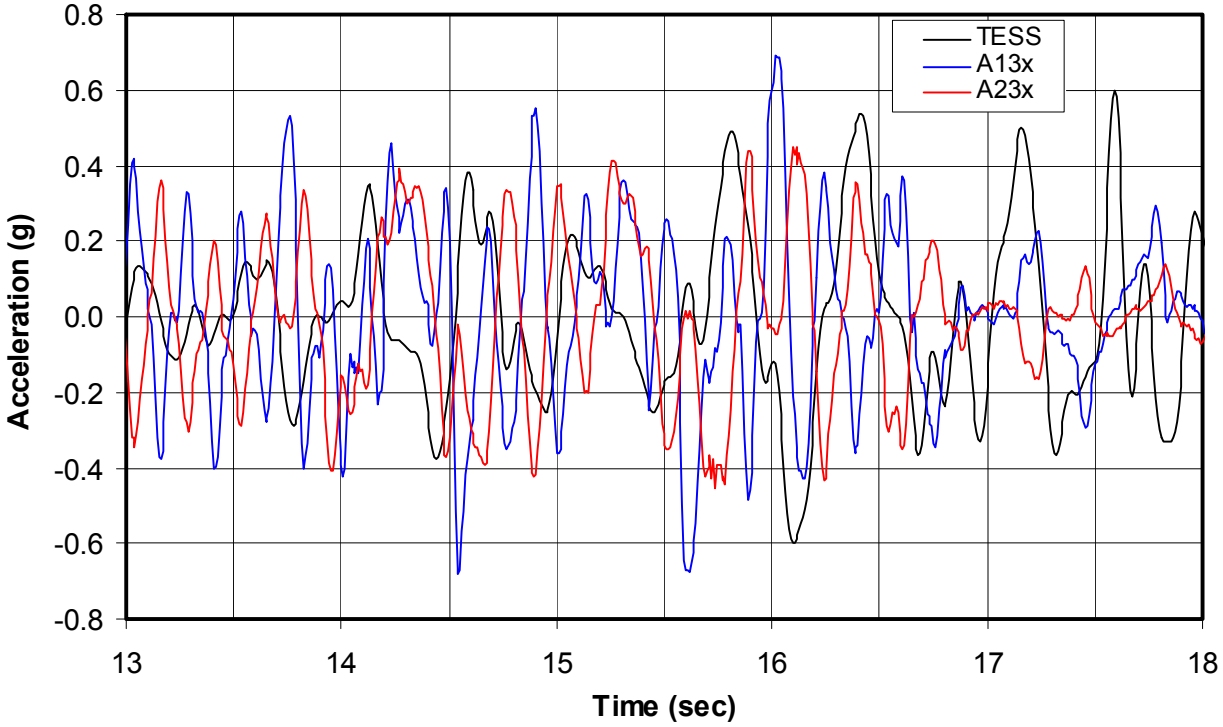

Figure 8-46 shows that the TESS motions are initially amplified significantly at the first-floor slab (A13x), and even more at the second floor (A23x). The model behavior is still fairly elastic at the beginning of the interval shown in Figure 8-46. At 12 seconds, the first-floor accelerations begin to exceed the second-floor values because of the greater amplification of the model in its second mode. Later, modal testing showed that, after this test, the model softened to the point that the first-mode frequency had fallen to 0.5 Hz. At 12 seconds, the diagonal straps are beginning to yield so that the first mode period increases, and after 13 seconds the first-mode response is not excited as much as the second mode. The second-mode frequency also begins to decrease at 12 seconds.

Figure 8-46 and Figure 8-47 show the TESS shake table motion oscillates significantly at periods corresponding to the period of the second mode of vibration of the model (0.2 seconds, or 5 Hz). The TESS motions were significantly influenced by the response of the model in the 100% SE32 test, and the TESS appears to have overcorrected in trying to prevent unwanted motions. Still, the objective of the test was accomplished, with significant nonlinear response and large lateral deformations. The actual achieved motions of the TESS and response of the model can be well documented, and the actual support motion can be used in the DRAIN2DX analysis to provide an evaluation of the ability to predict large deformation demand and capacity. Figure 8-47 shows that after 17 seconds, the diagonal straps have yielded and elongated to such an extent that the model has softened to the point that it is essentially isolated from the higher-frequency motions of the TESS. After this point, Figure 8-47 and Figure 8-45 show that the TESS accelerations are greater than the response accelerations at either the first or second floors of the model, measured at A13x and A23x, respectively.

8.9.2 Measured displacement response

Figure 8-48 shows the displacements for the entire 100% SE32 test, measured at the base beam, first-floor level, and second floor level. Figure 8-49 plots these displacements between 9 and 18 seconds, including the linear portion of the test before 12 seconds and the time of greatest model deformation. These displacements define the behavior of the model better than the accelerations. The base-beam, first-floor, and second-floor displacements are again averages of the measured displacements at these levels as explained in the linear test results.

Figure 8-48. Displacements at the base beam, first floor, and second floor.

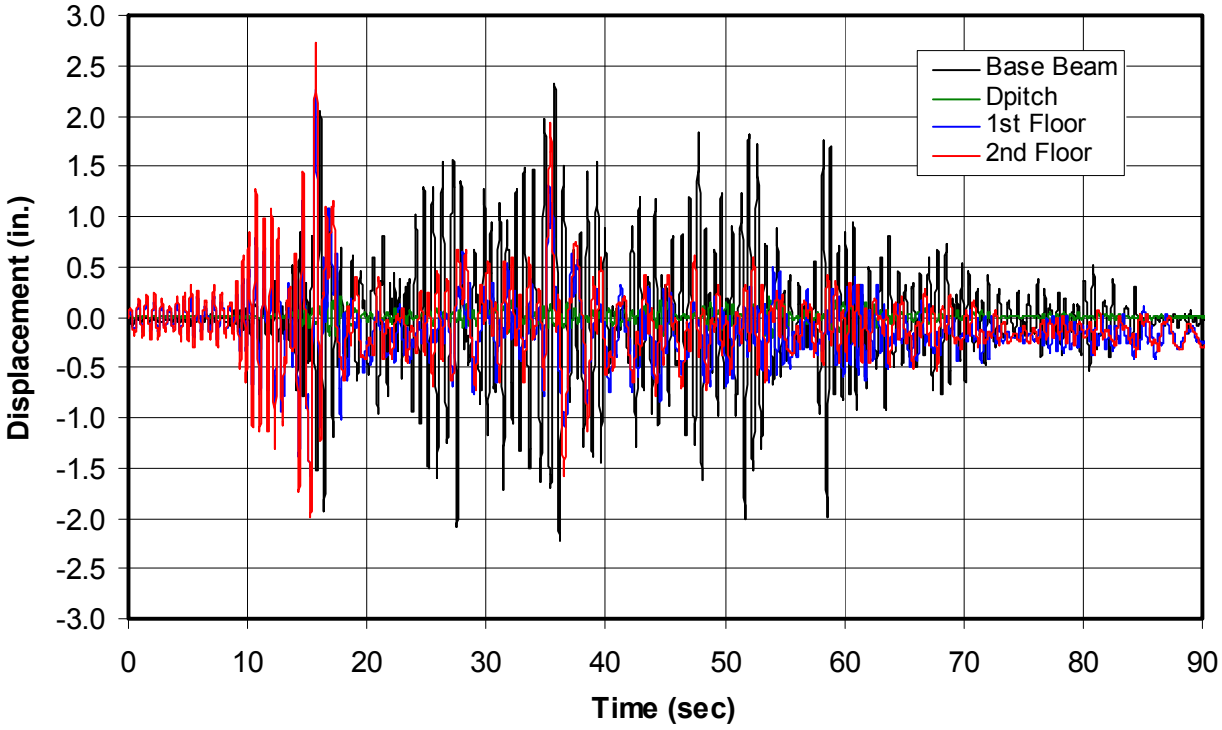

Figure 8-49. Displacements at the base beam, first floor, and second floor, 9–18 seconds.

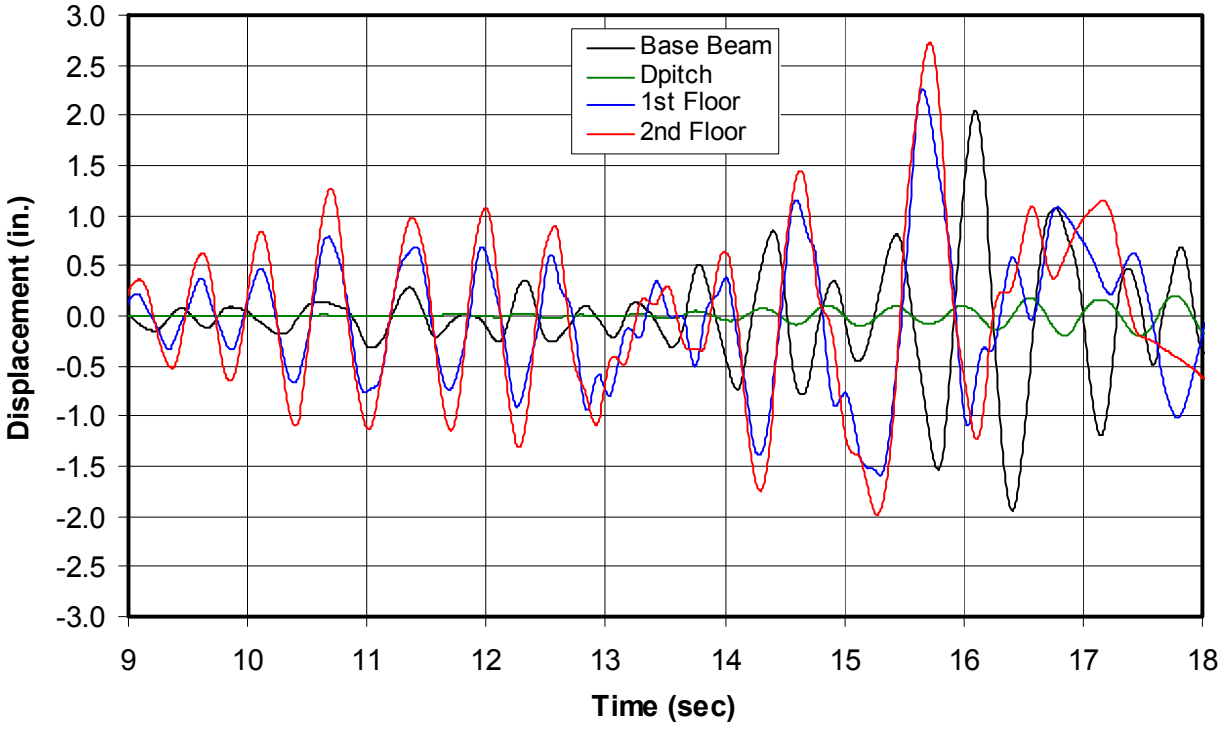

The pitch displacements, D_{pitch}, are also plotted in these figures. Figure 8-49 shows that the pitch displacements become quite large after 14 seconds. Figure 8-50 plots the first- and second-floor relative displacements, calculated from the measured displacement data according to Equations 8-1 and 8-2. Figure 8-51 plots the story drifts for both the first and second story, between 11 and 18 seconds, where the largest story drifts occur. The largest first-story drift is 3.43 in. at 15.728 seconds, and the largest second-story drift is 1.07 in. slightly later, at 15.752 seconds. This large first-story drift is the most critical deflection parameter defining the behavior of the model. The deformed model shape is plotted at 15.728 seconds in Figure 8-52. This peak first-story drift is almost nine times greater than the peak first-story drift in the 8% SE32 test (0.387 in.). Figure 8-52 shows that the peak drift was measured at a time when the first- and second-story floors were displaced to the right, while the base beam was displaced to the left. At this same time, the base beam was pitched counter-clockwise, indicating that the TESS and base beam was moving out-of-phase with the displaced shape of the model.

Figure 8-50. Relative displacements and first-story drift for the 100% SE32 test.

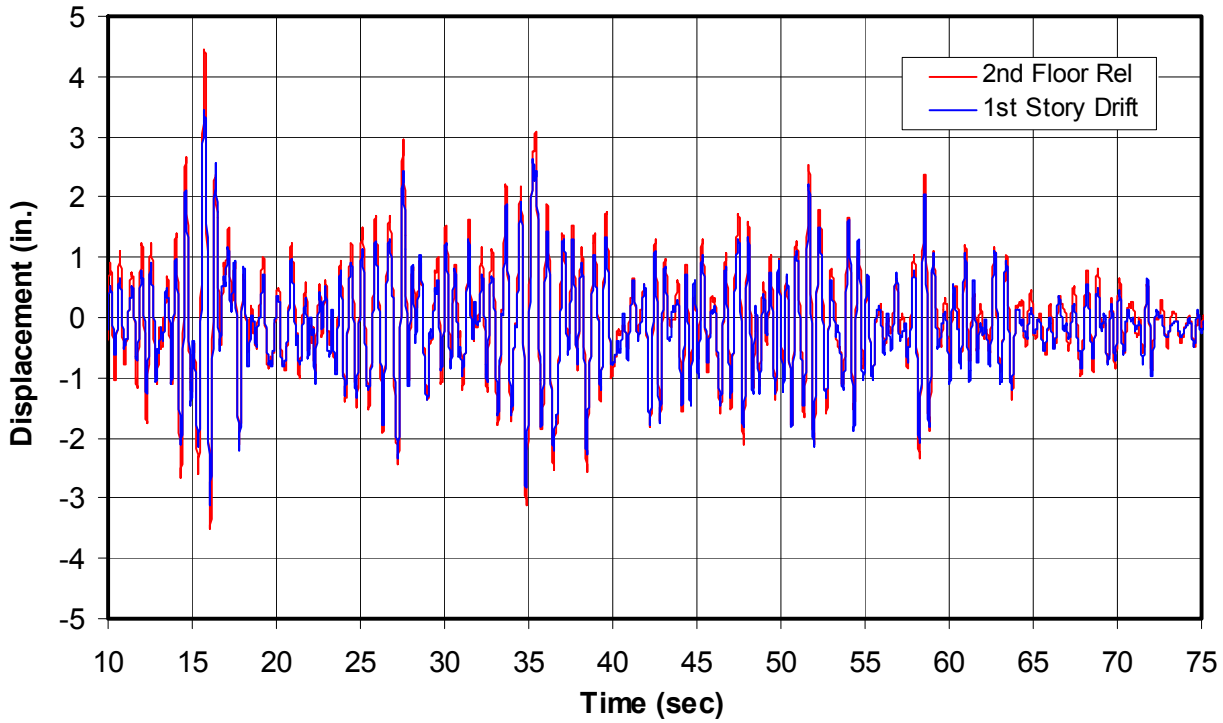

Figure 8-51. First- and second-story drifts for 100% SE32, 11 to 18 seconds.

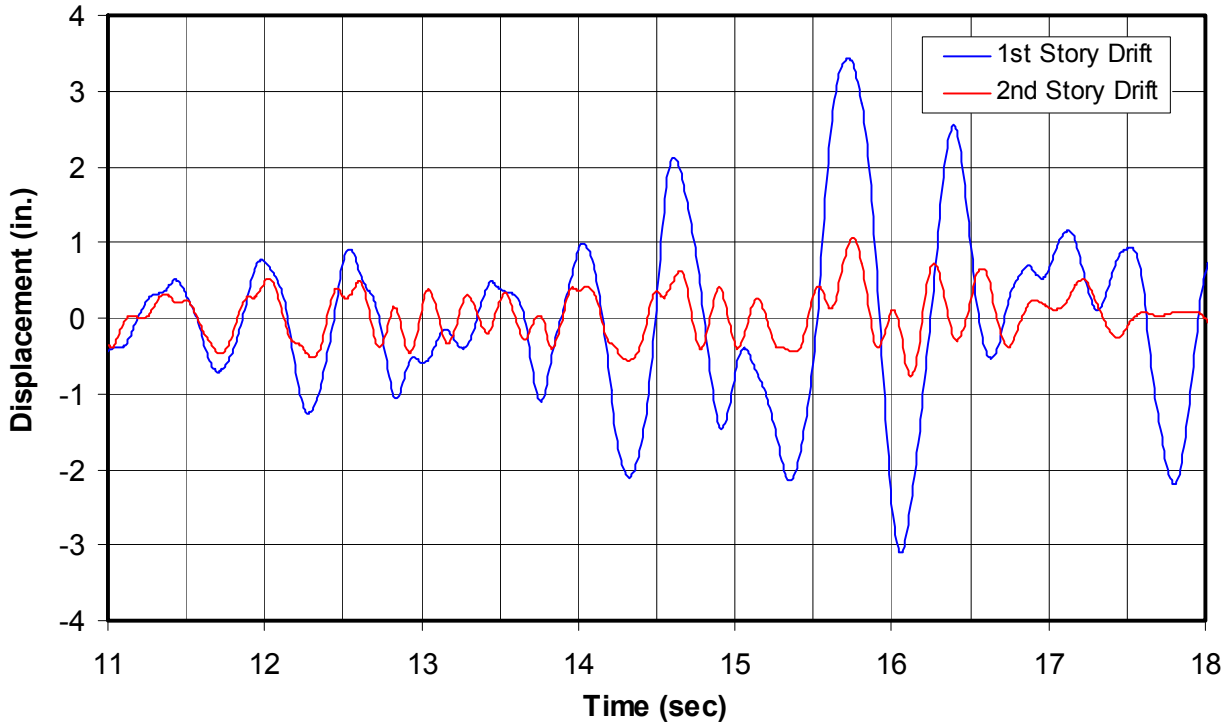

All shake table model tests were recorded with two digital camcorders, recording in a frame mode so that the video file consisted of individual photographs taken every 1/30th of a second. Figure 8-53, shows an overall view of the model taken from the east-northeast corner at approximately 15.7 seconds in the 100% SE32 test, near the time of largest model deformation shown in Figure 8-52. At this time the model was deformed to the left, which is to the south in the same direction that is to the right in Figure 8-52. The picture shown in Figure 8-53 should be very close to the shape that has been amplified by a factor of 10 in Figure 8-52. The first-story drift can best be seen in this picture by noting how the diagonal strap from the bottom-right to top-left corner of the panels are taut while they are slack in the opposite direction. Figure 8-53 shows how the diagonal straps at the second story remained almost taut, consistent with the small second-story drifts plotted in Figure 8-51. Figure 8-54 was taken by the other camcorder from the opposite west-southwest corner, having a perspective similar to Figure 8-52. This picture zooms in on the first story and it has almost the same perspective and the amplified deformed shape shown in Figure 8-52. Here the diagonal straps between the bottom-left to top-right corners were taut, while they were slack with multiple ripples in the opposite direction.

Figure 8-52. Model displacement and deformation
in the 100% SE32 test at 15.728 seconds.

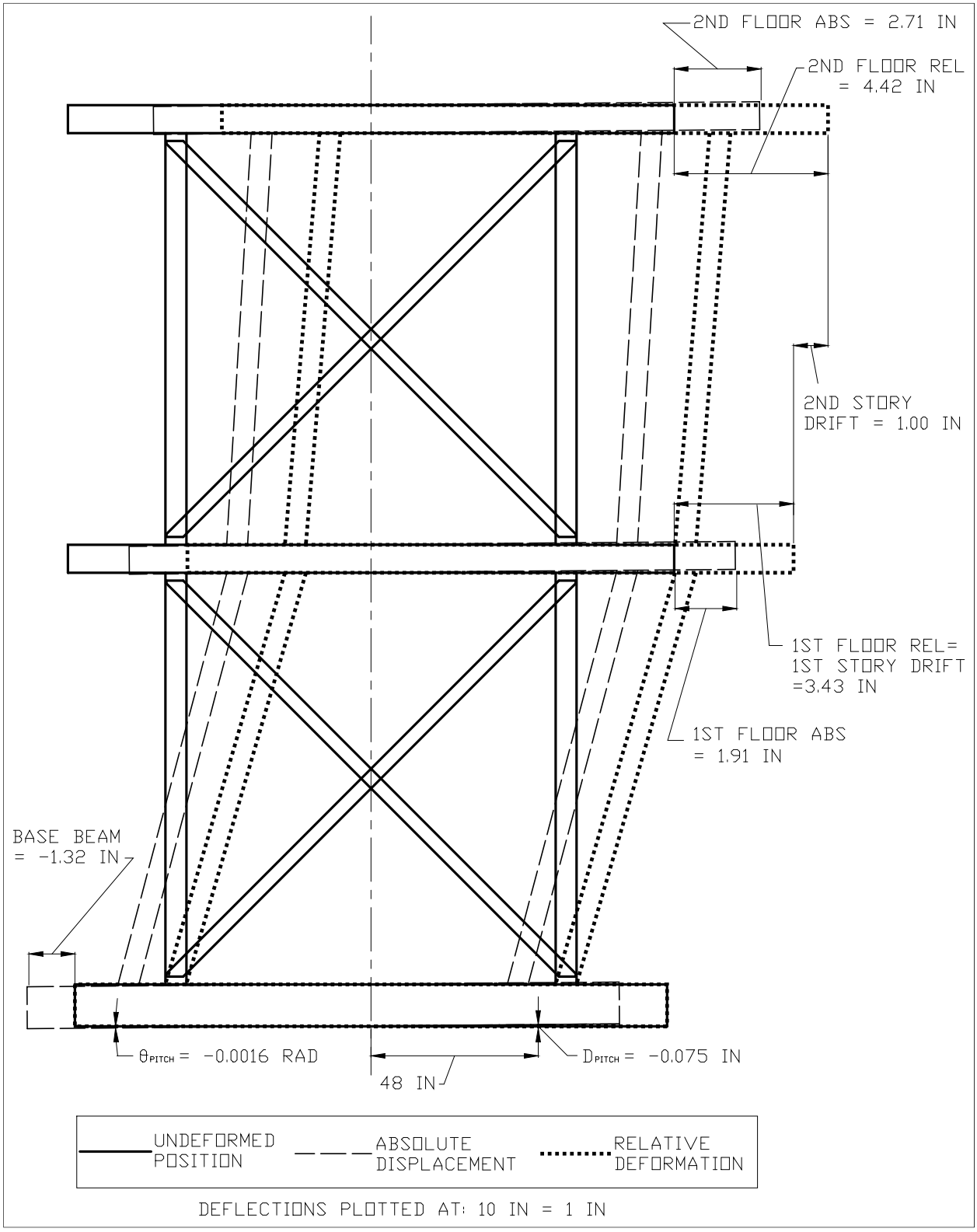

Figure 8-53. Overall view at largest positive cycle, 100% SE32 test near 15.7 sec.

Figure 8-54. First-story view at largest positive cycle, 100% SE32 test near 15.7 sec.

Inertia forces and applied lateral forces (base shear) at both story levels were calculated from the floor accelerations shown in Figure 8-45 through Figure 8-47. These forces were used to plot story shear versus story drift for both stories in Figure 8-55. This plot shows that the story shear and especially story drift was much larger at the first story. Figure 8-55 shows that the greatest first-story shear per shear panel was 20.6 kips, and the greatest second-story shear was 13.1 kips. The greatest first-story shear occurred at 14.55 seconds and the greatest second-story shear occurred during the next major cycle at 15.74 seconds. The first-story shear was 57% greater than the greatest reached at the second story. Figure 8-56 shows plots of the story shear versus story drift during the largest first-story drift cycle that occurred between 15.52 seconds and 16.25 seconds. The largest second-story shear occurred during this cycle, but the largest first-story shear occurred during the previous cycle. These plots indicate that nonlinear deformation occurred in both the first and second story, but much greater deformations occurred in the first story.

Figure 8-55. Story shear versus story drift for both stories for the 100% SE32 test.

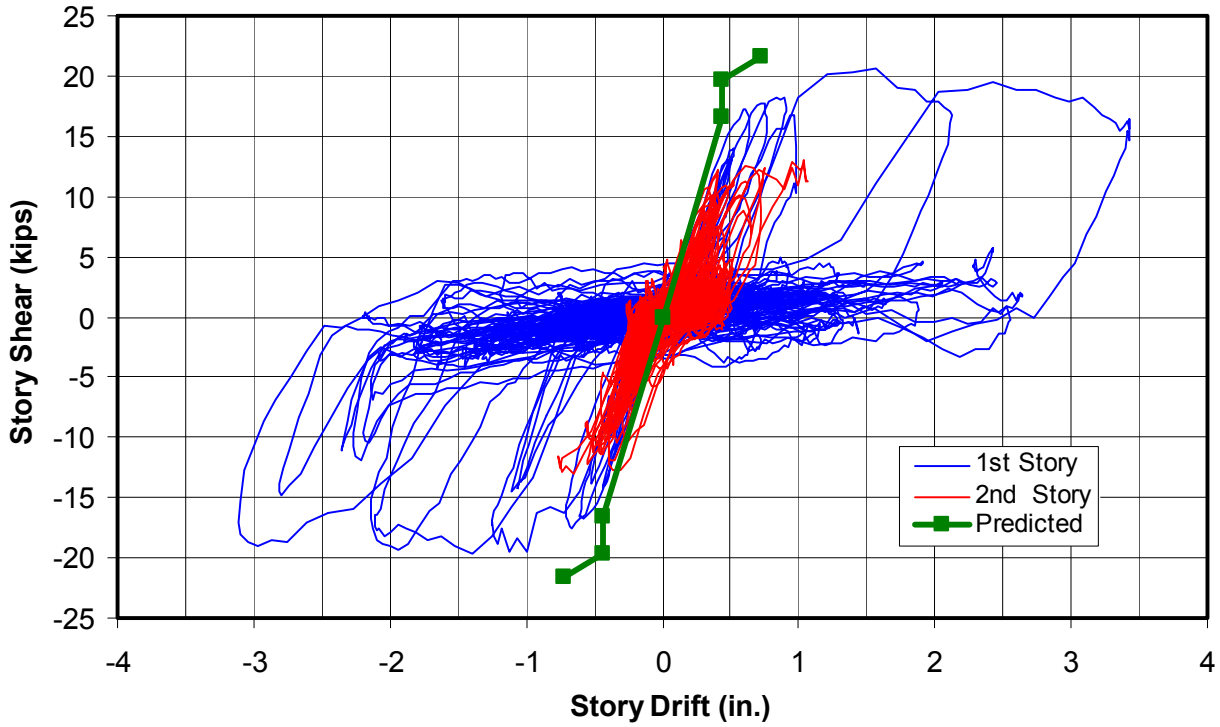

Figure 8-56. Story shear versus story drift
for 100% SE32 test, 15.52–16.248 seconds.

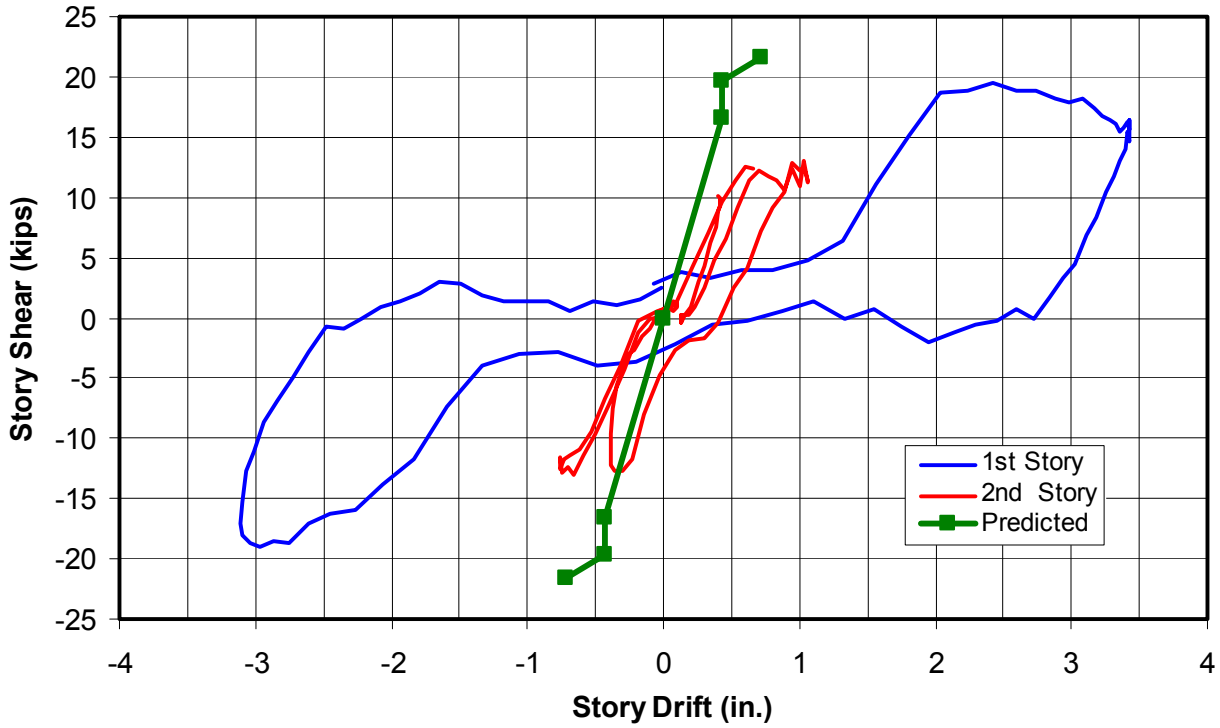

Both Figure 8-55 and Figure 8-56 plot the predicted lateral load versus deformation along with the measured data. The first-story panels reached the estimated lateral capacity of the panels from the diagonal straps alone at strap yielding at about 0.5 in. lateral deformation. Then at 1 in. drift in both directions, the panel applied story shear increased measurably, and this increase is attributed primarily to the contribution of the columns acting as moment frames. Further observation on the contribution of the columns can be made based on an examination of the column strain gage data in the following section. The plots of story shear versus story drift in Figure 8-55 and Figure 8-56 are very similar to the lateral load versus lateral deflection presented in Chapter 7. The relatively wide hysteretic plot of the single cycle shown in Figure 8-56 reveals substantial contribution of the columns acting as a moment frame.

8.9.3 Measured strains

Figure 8-57 plots strains measured at selected first-story diagonal strap gages and from one second-story diagonal strap gage. This figure shows that the first-story straps yielded repeatedly at increasing amplitudes between 10 and 16 seconds in the 100% SE32 test. Soon after 16 seconds, the

strains reached final elongation levels with only relatively small elastic variations for the remainder of the test. These data show that the diagonal straps did not yield or elongate further after 16.1 seconds. Figure 8-58 shows strains measured on diagonal straps that were oriented from the bottom-north panel corner to the top-south corner (NS orientation) on the first-story shear panels. Each of these sensors measured the greatest strain up to that time from among all the gages installed on the first-story panels in the NS direction. These strains are plotted between 10 and 16.5 seconds, when all the strap yielding and elongation took place. Figure 8-16 shows that the S2xz, S10xz, and S12xz first-story gages would all experience tensile elongation when the model was racked to the right (south). Figure 8-58 also plots the average strain of all NS-oriented strain gages on the first story (NSAvg). Similarly, Figure 8-59 plots strains measured at all the critical strain gages on straps oriented in the bottom-south to top-north (SN) orientation), along with the average of all gages in this direction (SNAvg).

Figure 8-57. Strains measured at several first-story and one second-story diagonal strap.

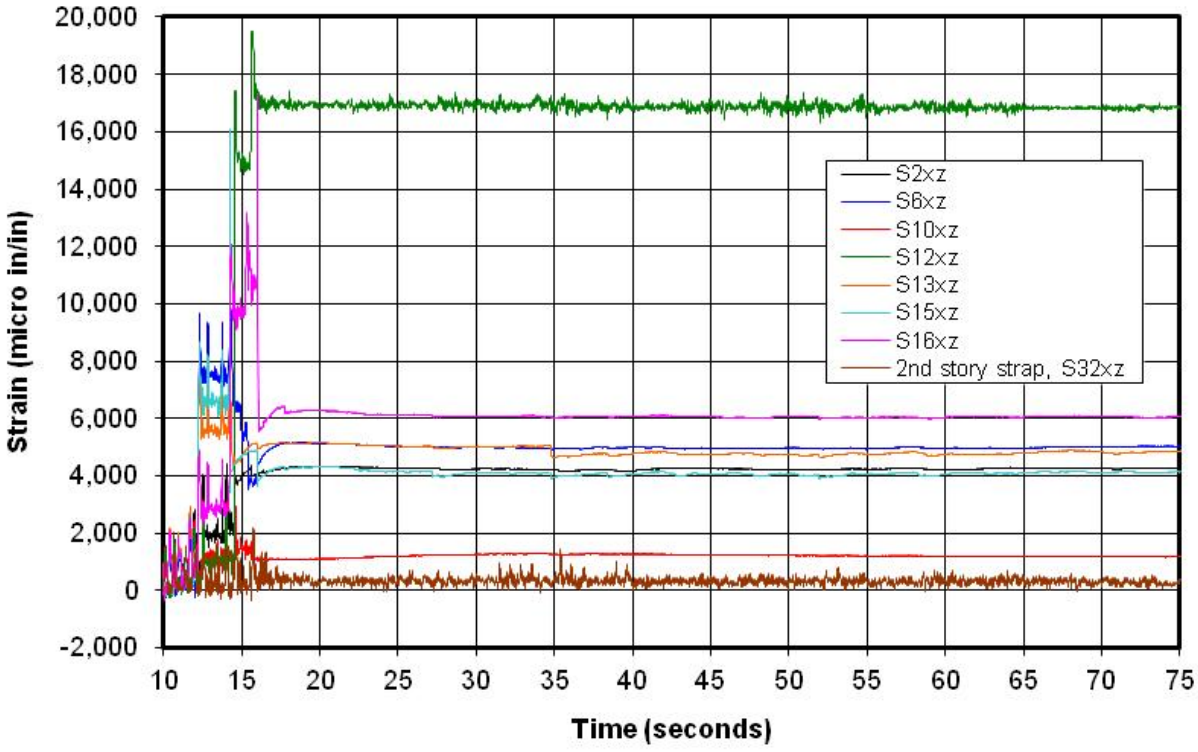

Figure 8-58. Strain measured at selected bottom-north to top-south first-story straps, 10– 16.5 seconds.

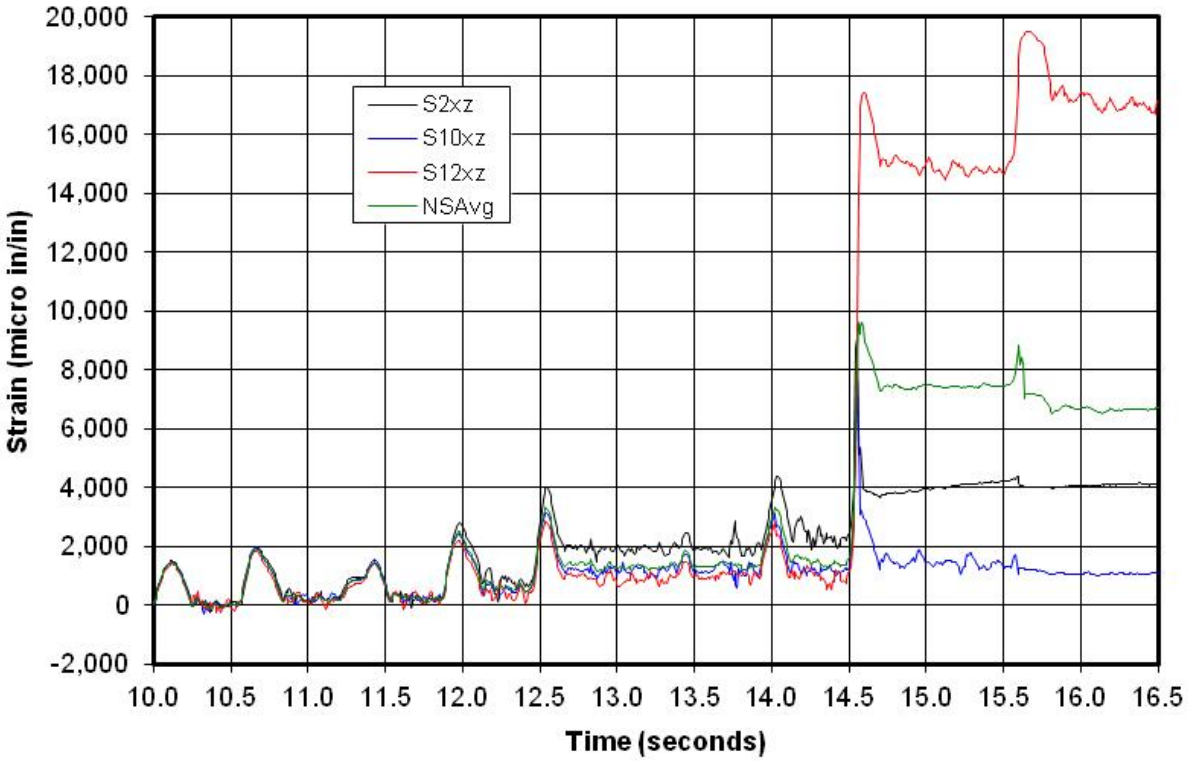

Figure 8-59. Strain measured at selected bottom-south to top-north first-story straps, 10–16.5 seconds.

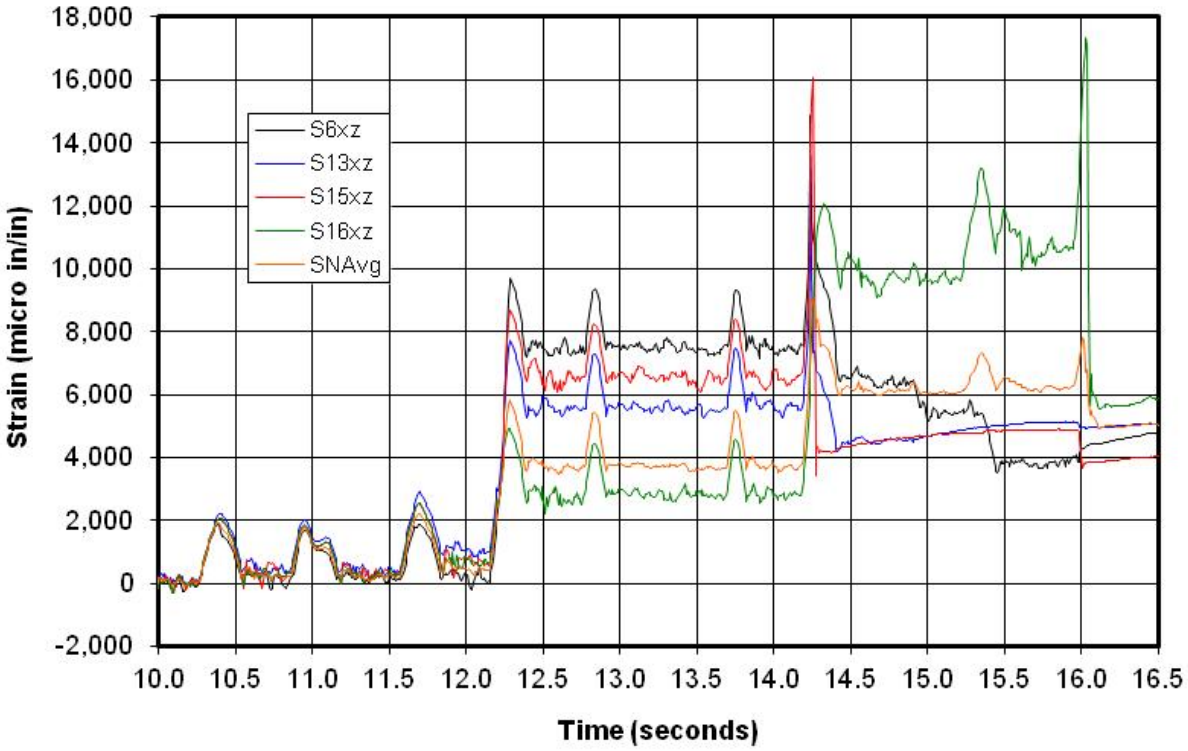

The strap coupon data plotted in Figure 8-22 show the straps begin to yield at 1,700 microinches/in., fully yield at 2,900 microinches/in. (see Table 8-6) and strain harden at 15,000 microinches/in. (0.015 in./in. in Figure 8-22). The strain plots for the first-floor straps in Figure 8-57 show these straps have yielded across their entire lengths, and many may have begun to strain harden having reached peak strains over 15,000 microinches/in. The straps would be expected to yield across their entire lengths before they begin to strain harden. This observation is consistent with the amount of elongation seen in the straps during and after the test. Comparison with the coupon data suggests the straps reached peak stresses up to 57.4 ksi, but not close to fracturing.

Comparison of the diagonal strap strain data shown in Figure 8-57 through Figure 8-59 with the strap coupon data in Figure 8-22 reveal that all the model damage related to elongation of the diagonal straps took place between 10.4 and 16.1 seconds. Table 8-18 summarizes each higher level of strain measured in the first-story straps, plus the average of all strains measured in the same direction during the same model deformation cycle. For example, the first evidence of diagonal strap yielding was seen at 10.4 seconds, with a peak measured strain at S13xz of 2,210 microinches/in. (see Figure 8-59). At this time the average of all strain gages in the SN direction was 1,930 microinches/in., and the first-story model lateral deformation, δ_s, at that time was calculated according to the following modification of Equation 5-2:

$$\delta_s = -SNAvg\left(\frac{H^2+W^2}{W}\right) \qquad \text{(Eq 8-10)}$$

The sign before Equation 8-10 is positive for the NS direction and negative for SN. Table 8-18 also provides an estimate of the strap stress for the average of all strain gage readings, based on the stress versus strain coupon data plotted in Figure 8-22. This stress can be used to estimate the panel capacity based on Equation 5.1. Table 8-18 provides average offset amplitudes for all strain gages in a given direction. In the SN direction the offset average was 200 microinches/in. This offset is a measure of the permanent elongation of the strap until further yielding takes place in a later cycle.

Table 8-18. Summary of Shake Table Model Diagonal Strap Yielding.

Strain Gauge Name	Time of Peak Strain (sec)	Peak Amplitude (mico in/in)	NSAvg (mico in/in)	SNAvg (mico in/in)	Lateral Defl, δ_s (in.)	1st Story Drift (in.)	Strap Stress, F_s (ksi)	Offset Amplitude (mico in/in)
S13xz	10.4	2210		1930	-0.46	-0.61	47.3	200
S10xz	10.7	2010	1930		0.46	0.64	47.3	200
S13xz	11.7	2910		2210	-0.52	-0.71	50.3	400
S2xz	12.0	2810	2510		0.59	0.77	51.9	600
S6xz	12.3	9690		5810	-1.37	-1.26	54.0	3700
S2xz	12.5	4020	3330		0.79	0.91	53.4	1300
S2xz	14.0	4400	3350		0.79	0.99	53.5	1400
S15xz	14.3	16110		9060	-2.14	-2.11	54.5	6000
S12xz	14.6	17440	9640		2.28	2.12	54.5	7400
S12xz	15.6	19520	8880		2.10	3.43	54.5	6600
S16xz	16.0	17320		7800	-1.84	-3.11	54.0	5100

The first-story lateral deformation, δ_s, can be compared with the measured story drifts shown in Figure 8-51. Values of measured story drift from Figure 8-51 are included in Table 8-18 for comparison. The values of measured story drift are consistent with but slightly greater than the values calculated based on the strain gage data. The overall story drifts are generally greater than the lateral deformation due to strap elongation alone, because the joints near the ends of the columns and anchors deform small amounts relative to the large values in the straps.

Figure 8-60 plots the strain data from the second-story shear panel diagonal straps, where the greatest strains were measured in the NS (S32xz) and SN orientation (S33xz). Also shown is the average of all the strain gages in both orientations of the diagonal straps (see locations of all gages in Figure 8-16). This plot shows that these straps clearly yielded at least in the NS direction (positive story shear), because the strains exceed 1,700 microinches/in., but some of the straps may have just begun to yield. The second-story drift plotted in Figure 8-51 is fairly large, reaching 1.06 in. at 15.76 seconds, but the amplitude is much less in the negative direction, reaching only -0.76 in. at 16.13 seconds. These values agree with both the time and amplitude of strains plotted in Figure 8-60. This information on diagonal strap strain gage measurements defines the nonlinear behavior of the shake table model.

Figure 8-60. Strain measured at greatest and average NS and SN second-story straps, 15.6–16.2 seconds.

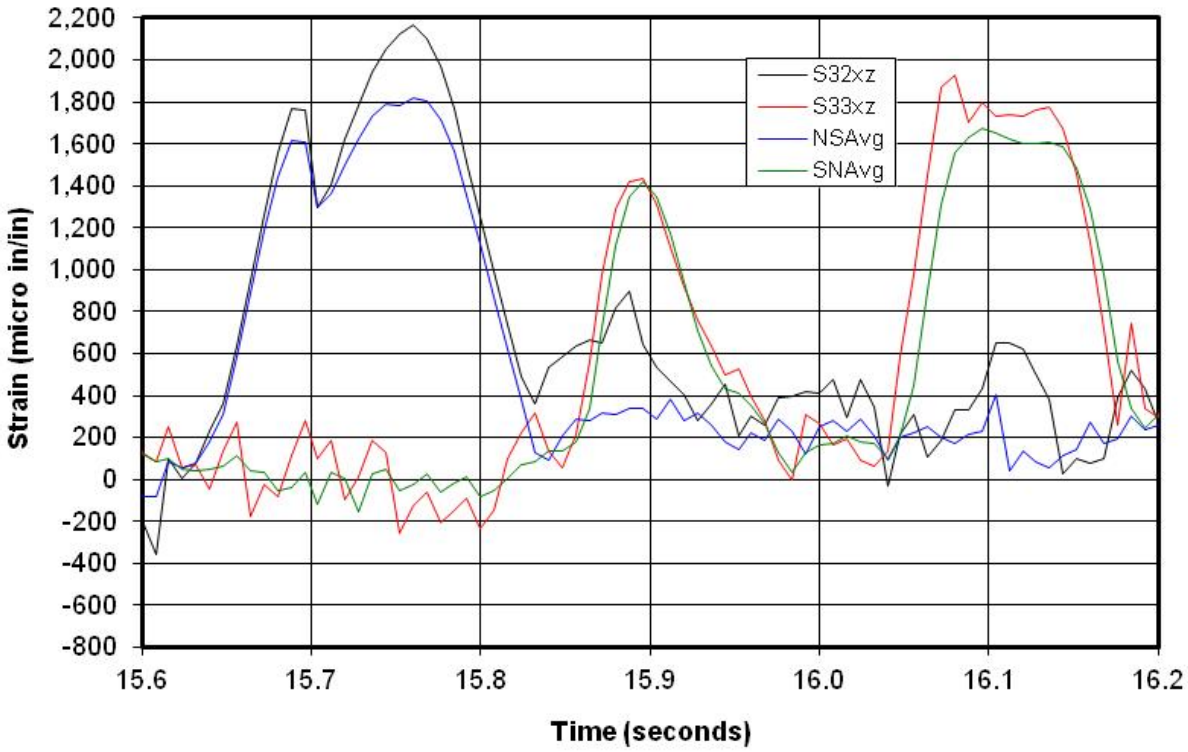

Figure 8-61 plots strains measured on the northwest column, which like for the 8% SE32 tests have been reduced by 256 microinches/in. to account for the effects of gravity. This plot shows the effects of gravity were overcome, and small tensile strains were measured at the locations of the strain gages. Scaling these strains to the location of the anchors suggests the columns would have yielded in compression. For example, the strain measured at S23z at 15.72 seconds (plotted in Figure 8-63) scales to -1,837 microinches/in. at the bottom of the top anchor leg of the southwest column. Since the column coupon data in Figure 8-22 show that it begins to yield at 1,300 microinches/in., these columns likely yielded in compression near their anchors. The greatest tensile strain of 489 microinches/in. was measured at S22z at 36.48 seconds, and this equates to 1,078 microinches/in. when scaled to the top of the bottom anchor leg, suggesting that the columns never yielded in tension. Post-test visual observations indicate that the columns did permanently buckle locally, agreeing with minor compression yielding. Figure 8-62 plots the same corrected strain data for the 12–18 second region of these records.

Both Figure 8-61 and Figure 8-62 show that the strains measured at S17z have a permanent positive increase of 200 microinches/in. beginning at either 15.6 or 16.4 seconds. This indicates that the columns may have yielded in tension at the S17z strain gage location, even though the positive tensile strains are well below the amplitude that should cause yielding. Figure 8-62 shows the same pattern of strain oscillations as explained in the linear 8% SE32 test results. Figure 8-63 plots similar strain measurements for the southwest column for the 12–18 second region, showing slightly greater measurements than on the northwest column. This figure shows a positive tensile offset at S22z of 300 microinches/in. and a negative compressive offset at S21z of 200 microinches/in. at 16 seconds, suggesting column yielding in both tension and compression at this time.

Figure 8-61. Strain measurements
on the first-story northwest column, 100% SE32 test.

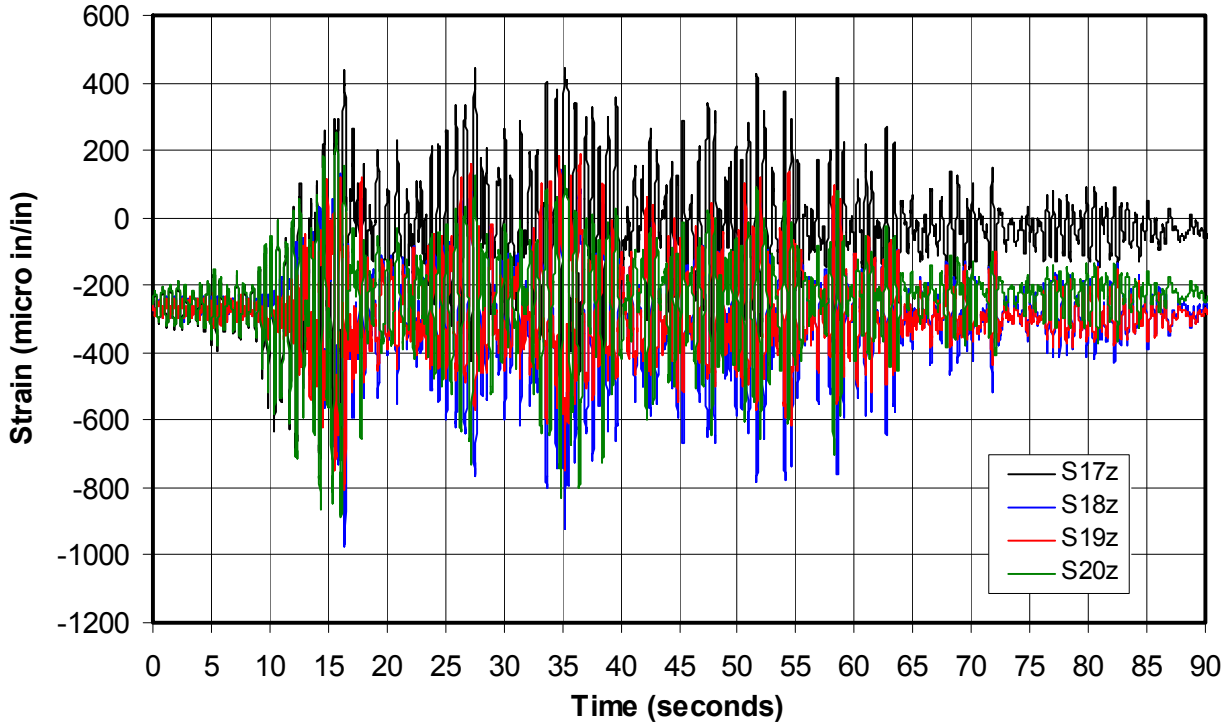

Figure 8-62. Strains on the first-story northwest column, 12–18 seconds.

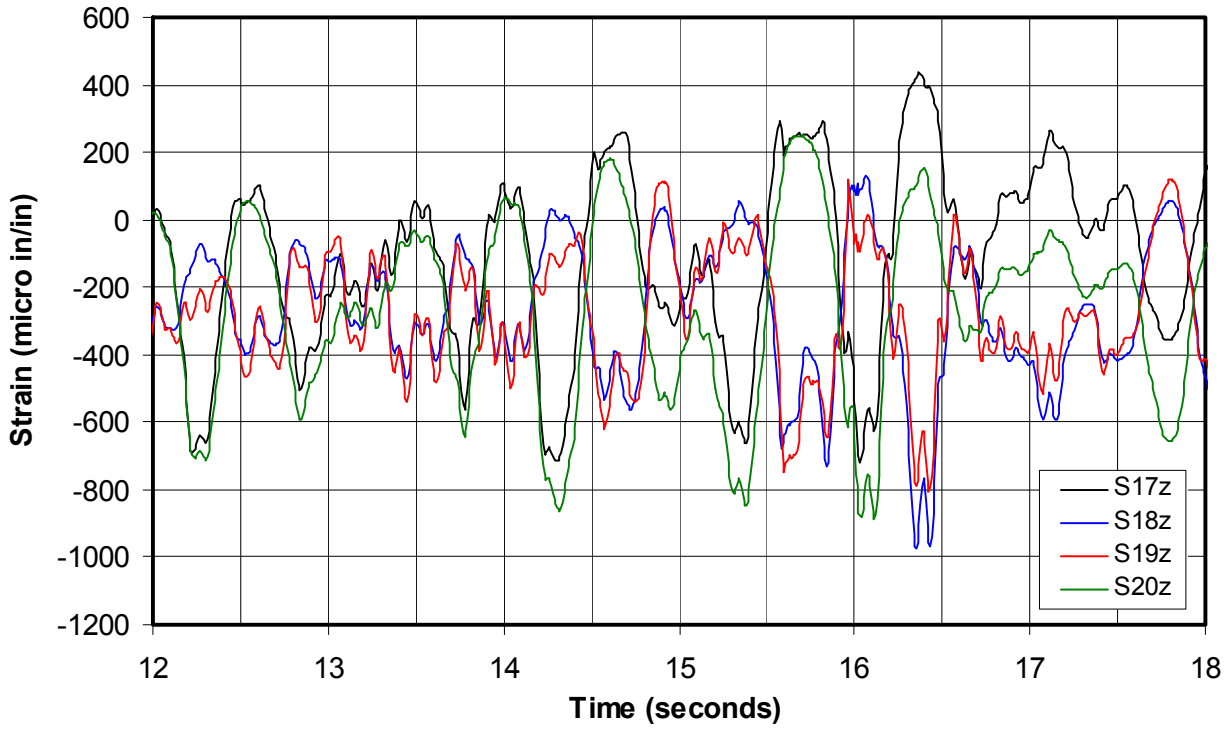

Figure 8-63. Strains on the first-story southwest column, 12–18 seconds.

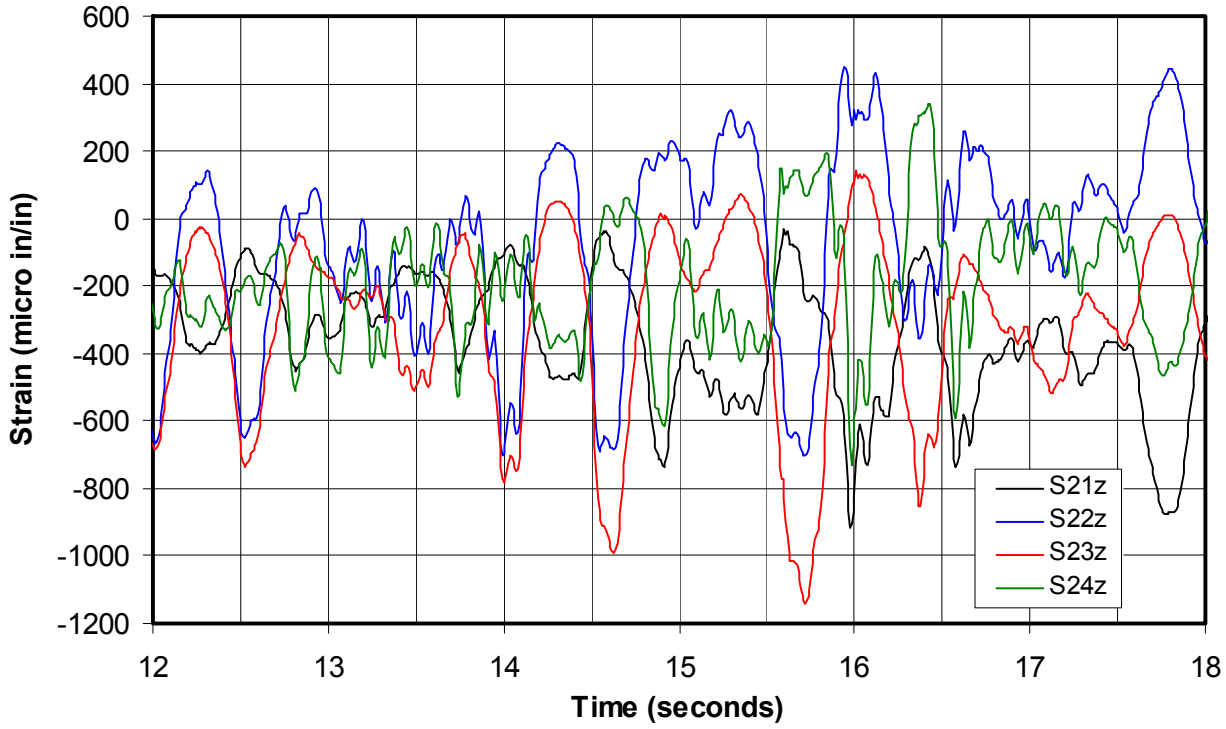

8.9.4 Column axial load, moments and shears

The column strains are again used to estimate the column axial load, load carried in shear by the columns, and column moments at their tops and bottoms. Only the columns at the west first-story shear panel were instrumented, and Equation 8-6 defines how the strain measurements were used to calculate the axial load in the northwest column, P_{aNW}. The axial load applied to the southwest column, P_{aSW}, was calculated in a similar way using the strain measurements from it. Figure 8-64 plots the applied axial load for both the north and south columns of the first-story west shear panel. The previous section describes permanent strain offsets (yielding) of 200–300 microinches/in., measured at strain gages S17z, S21z, and S22z at 16 seconds. The load calculated based on these strains should not include the effects of these offsets. The axial loads plotted in Figure 8-64 do not correct for the strain offsets, so that axial loads plotted after 16 seconds include a small error. However, the diagonal strap strain gage data showed most of the nonlinear response of the model had already taken place by 16 seconds, indicating that accurate loads after this point were less important.

Figure 8-64. Axial load for first-story west panel columns 100% SE32, 11–18 seconds.

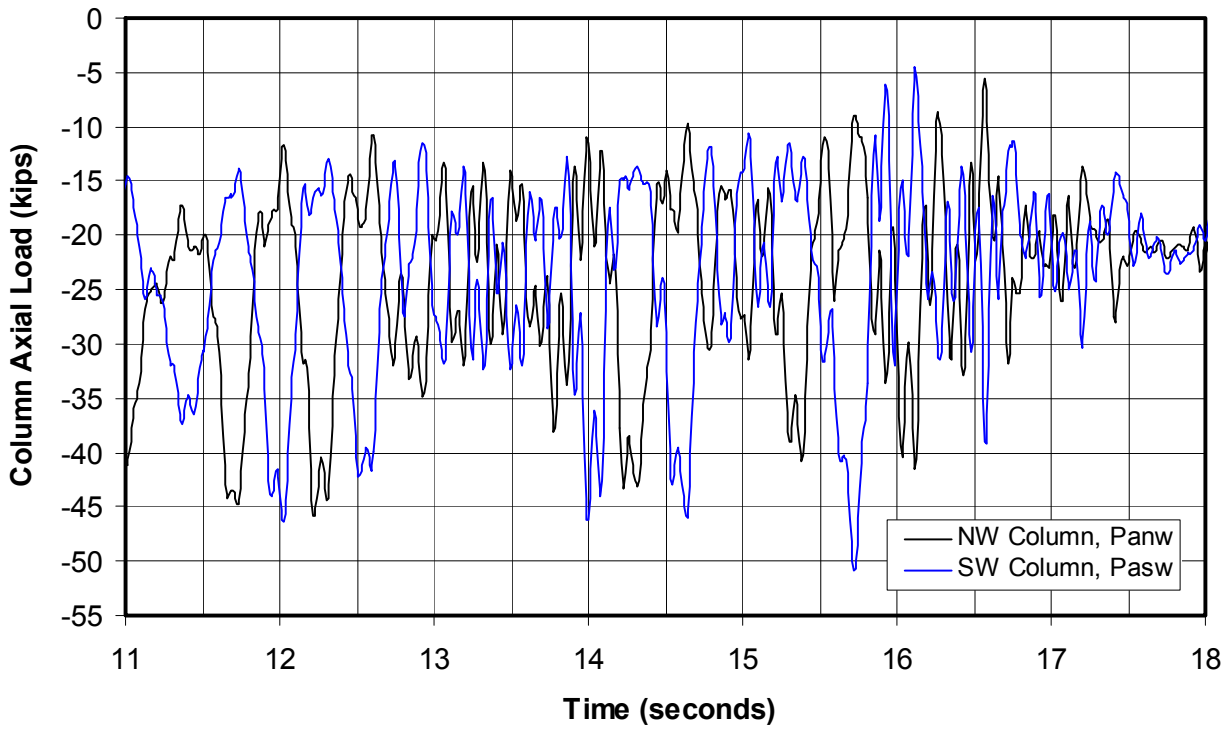

Figure 8-64 shows that the column axial loads oscillate about the 26 kip static gravity load per column. This figure shows that the overall column cross-section remains in compression throughout the test, reaching the smallest compression force of 4.4 kips at 16.1 seconds in the southwest column. Figure 8-64 also shows that the maximum compressive force in the columns is almost twice the static load, reaching a peak value of 50.8 kips at 15.7 seconds in the southwest column. Incidentally, this peak axial load in the southwest column is exactly the same as the spreadsheet-calculated column axial load at strap ultimate, P_{vumax}, shown in Table 8-8. After 16 seconds this plot erroneously shows the axial force oscillating about 21 kips (it should still be 26 kips) due to the permanent offset in the column strain measurements.

Figure 8-65 plots the moments applied to the top and bottom of both the north and south columns of the first-story west shear panel, calculated according to Equation 8-7. The same sign convention for moments is used as in the section 8.8 so the relative magnitudes can be easily compared.

Figure 8-65. Moment for first-story west shear panel columns, 100% SE32, 10–18 seconds.

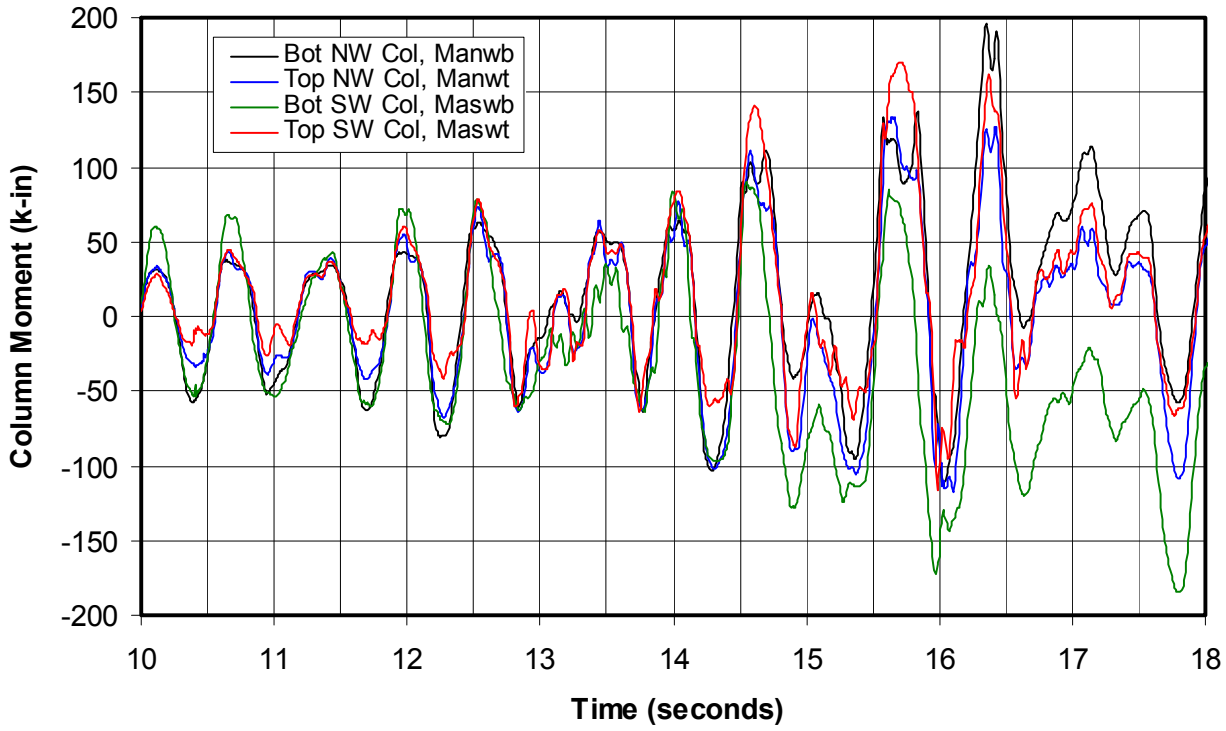

Before 12 seconds, the moments at the bottom of the columns are consistently greater for the southwest column, and also for the northwest column

when the model is deformed to the left (north), resulting in negative moments in Figure 8-65. The applied moments at the bottom of the columns are expected to be larger while the columns are behaving linearly, but after 12 seconds moments at the column tops equal or exceed values at the bottom, indicating that the columns have reached their yield capacities at their bottoms and that no greater moment resistance can be developed. After 16 seconds, the moments are inaccurate at both the bottom northwest column, M_{anwb}, and bottom southwest column, M_{aswb}, where they no longer oscillate about zero. This offset is due to the permanent offset in the column strains

Figure 8-66 plots the applied shear at the north and south columns of the first-story west shear panel. After 16 seconds, the shears at both columns are inaccurate where the northwest column shear, V_{anw}, is offset positively and the southwest column shear, V_{asw}, is offset negatively. The greatest shear prior to these offsets was at 15.7 seconds, where the northwest column reached 2.13 kips and the southwest column reached 2.08 kips.

Figure 8-66. Shear for first-story west shear panel columns, 100% SE32, 12–18 seconds.

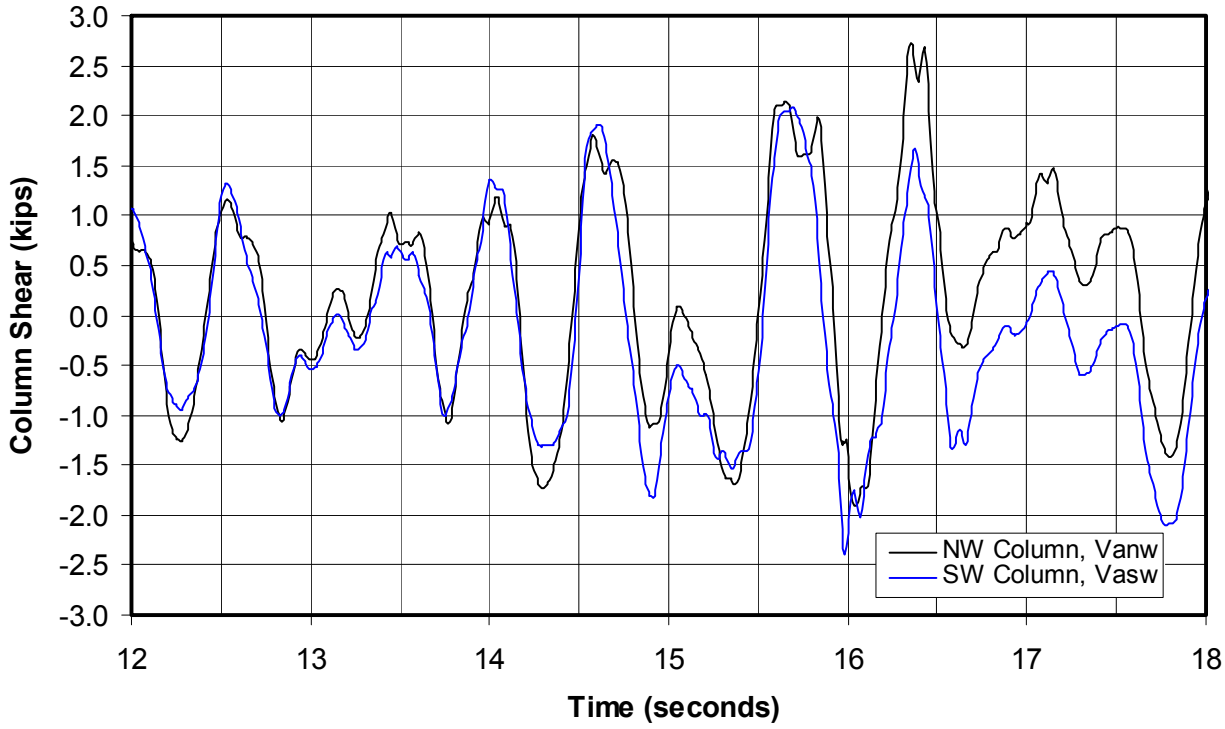

Figure 8-55 and Figure 8-56 plotted the story shear per shear panel, calculated based on the inertia forces defined by the model acceleration and

weight. This story shear at the first story carried by the columns is the total for the northwest and southwest columns, shown in Figure 8-66; and the portion carried by the diagonal straps is the amount in Figure 8-55 and Figure 8-56 minus the total carried by the two columns. For the cycle between 15.52 and 16.248 seconds shown in Figure 8-56, the total positive column shear was 4.21 kips at 15.7 seconds (Figure 8-66), which is 22% of the panel story shear of 19.45 kips (Figure 8-56). In the negative direction, the peak negative column shear at the southwest column is 2.40 kips at 15.98 seconds, but the calculated shear based on the columns strains is already offset by 0.5 kips in the negative direction, so a corrected estimate of the shear at this column is 1.9 kips. The peak negative shear at 16.04 seconds for the northwest column is 1.91 kips, giving a total negative shear at both columns of 3.81 kips, which is 20% of the negative panel story shear of 19.07 kips (Figure 8-56). The percentage of shear carried by the columns grew 10 and 9% in the positive and negative directions, respectively, in the linear 8% SE32 test to the values of 22 and 20% in this 100% SE32 test. This is because the contribution of the straps only increased from the linear 8% SE32 test to the point that the straps fully yielded, while the columns remained elastic almost to the full amplitude of the nonlinear 100% SE32 test. The added contribution of the columns after strap yielding can be seen graphically in the story shear (lateral load) versus story drift plot shown previously in Figure 8-55. A bilinear approximation or envelope of the panel capacity shown in that figure suggests the straps had fully yielded at 0.6 seconds.

8.10 Shake table model damage observations following cyclic tests

Following the 100% SE32 nonlinear test the natural frequency of the model was 0.5 Hz, based on random-motion shake table tests. In the low-level random tests only, the model columns at the first floor would have contributed to the stiffness of the model because the diagonal straps were significantly elongated and slack. Therefore, the model stiffness was much lower, explaining the decrease in the first mode of vibration frequency from 1.65 Hz to 0.5 Hz. The model was next tested using sinusoidal motions at the model new natural frequency of 0.5 Hz, in order to cause even greater deformation of the model. However, these tests resulted in relatively minor increased lateral deformation. The model behaved as a 0.5 Hz SDOF oscillator with a 115.1 kip mass at the top of the first-story columns. The model acceleration needed to produce lateral deformation large enough to further elongate the diagonal straps can be approximated by determining the acceleration of the oscillator that is large enough to produce

absolute first-floor displacements equal to the greatest measured displacements in 100% SE32 test. This approximation is fairly crude because it assumes that the dynamics of the model and the ratio of the greatest first-story drift over the absolute displacements in the 100% SE32 test are proportional to the same ratio in the 0.5 Hz sinusoidal tests. The expression below can be used to calculate this approximate acceleration, a_{SDOF}:

$$a_{SDOF} = \frac{d_{1stFloor}(2\pi f_{SDOF})^2}{386 in/sec^2/g} \quad \text{(Eq 8-11)}$$

where

$d_{1stFloor}$ = the peak absolute displacement from the 100% SE32 test. Close inspection of Figure 8-48 and Figure 8-49 show this is 2.26 in. at 15.656 seconds.

f_{SDOF} = 0.5 Hz as measured in the random shake table test described above.

At this low frequency of 0.5 Hz, Equation 8-11 shows that the model acceleration that would lead to the diagonal straps becoming taut again is only 0.058 g, which is much less than the higher frequency and much higher accelerations (see Figure 8-47) that produced the inertia forces (see Figure 8-55). The 115 kip model responding as a SDOF oscillator at 0.058 g would apply lateral forces of only 3.33 kips per shear panel. These forces are much less than the lateral forces required to further elongate the diagonal straps. These forces are actually even less than the restoring forces from the columns approximated from the column strain gages (i.e., 4.2 kips in the positive direction or 3.8 kips in the negative direction). When testing with sinusoidal motions at 0.5 Hz, there would be a sudden impact loading increase in force in the diagonal straps when their slack is overcome, but this force would almost certainly not be enough to exceed the full lateral capacity that still is available in the straps and columns. At the very small accelerations of only 0.058 g, the velocities would also be small. As the amplitude of the sinusoidal base motions at 0.5 Hz were increased, the straps "caught" the oscillating mass, so that sinusoidal motions at 0.5 Hz never did amplify significantly in the model. If higher-frequency sinusoidal or other shake table motions were used to excite the model, the low-frequency lightly damped 0.5 Hz model would isolate the model from these motions. Therefore, the only way to deform the model further with shake table base motions appeared to be use of higher-frequency motions whose displacement amplitudes exceeded the existing first-story de-

formation of the model. Because of the stroke limitations of the TESS in the in-plane direction (2.75 in. or 5.5 in. peak to peak), this could only have been done using very artificial motions of the shake table. In a single half-cycle test, the TESS could have been offset completely in one in-plane direction and then quickly displaced close to the full 5.5 in., thereby exceeding the first-story drift equivalent to the slack diagonal straps. In such a test the TESS and model base beam would have moved quickly, and the SDOF model would have been isolated from these motions, slowly tailing behind until the straps tightened. This would have caused larger deformation of the model in the one direction tested, with first-story deformations perhaps as great as 5 in. This process could have been repeated in the other direction, but the test would provide little value for comparing the DRAIN 2DX analysis with the nonlinear response of the model. Therefore, the 100% SE32 test was judged to have produced the best experimental results to compare its measured large deformation with the DRAIN 2DX analysis. The test was also very useful to evaluate the ductile performance of the model under large nonlinear deformations.

Several observations of the performance of the model can be made from pictures taken after the 0.5 Hz sinusoidal tests were completed. These sinusoidal tests did cause minor additional damage to the column (local buckling) and column anchors. Figure 8-53 and Figure 8-54 provided the best overall view of the deformed model at the greatest lateral deformation. These figures show significant elongation in the diagonal straps that are taut in one direction and slack in the other. The columns and anchors did experience somewhat greater damage at the south column of the west shear panel and the south column of the east panel. Figure 8-67 shows the bottom of the southeast column facing west toward the interior of the model. Local elastic buckling can be seen near the column knockout near the top of this photograph. When the model was deformed laterally to the south (left in Figure 8-67) the diagonal strap connected to the top of this column would be loaded in tension, applying compressive forces to this column. At this same time the column would be deformed in bending so that the compression side of the column is the face shown with the knock-out in Figure 8-67. Deformation to the south is the same direction as positive drift in Figure 8-51 and Figure 8-52. Figure 8-51 and Figure 8-52 show the model reaches a peak positive first-story drift in the 100% SE32 test at 15.728 seconds.

Figure 8-67. Bottom of southeast column facing west, showing local column buckling and anchor and column bending at top of the anchor.

The columns of the east shear panel were not instrumented, but Figure 8-16 shows the that S22z strain gage was on the south face of the south-west column, and this column would have been similarly loaded at the same point in time as the southeast column. The top of the knockout shown Figure 8-67 is 12 in. above the bottom of the column, so the S22z strain gage was centered 16 in. above the top of a similar knock-out in the southwest column. Figure 8-63 shows that the S22z strain gage shows a negative (compressive) peak strain measurement near 15.728 seconds (peak value of -702 microinches/in. at 15.72 seconds). Since the knockouts are closer to the bottom of the columns, the compression strains near

them would be greater than at S22z. They would have been further increased due to the stress concentration around these knockouts.

Local column bending can also be seen in Figure 8-67 at the center of the column south face directly above where it is welded to the horizontal top edge of the anchor angle. Close inspection of Figure 8-67 shows that the top of the angle is bent to the north at both the east and west faces of the column. This minor local inelastic deformation of both the column and the anchor is part of the intended behavior of the anchor-to-column connection configuration under load when the connected diagonal strap is in tension. Even if the diagonal strap material has a yield strength equal to its maximum value, F_{symax}, the column-to-angle connection must resist the load applied without fracture. Still, the local yielding and deformation shown in Figure 8-67 is good because it would dissipate energy in large seismic events. The load path facilitated through the strap-to-column and column-to-anchor connection configurations is intended to permit large nonlinear deformation without risk of brittle failure.

A shear panel can be designed with diagonal straps on either one or both faces. When the panel racks laterally in an earthquake, the diagonal straps in tension load the face of the column to which they are connected in shear. Like the welded connection shown in Figure 8-67, these connections should be centered below the top of the anchors so that a direct load path exists between the application of shear load to the column face and the resistance provided by the anchor. The column face then only needs to resist these shear forces locally in tension. It is critical that much of the strap is connected to the outside stud of the column (left stud in Figure 8-67) because this stud is welded to the anchor. It is also important that the column intermittent welds at the ends of the columns are placed at the column ends, behind the track, so that loads applied to the other studs at the strap welds will be carried directly between the studs in tension into the exterior stud that is in turn welded to the anchor, or in compression through the studs and groove welds that connect them.

The load path between the strap-to-column connection, along the column face where the corner of the column is welded with a vertical groove weld to the edge of the anchor edge, is all very rigid and will behave elastically in seismic motions. Some of the lateral load in the column coming from the strap connected to the interior column studs will carry this load in tension through the weld to the anchor into the horizontal portion of the an-

gle at the bottom of this connection, which is in turn carried directly into the concrete foundation or diaphragm in friction or is carried to the anchor bolts through this bottom portion of the angle in tension. A portion of this load is also carried in compression into the interior anchor at the interior side of the column. These portions of the load path are also fairly rigid, especially in tension to the exterior anchor, but much of the load will be carried into the anchor above these horizontal portions of the angle. Most of the remaining lateral load will be carried to the foundation or diaphragm through the vertical welds between the exterior anchor angle and the exterior stud, or to the horizontal weld along the top edge of the angle. These vertical welds are 3.5 in. tall in Figure 8-67 and the horizontal weld is 6 in. long (i.e., depth of the panel). The load path or stress flow between the column and the anchor is dependent on the relative stiffness of the column face welded to the anchor and the vertical leg of the anchor. The vertical leg of the anchor is stiffened with a triangular in-plane vertical stiffener plate, which is positioned at the center of the anchor in the out-of-plane direction as shown in Figure 8-67. This stiffener plate is very rigid in carrying lateral load in tension and also uplift forces down into the anchor bolts. The ductility in this joint is introduced by the flexural deformation of the vertical leg of the angle and the face of the column to which it is welded. The tensile force from the straps pulls through the column corners and applies bending load to the vertical edges of the angles. This causes them to deform in bending and even yield if the full maximum strength exists in the straps. However, the anchor welds, stiffening plate, and anchor bolts are designed to support significant yielding in this vertical leg of the anchor without loss of capacity. These anchors will only deform in the direction that the tension-only straps pull. The vertical legs of the anchors on the interior side of the columns could possibly also be loaded to the point of yielding, through the columns in horizontal compression, but only after significant deformation of the more rigid tensile load path to the exterior anchors.

The anchor bolts are placed very close to this stiffener plate to provide a relatively direct and rigid load path between the stiffener plate and anchor bolts. A small amount of flexural deformation could take place in the horizontal leg of the anchor near the anchor bolts, due to prying action, but even this deformation would be ductile if it were to exceed the yield capacity of the anchor.

Figure 8-68 shows the bottom of the southwest column facing northeast, and Figure 8-69 zooms in on the same column anchor connection at the top of the anchor angle. The diagonal strap-to-column weld connections were undamaged at all these connections even though the weld lengths were the minimum needed to develop the capacity of the straps. The discussion prior to Table 8-11 explained that the maximum strap force, P_{su}, was actually slightly greater than the welded connection capacity in order to test the ability of these welds to perform at their design limit, thereby verifying the welded connection design recommendations. The bottom-right corner of Figure 8-67 shows this connection at the bottom of the southeast column, and left side of Figure 8-68 shows it at the bottom of the southwest column.

The discussion prior to Table 8-13 explained that the height of the angles, H_A, was only 3.5 in. so that the total angle weld strength, P_A, would barely exceed the maximum applied tensile force per anchor angle ($P_{vymax}/2 + P_M$) at the first-floor anchors. Therefore, this 100% SE32 test verified the weld design recommendations for these anchor connections.

Figure 8-68. Bottom of southwest column facing northeast, showing local column buckling and anchor and column bending at top of the anchor.

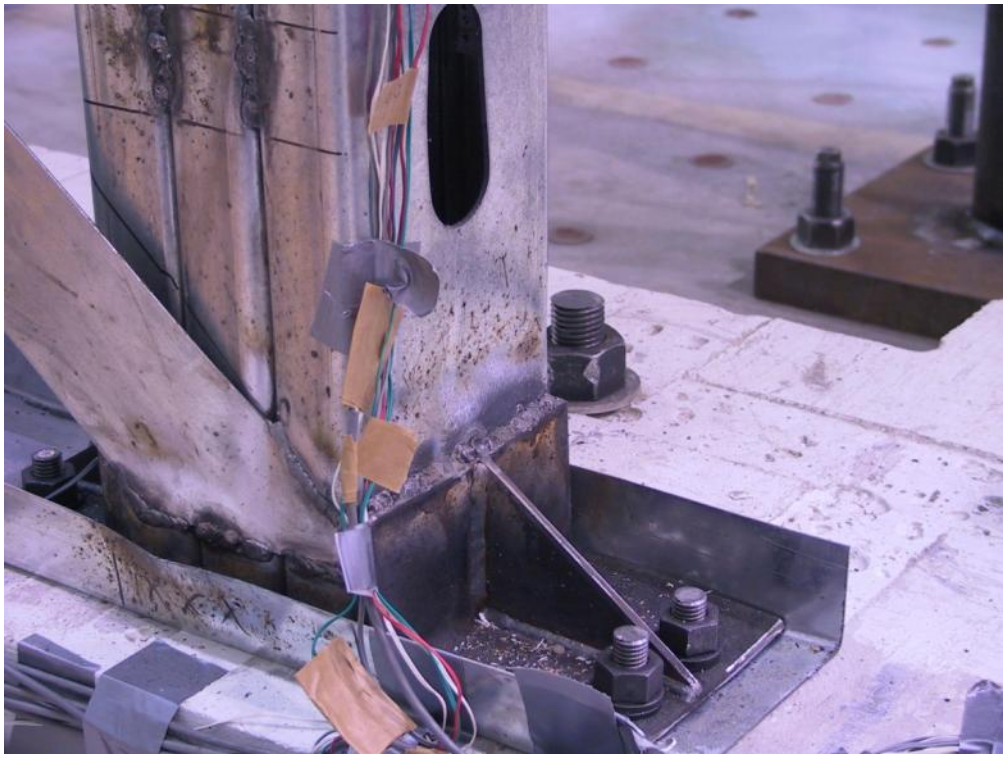

Figure 8-69. Zoomed in view of the vertical anchor leg
and stiffener plate at the bottom of the southwest column, facing northeast.

Figure 8-68 and Figure 8-69 show that bending of the vertical leg of the anchor and column where it is welded to the top of the anchor is greater here than it was at the southeast column. When the attached strap is in tension, it pulls the top corners of the vertical leg of the angle so that it deforms in bending, while the center of the anchor and attached column is held back by the stiffener plate. Then when the model racks back in the other direction, the column is loaded with large compressive forces, and it buckles locally near the stiffener plate because the relatively thin column steel has already been deformed out in the direction of the stiffener plate. However, there is no risk of buckling the entire column because of the bracing that comes from the column shape and the support of the vertical leg of the angle.

The 100% SE32 shake table test of a two-story model provided significant nonlinear response that could be compared with the ability to analytically predict both the deformation-based demand and capacity using the DRAIN 2DX analysis for cold-formed steel construction. This test also provided data to validate the cold-formed steel seismic design provisions that are presented in Part II of this report. The cyclic tests presented in an earlier chapter together with the shake table test presented in this chapter demonstrate that cold-formed steel shear panels can be designed to re-

spond in a ductile way, effectively resisting the lateral loads applied to them at very large lateral drifts. This provides the justification needed for use of the recommended response modification coefficient, R, of 4. Because of the significant contribution of the column moment frames, the R coefficient could arguably be increased to 5, but a coefficient of 4 is still conservatively recommended.

9 Special Design Considerations for Seismic Loads

The philosophy underlying building design for seismic loads may be unknown to or misunderstood by some structural engineers, even those practicing in regions of significant seismic activity. Familiarity with special design considerations for seismic loads can help to clarify certain code specifications and identify potential design errors that may, on the surface, appear to comply with the code.

Wind loads are well understood by structural engineers. Statistics on wind velocities are recorded regularly and have been for nearly 100 years. Once the design return period for wind is decided by code officials — usually 300-, 700-, or 100-year wind velocities (ICC 2011, Figures 1609A through 1609C) — the horizontal and vertical wind pressures can be calculated for design from simple equations that appear in the building code. The structural engineer includes these forces with dead, live, and other loads, and designs the building to remain elastic under the factored load combinations. The design resistance is reduced by a resistance factor, ϕ, to account for uncertainties in material properties. The load and resistance factors take the place of factors of safety used in earlier codes.

Incorporating seismic resistance specifications within this design framework is difficult for two reasons: (1) the effective seismic loads on the building that would arise due to the "design earthquake" are much greater than all of the other referenced loads and (2) they occur less frequently than the design wind load. If buildings were designed to remain elastic under the design earthquakes, the design forces would be as much as eight times greater than those currently used. This would place a large economic burden on society for the purpose of addressing seismic forces that have only a very small probability of occurring during a building's life cycle.

The current design codes are based on a maximum considered earthquake (MCE) earthquake with a return period of 2,475 years. Such an earthquake has a 2% probability of exceedance in 50 years. These forces can be compared to wind loads that have a 700-year return period.

Earthquake ground motions are both horizontal and vertical, causing building deformation and inertial loading in both directions. All of the building's mass contributes to the seismic inertial forces that occur. The dynamic response of the building amplifies ground motion, producing greater inertia forces than might be calculated by simply multiplying the ground acceleration by the building mass.

The design base shear used for building design has a coefficient, R, that appears in the denominator. This is called the *response modification coefficient*. If this coefficient were taken as 1.0, that would represent the force for which the building would have to be designed in order for the building to remain elastic under the design earthquake. In the current seismic design provisions, this coefficient may be as large as 8 for some structural systems. So it is obvious that a great deal of damage will occur in these buildings when a large earthquake occurs.

The value of R that is specified for a building type depends on

- the redundancy of the vertical load-carrying system
- the redundancy of the horizontal load-carrying system
- the expected overstrength of the building
- the ductility capacity of the building type
- the building occupancy type
- acceptable risk.

Shown in Figure 9-1 are idealized models of building frames, the first using cold-formed steel members with diagonal straps for cross-bracing. The diagonal straps resist lateral forces. The member joints themselves behave as pinned connections. The gravity frames also behave as if all of the connections are pinned. Therefore, the diagonal straps must provide all of the stability against collapse under gravity loads and also resist horizontal forces arising from wind or earthquakes. As a result, if the diagonal straps fracture or lose their lateral load-carrying capability, the building may readily collapse. This type of structural system is referred to as a *bearing wall system*.

Figure 9-1. Idealized models of building frames.

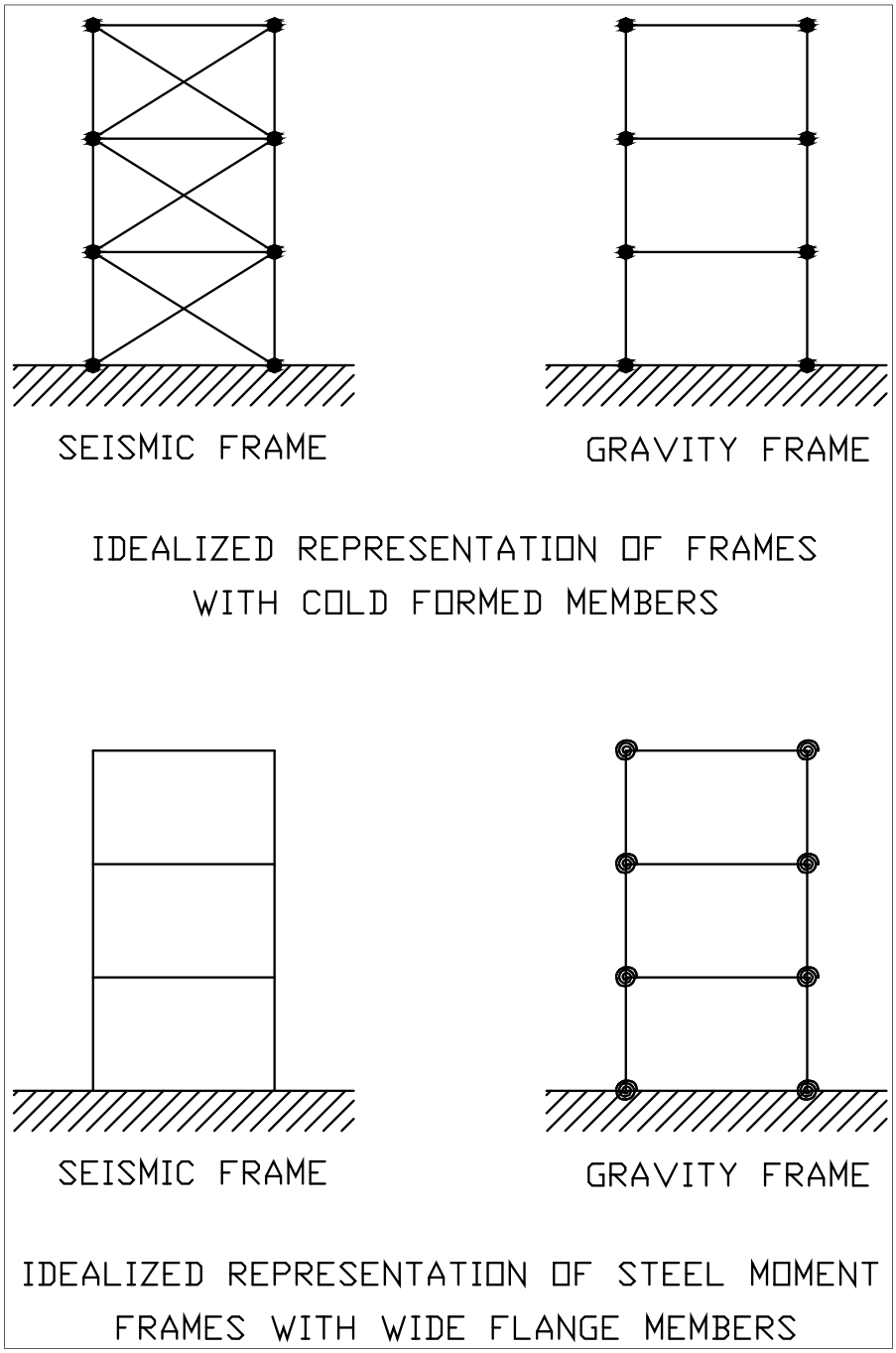

For a moment frame, all of the lateral forces are resisted by frame action, which results in shear and moment developing in the beams and columns under wind or earthquake loads. Usually only two or three frames in each direction are designed as moment frames. The rest are gravity frames. The schematic of a typical gravity frame is shown in the bottom drawings of Figure 9-1. Although the beam-to-column connections are assumed to be

pinned, they can actually develop significant moments. The mechanism for this is shown in Figure 9-2. The web shear connections, acting alone or in composite behavior with the floor slab, are able to develop significant moment resistance. As a result, the building will be able to stand up under gravity loads even if all of the moment connections in the moment frame fail during the earthquake. Thus, there is much redundancy against gravity loads in the moment frame building.

Figure 9-2. Schematic drawing showing unintended moment resistance in gravity frames with wide flange members.

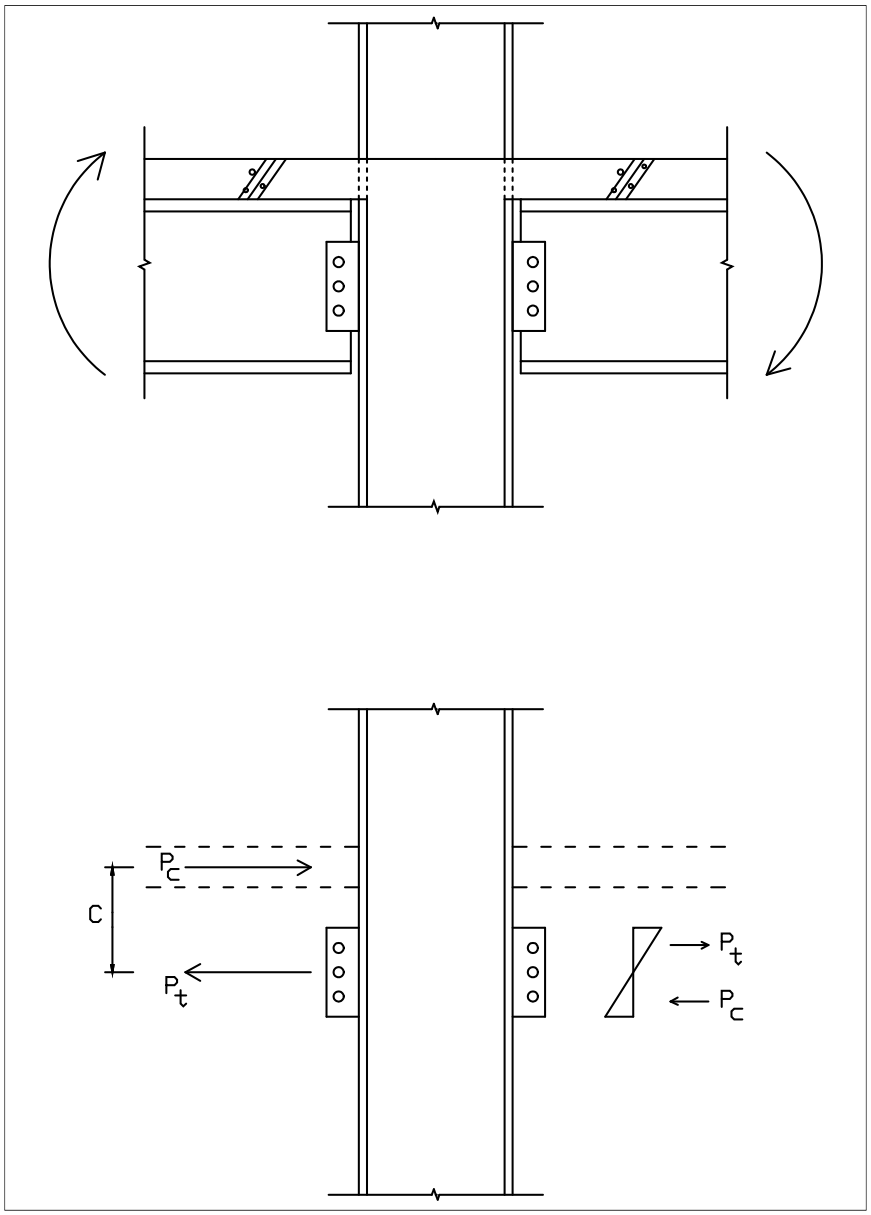

There is a rule of thumb in seismic design that is only approximately true, but which is useful for describing the function of ductility in seismic design. If a horizontal force, Q_E, taken from the elastic response spectrum of an earthquake is applied to a structure, an elastic displacement that can be called δ_E will occur. This means that if the earthquake actually occurred, the maximum deflection would be δ_E. If the structure is only designed to withstand a force of $Q_y = Q_E/\mu$ where μ is greater than 1.0, then the maximum displacement during the earthquake will be $\mu\delta_y$ where δ_y is the yield displacement that would occur if a static force is applied equal to Q_y; and μ is the *ductility factor*, which is the maximum displacement divided by the yield displacement. As a result, the larger the ability of a structure to experience lateral displacement beyond yield without failure, the greater is its ductility capacity. The larger the ductility capacity of a structure, the smaller is the seismic design force that can be used in its seismic design without risk of catastrophic failure.

Based on this discussion, one could infer that the response modification coefficient, R, is equal to the ductility factor, μ. This is not the case, however, because the actual effective strength of a building should always be greater that the design strength. This extra strength comes from many sources, including architectural partitions, stairway structures, piping, cladding, moment redistribution resulting from redundancy, material overstrength, material strain hardening, and gravity frames. The most important of these are the last three.

The total (inelastic) lateral strength of a typical cold-formed steel building may be two times greater than the design value while the total strength of a moment frame building may be six times greater than the design. This assumes that only material overstrength, strain hardening, gravity frames, and moment redistribution are considered. This extra strength beyond design means that the displacement experienced by the building under the design earthquake will be less than $R\delta_y$, because the strength is greater than Q_y. This is also why the deflection amplification factor C_d is needed and why C_d is always less than R. The strength for design is $Q_y = Q_E/R$, but the expected displacement is only $\delta_{max} = C_d\delta_y$, not $R\delta_y$.

So for a given building system, the value of R is greater if its ductility capacity is greater. The value of C_d will be smaller than R as a function of the expected overstrength. For a special moment frame, the large value for R (equal to 8) is because it has a large ductility capacity, great redundancy

for gravity loads, and it is expected to possess substantial overstrength. The value of C_d is small compared to R because it has large overstrength. For the cold-formed steel frame, the ductility capacity is large but the redundancy against collapse under gravity loads is small. As a result, R equals 4 for a cold-formed steel frame. Because the overstrength for a cold-formed steel frame is not substantial, the value of C_d equal to 3.5 is only slightly smaller than R.

10 Summary and Recommendations

This chapter concludes Part I of this technical report, which documents the technical basis for effective seismic design using cold-formed steel materials. Below is a summary of the results and areas for further research.

10.1 Summary

Previous cold-formed steel research and seismic design guidance developed by the AISI may not produce the desired ductile performance for load-bearing applications. Cold-formed steel has high strength variability, and light-gage materials are vulnerable to local buckling. Together, these characteristics can lead to brittle failures and collapse of buildings constructed with these materials. In the 1990s, USACE observed poor detailing and construction practices, which led to a moratorium on the use of cold-formed steel for load-bearing construction.

This report reviews previous CFS design research by others; presents a design philosophy encompasses special considerations for seismic loading; defined shear panel configurations; develops a design model and test panel specimens; defines material properties; defines test panel configurations and tests results that demonstrate ductile behavior; develops seismic design recommendations; and verifies those recommendations through shake table testing. Preliminary design recommendations emerging from USACE-funded research led to the lifting of the Corps moratorium on CFS construction. The data produced by the studies documented in Part I of this report serve as the basis for the detailed CFS design recommendations presented in Part II, which follows the conclusion of this chapter.

10.2 Recommendations

The test panels and design recommendations provided in this report focused on shear panels with diagonal straps as the primary lateral-load-resisting element. Other configurations that were considered in Chapter 2 used full-panel steel sheets as the lateral-load-resisting element. Further research on the G and H panel configurations is recommended. Those configurations use welded connections to fasten a steel sheet to the panel framing. The weld strength should always exceed the strength of the sheet material, so that an increase in strength of the steel sheet should require a

proportionately greater strength in the welded connection to the sheet. Chapter 2 presented two configurations: (1) the G configuration, in which the columns are built up from studs, similar to the C1 test panels; and (2) the H configuration, in which the columns are hollow structural sections (HSS). Effective design with either configuration should result in panels with greater overstrength than any of the diagonal strap configurations, because as the sheet yields, the diagonal tension field should widen, increasing the panel strength. These panels should also dissipate more energy, because as the panel deforms in the opposite direction after a peak excursion, the sheet will be buckled perpendicular to the tension field and the buckles will be forced to straighten out, picking up some load in the process. This should result in the load versus deflection hysteretic plots being less pinched than the diagonal-strap panels. The steel sheet welded to both the columns and heavy track that is braced by the anchors would also add to the column moment frame stiffness, further increasing the energy dissipation after a peak excursion. The steel sheet must be pulled taut before welding to the frame. Below are more thoughts about promising configurations using these two panel types that warrant further investigation.

10.2.1 Panel G

The panel G configuration uses columns built up from studs and anchors similar to those used in the panel C1 configuration. The sheet should be welded around its entire perimeter to the columns at the sides and to the track at the top and bottom. The track should be very heavy, and would be braced at the interior of the columns with the column anchors. The diagonal tension field should develop at close to a 45 degree angle, so panels that have an aspect ratio of 1 would be most efficient. Panels that are slightly taller, will result in increased bending load applied to the columns, while shorter panels will apply greater loads to the tracks. Even the heavy tracks should not be loaded significantly in bending. Initially the tension field will be relatively narrow, but it would widen as the sheet yields and elongates. This would result in greater loading of even the unbraced portions of the track. Therefore, it is likely that panels which are slightly taller than they are wide (i.e., aspect ratio greater than 1) would be more effective. The earlier test panels demonstrated that the diagonal straps should not be spot welded to the interior studs. Therefore, the interior studs resist only a relatively small portion of the gravity loads. For panels that have an aspect ratio much greater than 1, a mid-height horizontal compression member should be installed that should reduce bending loads on the col-

umns. As stated in Chapter 2, a method is needed to define the width of the diagonal tension field. Therefore, the research needed would require both analytical studies (e.g., Abaqus finite element analysis) and experimental testing of shear panels to define this width. The tension field width would be influenced by the thickness of the sheet and relative stiffness of the sheet and panel framing. Panels with varying dimensions of sheet thickness, frame thickness and stiffness, and aspect ratios, with and without mid-height compression members should be designed and tested. The maximum strength of the steel sheet material must be considered. Guidelines would need to be developed for designing panels of this type in a proportionate way so that the steel sheet yields significantly without any brittle failures of the sheet welded connections, columns, tracks, or anchors.

10.2.2 Panel H

The H configuration panel is identical to the panel G, except it uses HSS members for the columns. These columns would be thicker than the G columns that are built up from studs. The greater thickness would make these columns less vulnerable to tearing at the welded connections to the sheet and anchors. The heavier columns would also be less vulnerable to local buckling.

References

ACI. 2011a. *Building Code Requirements for Structural Concrete and Commentary (ACI 318-11)*. Farmington Hills, MI: American Concrete Institute.

ACI. 2011b. "Guide for Design of Anchorage to Concrete: Examples Using ACI 318 Appendix D." ACI 355.3R-11. Farmington Hills, MI: American Concrete Institute, ACI Committee 355.

AISC. 2010a. "Specification for Structural Steel Buildings." ANSI/AISC 360-10. Chicago, IL: American Institute of Steel Construction.

AISC. 2010b. "Seismic Provision for Structural Steel Buildings." ANSI/AISC 341-10. Chicago, IL: American Institute of Steel Construction

AISC. 2011. *Steel Construction Manual*. 14th Edition. AISC 325-11. Chicago, IL: American Institute of Steel Construction.

AISI. 2007a. "North American Specification for the Design of Cold-Formed Steel Structural Members." AISI Specification S100-07. Washington, DC: American Iron and Steel Institute.

AISI. 2007b. "Commentary on North American Specification for the Design of Cold-Formed Steel Structural Members." AISI S100-2007-C. Washington, DC: American Iron and Steel Institute.

AISI. 2008. *AISI Manual: Cold-Formed Steel Design*. Washington, DC: American Iron and Steel Institute.

ASCE. 2010. *Minimum Design Loads for Buildings and Other Structures*. ASCE/SEI 7-10. Reston VA: American Society of Civil Engineers. doi: http://dx.doi.org/10.1061/9780784412916.

ASTM. 1995. "Standard Practice for Static Load Test for Shear Resistance of Framed Walls for Buildings." E 564-95. West Conshohocken, PA: ASTM International.

ASTM. 2013a. "Standard Specification for Steel Sheet, Zinc-Coated (Galvanized) or Zinc-Iron Alloy-Coated (Galvannealed) by the Hot-Dip Process." ASTM A653. West Conshohocken, PA: ASTM International.

ASTM. 2013b. "Standard Specification for Steel Sheet, Carbon, Metallic- and Nonmetallic –Coated for Cold-Formed Framing Members. Standard ASTM A1003/A1003M-13b. West Conshohocken, PA: ASTM International.

ASTM. 2013c. "Standard Specification for Cold-Formed Welded and Seamless Carbon Steel Structural Tubing in Rounds and Shapes." ASTM A550/A500M. West Conshohocken, PA: ASTM International.

ASTM. 2014a. "Standard Specification for Structural Bolts, Steel, Heat Tread, 120/105 ksi Minimum Tensile Strength. Standard ASTM A325. West Conshohocken, PA: ASTM International.

ASTM. 2014b. “Standard Test Methods and Definitions for Mechanical Testing of Steel Products. ASTM A370. West Conshohocken, PA: ASTM International.

ATC. 1992. “Guidelines for Cyclic Seismic Testing of Components of Steel Structures.” ATC-24. Redwood City, CA: Applied Technology Council.

_____. 1995. “Structural Response Modification Factors.” ATC-19. Redwood City, CA: Applied Technology Council.

_____. 1997. *A Critical Review of Current Approaches to Earthquake-Resistant Design*. ATC-34. Redwood City, CA: Applied Technology Council.

AWS. 2008. “Structural Welding Code - Sheet Steel.” AWS D1.3/D1.3M:2008. Doral, FL: American Welding Society.

_____. 2012. “Recommended Practices for Resistance Welding.” AWS C1.1M/C1.1:2012. Doral, FL: American Welding Society.

Caccese, Vincent, Mohamed Elgaaly, and Ruobo Chen. 1993. “Experimental Study of Thin Steel-Plate Shear Walls under Cyclic Load.” *Journal of Structural Engineering* 119(2): 573–587. doi: http://dx.doi.org/10.1061/(ASCE)0733-9445(1993)119:2(573).

Driver, Robert G., Geoffrey L. Kulak, Alaa E. Elwi, and D.J. Laurie Kennedy. 1998a. “FE and Simplified Models of Steel Plate Shear Wall.” *Journal of Structural Engineering* 124(2): 121–130.

Driver, Robert G., Geoffrey L. Kulak, D.J. Laurie Kennedy, and Alaa E. Elwi. 1998b. “Cyclic Test of Four-Story Steel Plate Shear Wall.” *Journal of Structural Engineering* 124(2): 112–120. doi: http://dx.doi.org/10.1061/(ASCE)0733-9445(1998)124:2(112).

Elgaaly, Mohamed, Vincent Caccese, and C. Du. 1993. “Postbuckling Behavior of Steel-Plate Shear Walls under Cyclic Loads.” *Journal of Structural Engineering* 119(2): 588–605. doi: http://dx.doi.org/10.1061/(ASCE)0733-9445(1993)119:2(588).

Foutch, Douglas A., and James Wilcoski. 2005. “A Rational Approach for Determining Response Modification Factors for Seismic Design of Buildings Using Current Code Provisions.” *Earthquake Spectra* 21(2): 339–352.

ICC. 2011. “Cold-Formed Steel Light-Frame Construction.” Section 2211 in *2012 International Building Code*. Washington, DC: International Code Council.

Larson, Jay W. 1998. In-house report. Bethlehem, PA: Bethlehem Steel Corporation.

Matsen Ford Design Associates. 1997. *U.S. Army Corps of Engineers Barracks Prototype, Department of the Army*. Prepared for the National Association of Architectural Metal Manufacturers (NAAMM), Glen Ellyn, IL. Waukesha, WI: Matsen Ford Design Associates.

NEHRP. 2009. *Recommended Seismic Provisions for New Buildings and Other Structures*. FEMA P-750. Gaithersburg, MD: National Earthquake Hazard Reduction Program.

SAC Steel Project. 1997. "SAC Testing Programs and Loading Histories" (unpublished guidance).

Serrette, Reynaud. 1997. *Additional Shear Wall Values for Light Weight Steel Framing*. Final report. Washington, DC: American Iron and Steel Institute.

USACE. 1997. *After-Action Report: Shear Wall Testing and Cold Formed Steel Design, Whole Barracks Renewal*. Fort Lewis, WA: MCA PN 41545 and PN 46748. Seattle, WA: U.S. Army Corps of Engineers, Seattle District.

_____. 1998. *Design of Cold-Formed Load Bearing Steel Systems and Masonry Veneer / Steel Stud Walls*. Technical Instructions TI 809-07. Washington, DC: Headquarters, U.S. Army Corps of Engineers, Engineering and Construction Division, Directorate of Military Programs. https://www.wbdg.org/ccb/ARMYCOE/COETI/ARCHIVES/ti809_07.pdf

Wilcoski, James. 2014. "Excel Cold-Formed Steel Seismic Design Tool." Champaign, IL: Engineer Research and Development Center. Spreadsheet available at http://nees.org/warehouse.

APPENDICES

Appendix A: Prototype Barracks Building and Cold-Formed Steel Test Panel Drawings

This appendix shows a typical three-story barracks framing layout and the six panels tested by ERDC-CERL. The elevation views are a good representation of the typical shear wall panel layout. However, the connection details have been modified since testing the earlier panels and only the details shown in test panels C1 and D2 are recommended. Designers should use the new diagonal strap-to-column connection and column anchorage details shown in the design example in Chapter 12.

Figure A-1. Prototype 3-story barracks 3-D drawing.

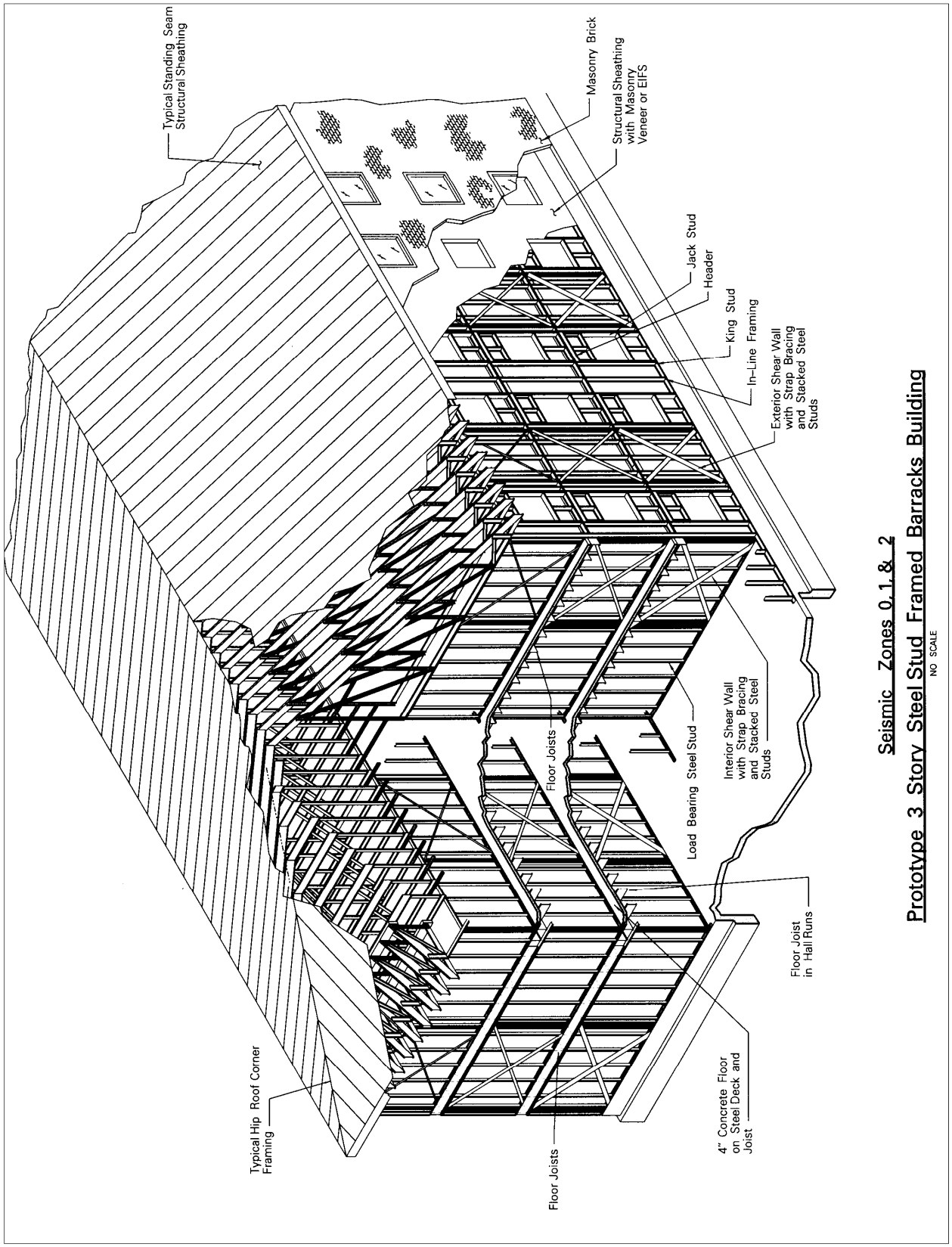

Figure A-2. Test panel A1.

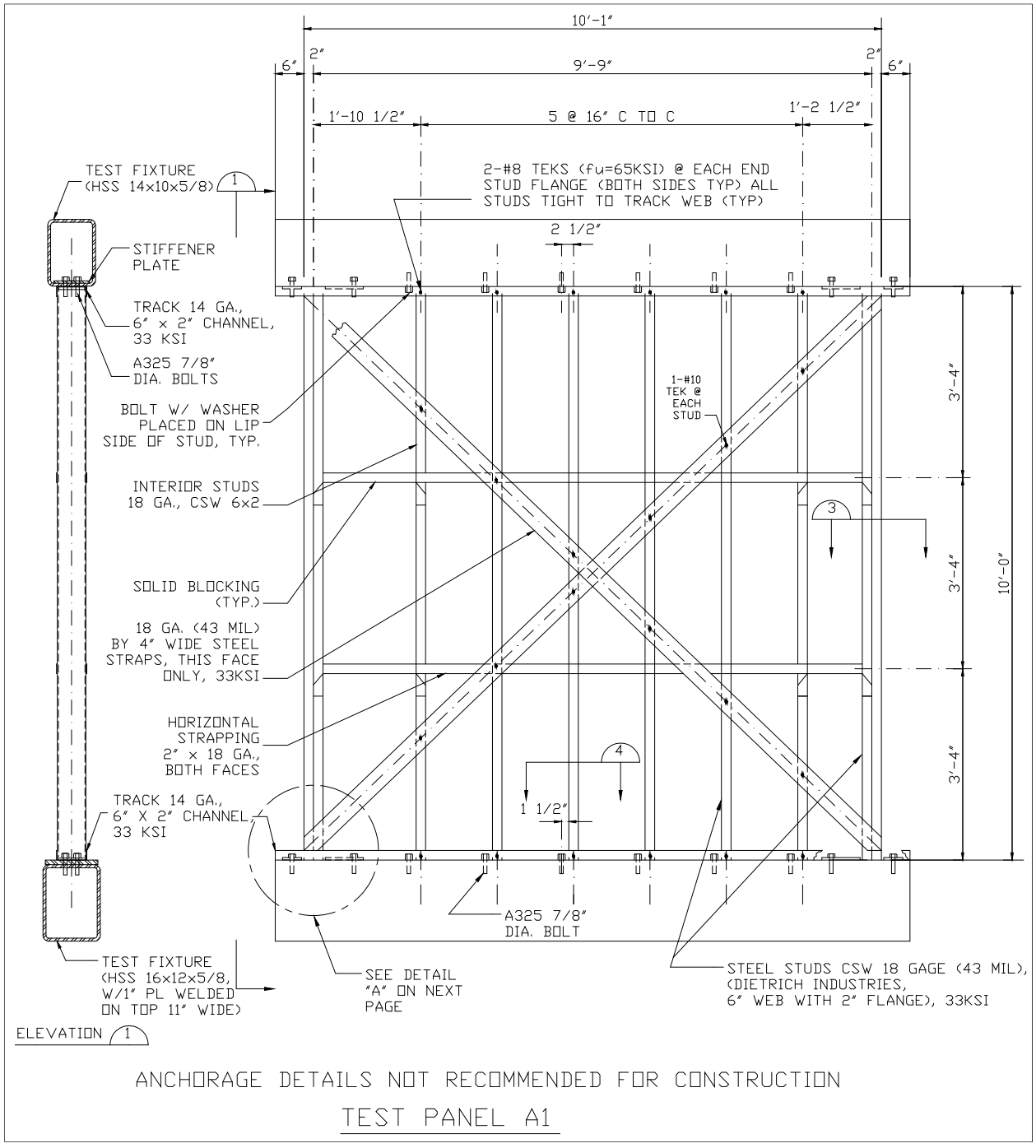

Figure A-3. Test panel A1 details.

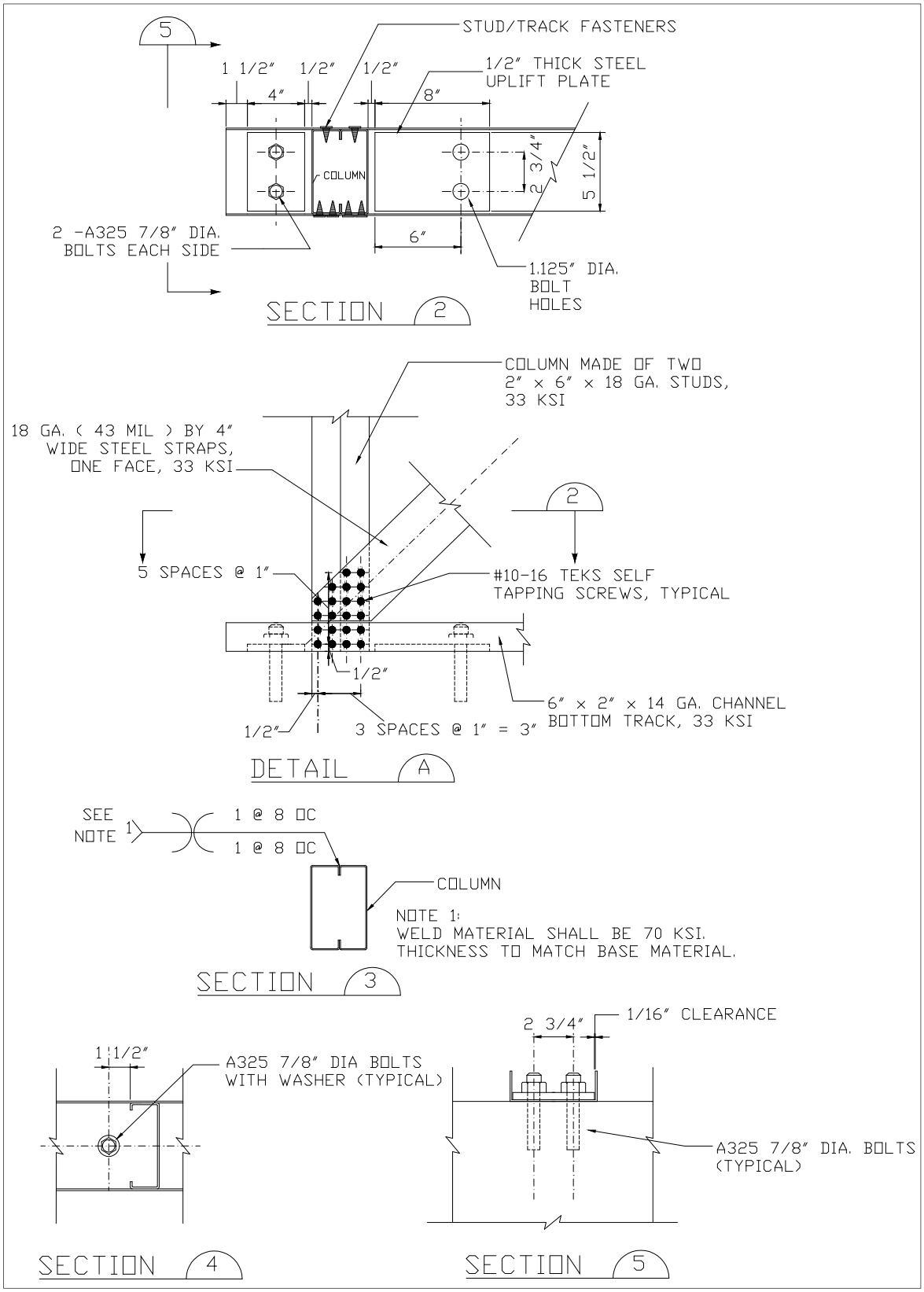

Figure A-4. Test panel A2.

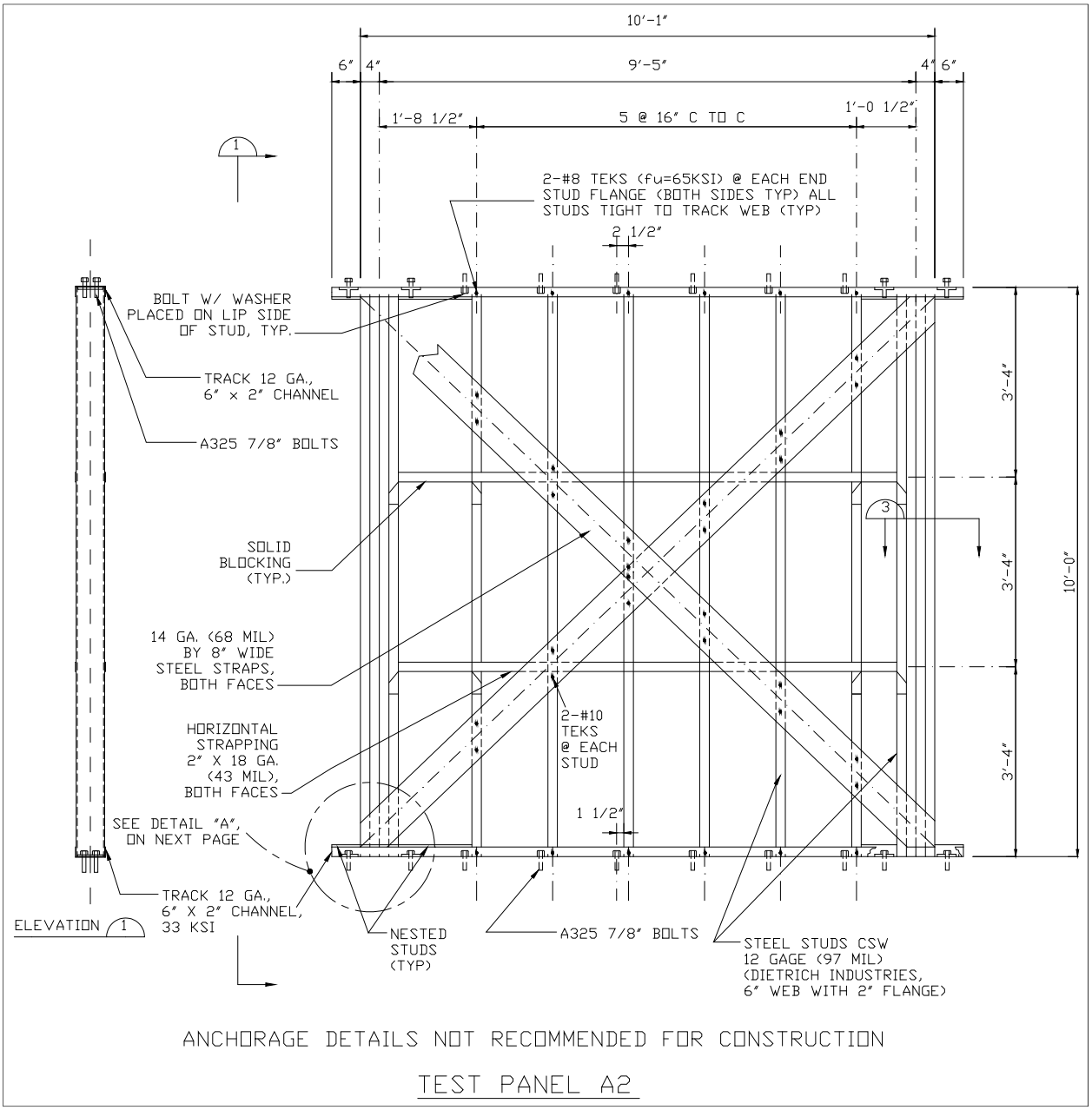

Figure A-5. Test panel A2 details.

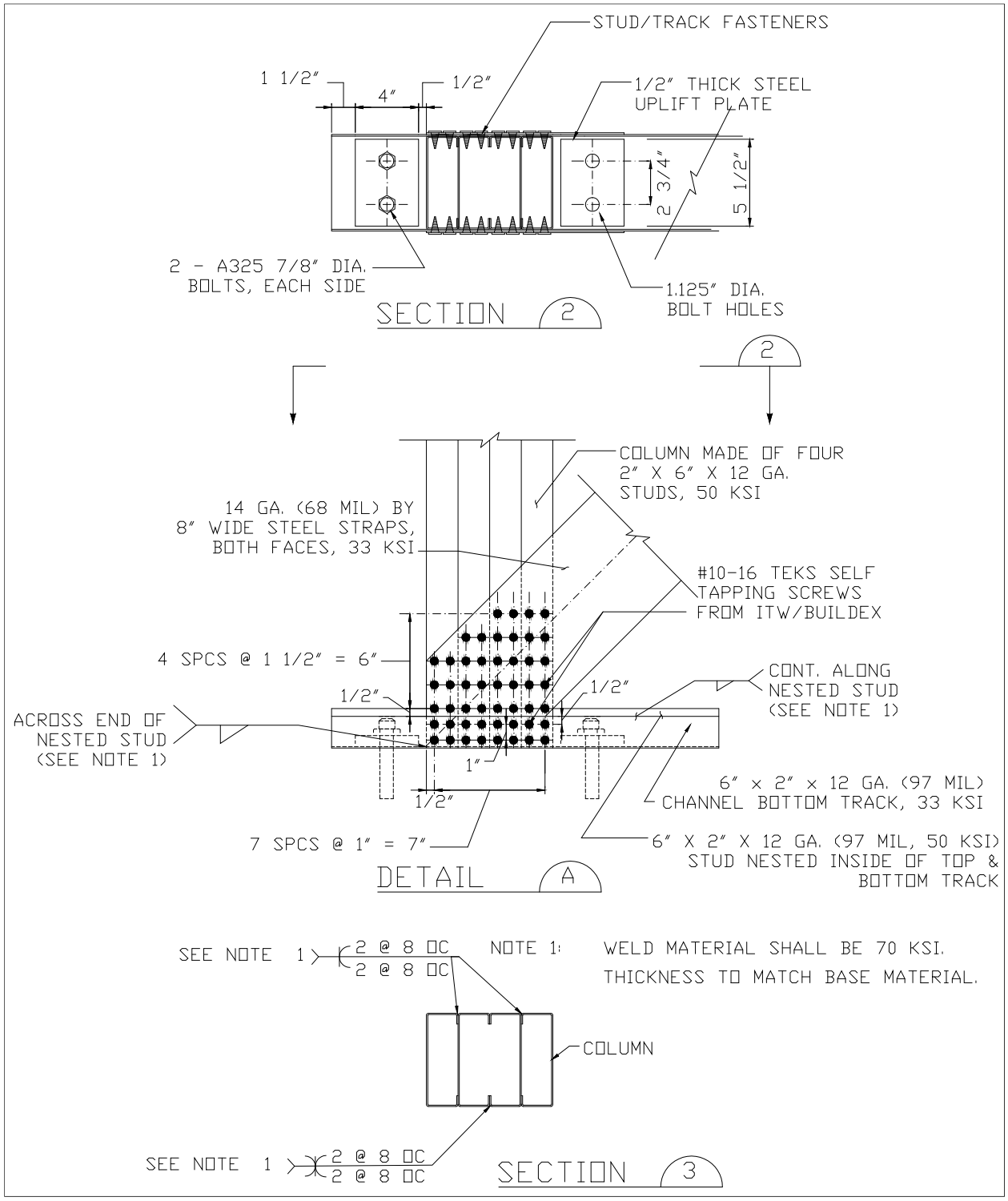

Figure A-6. Test panel A3.

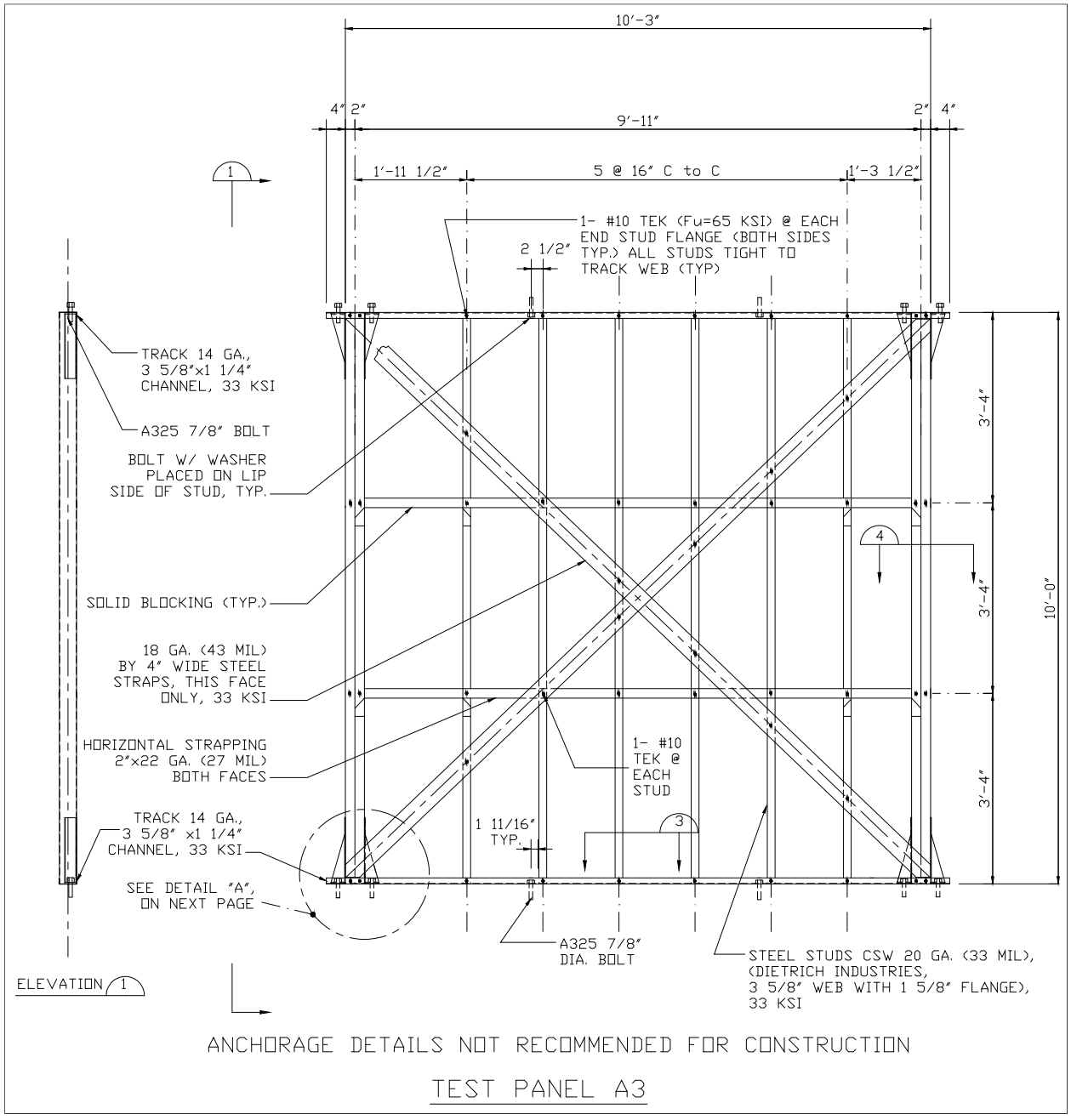

Figure A-7. Test panel A3 details.

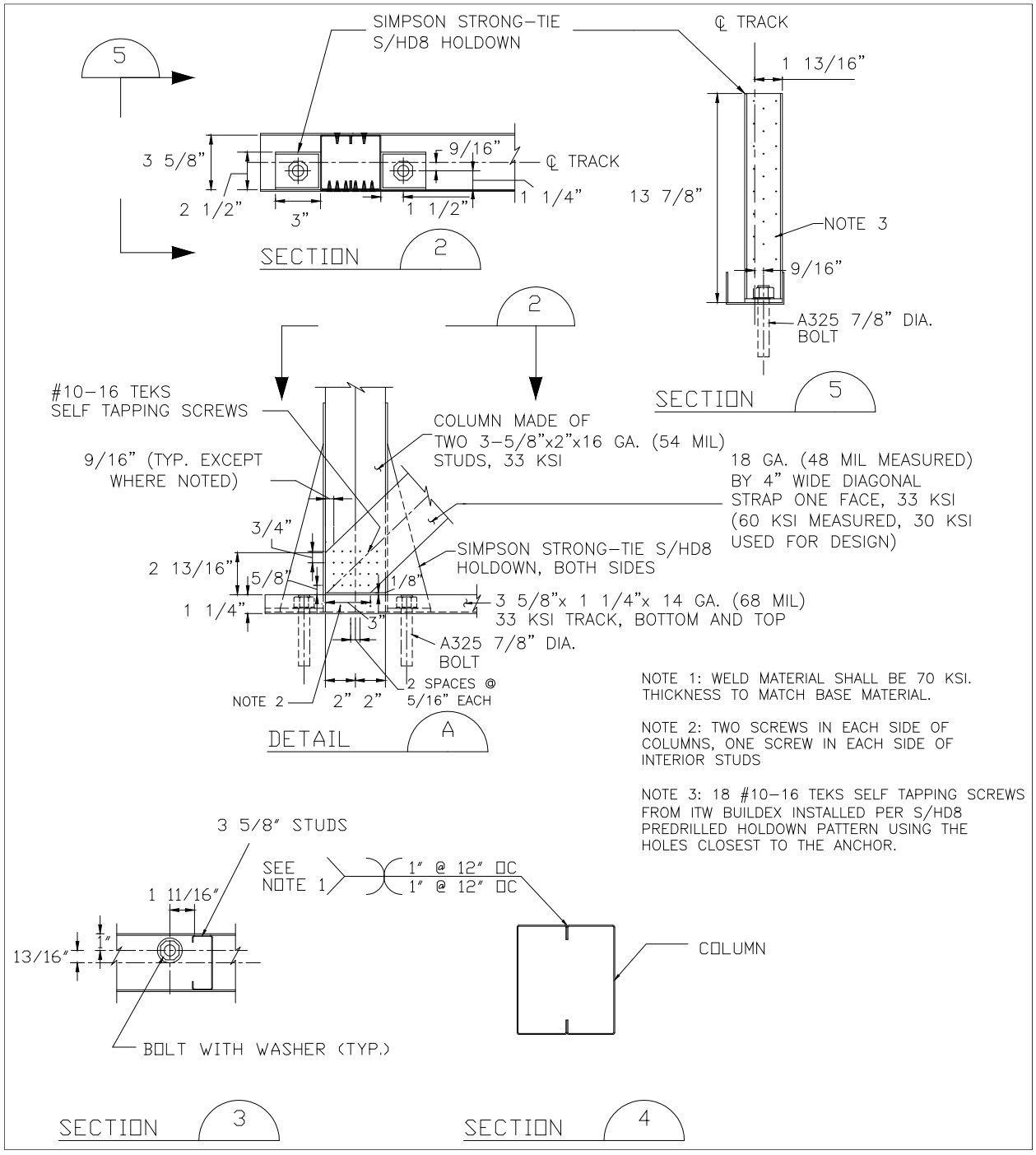

Figure A-8. Test panel C1.

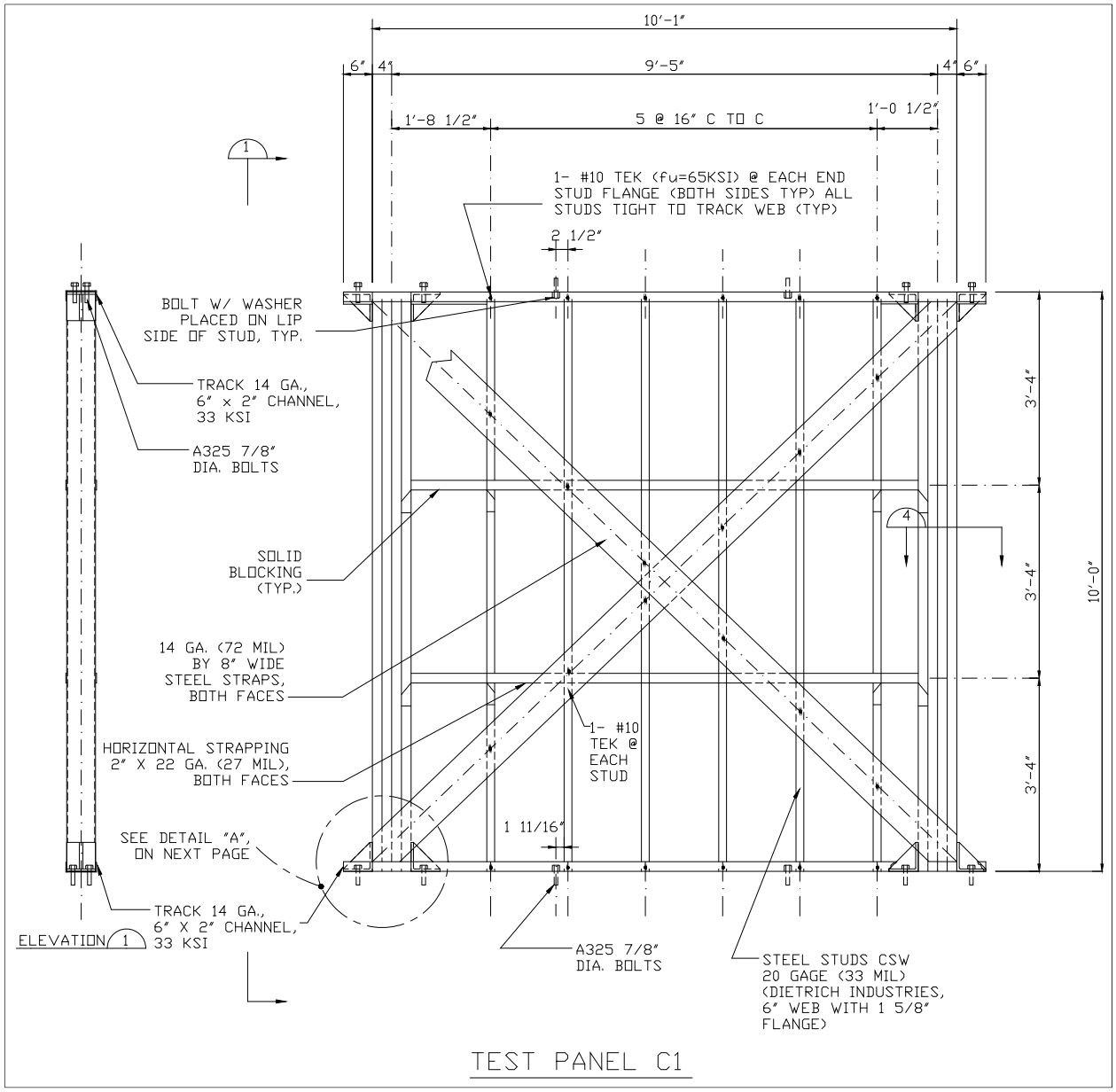

Figure A-9. Test panel C1 details.

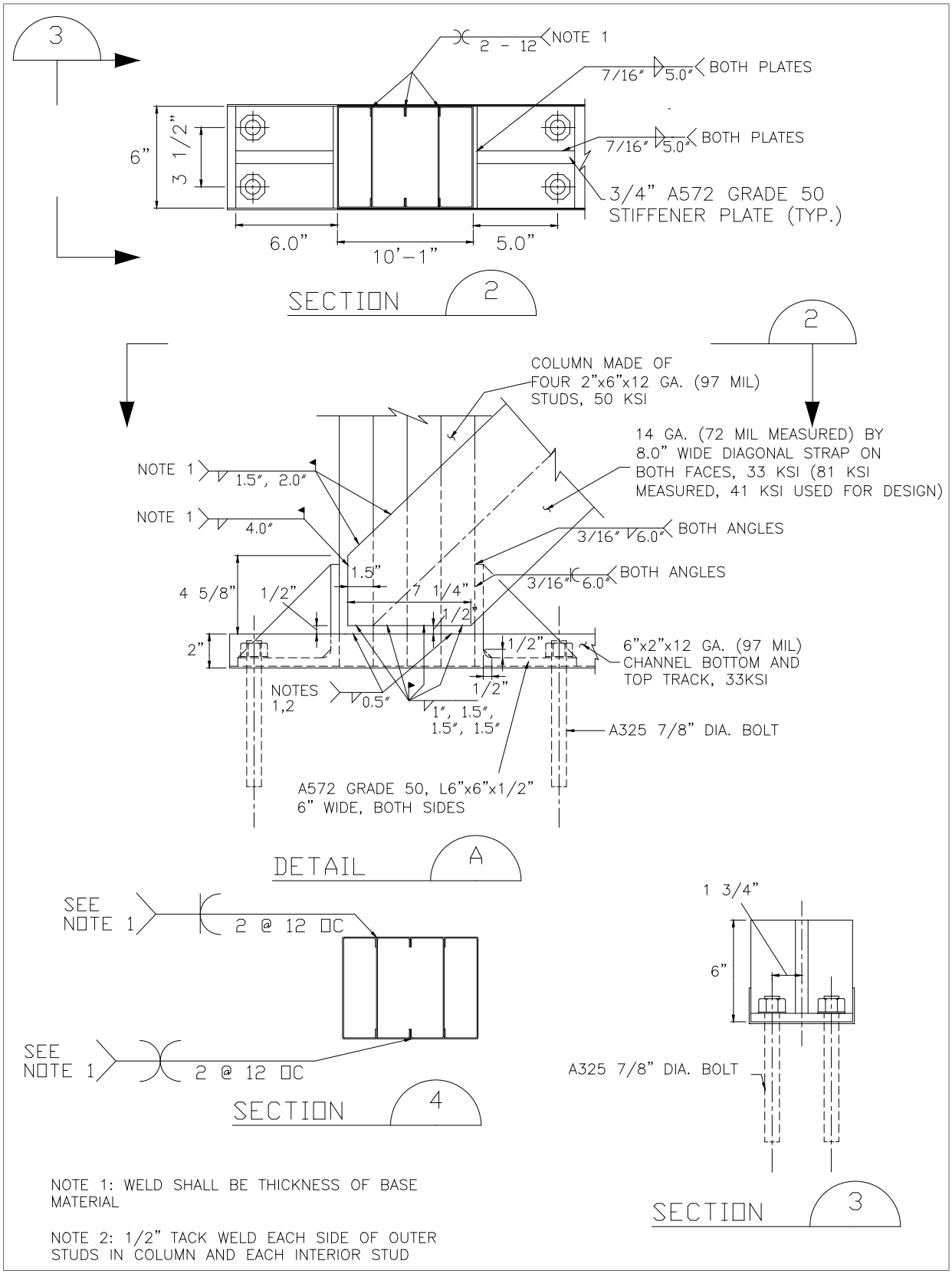

Figure A-10. Test panel D1.

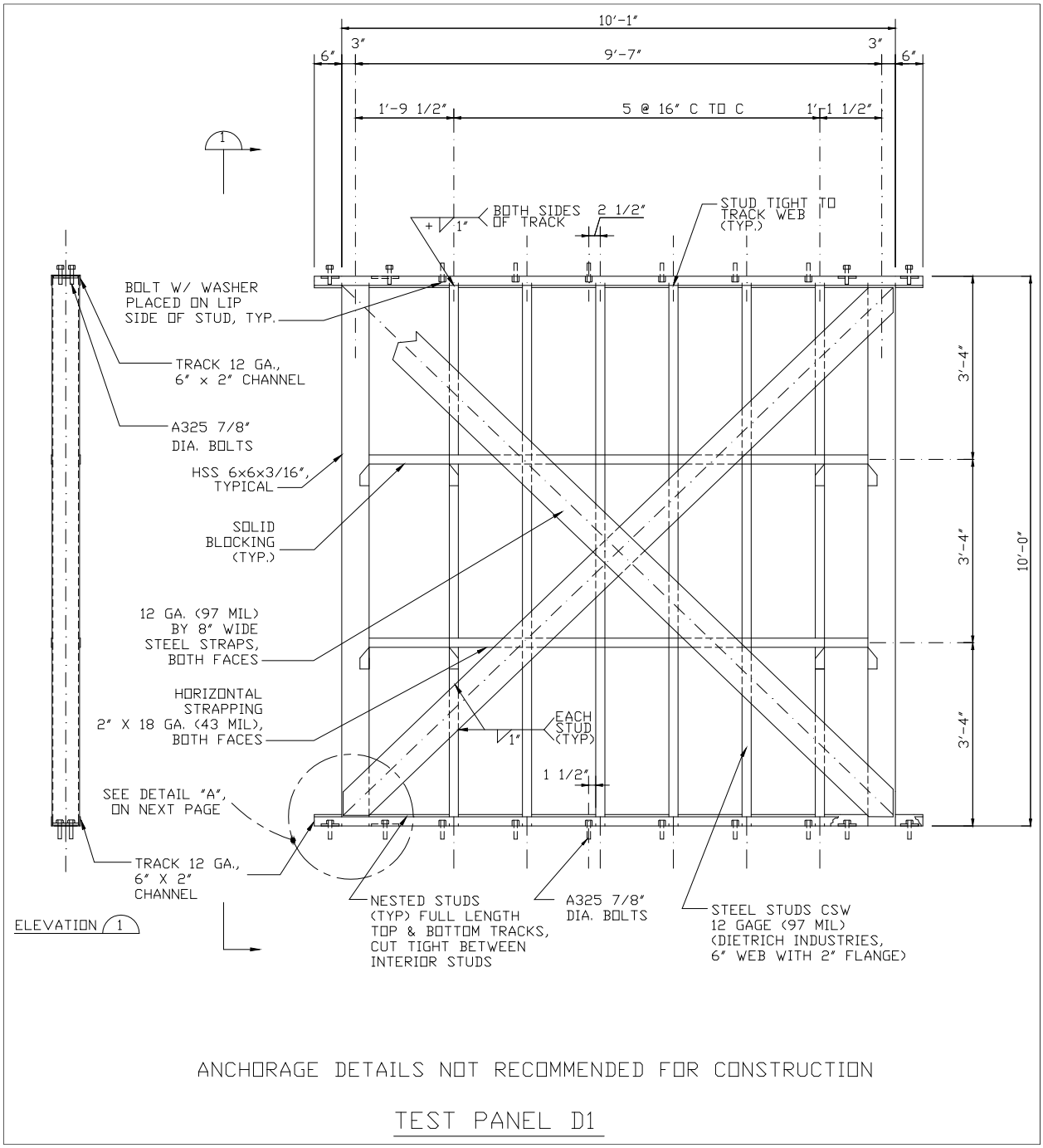

Figure A-11. Test panel D1 details.

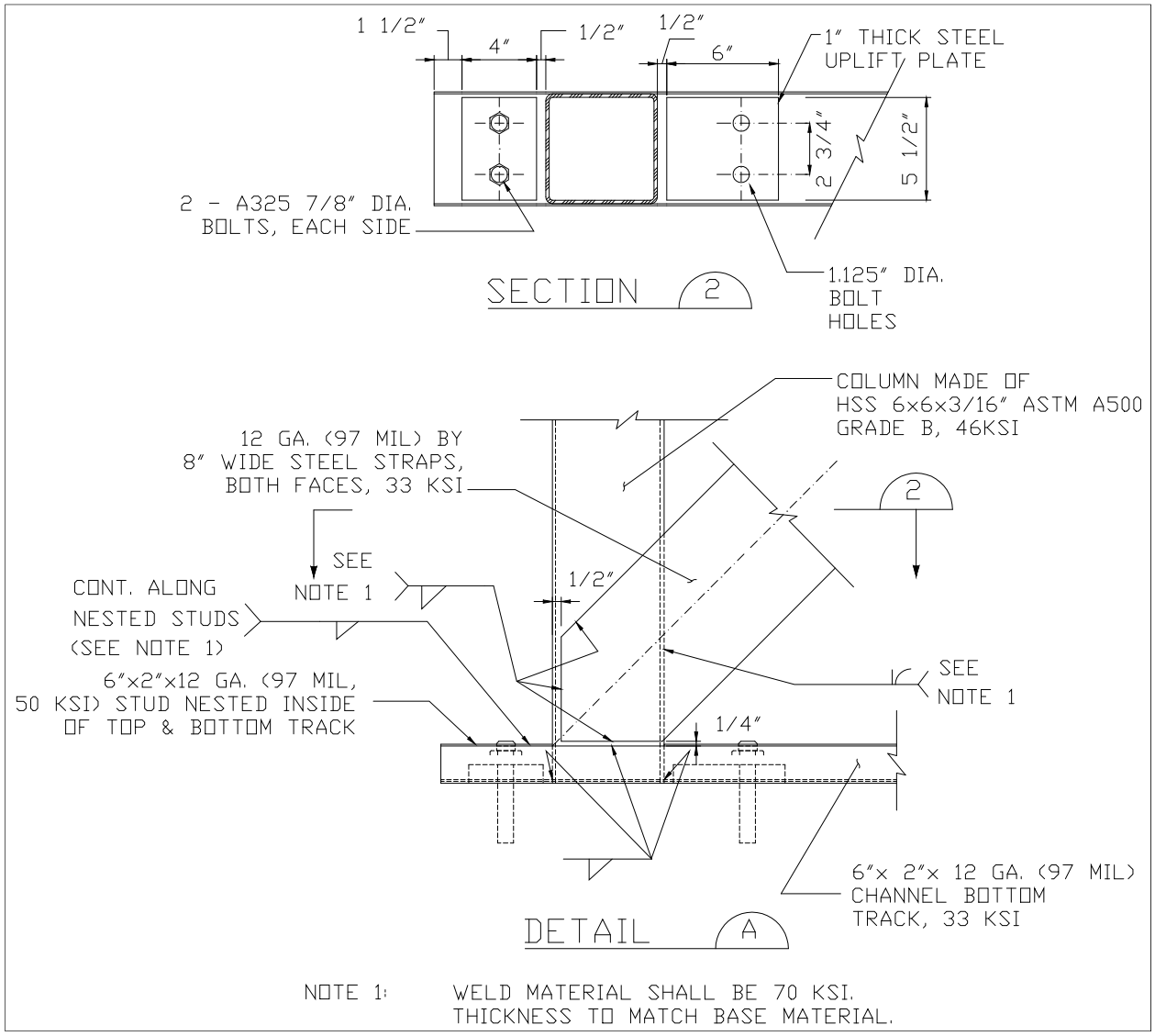

Figure A-12. Test panel D2.

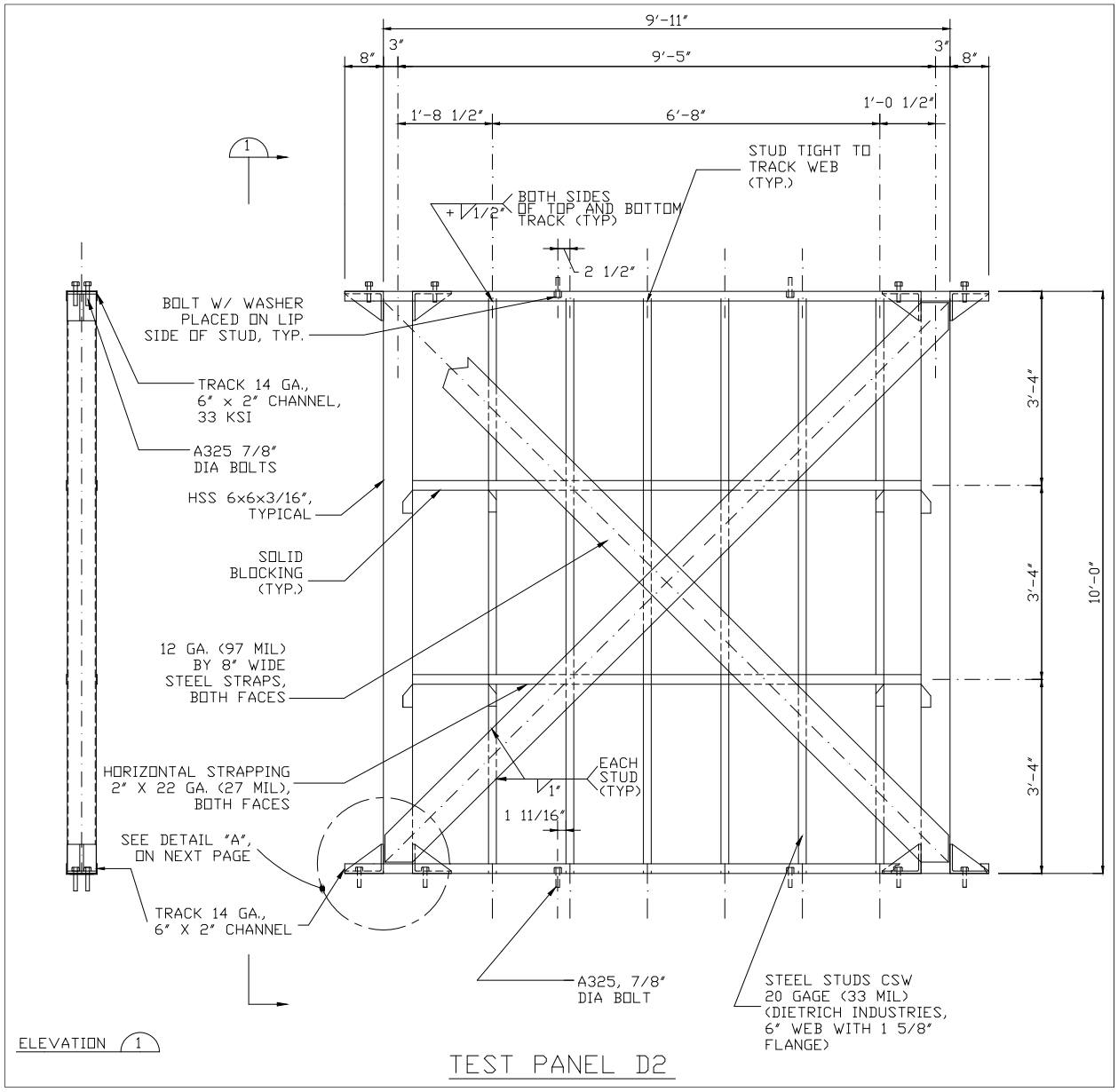

Figure A-13. Test panel D2 details.

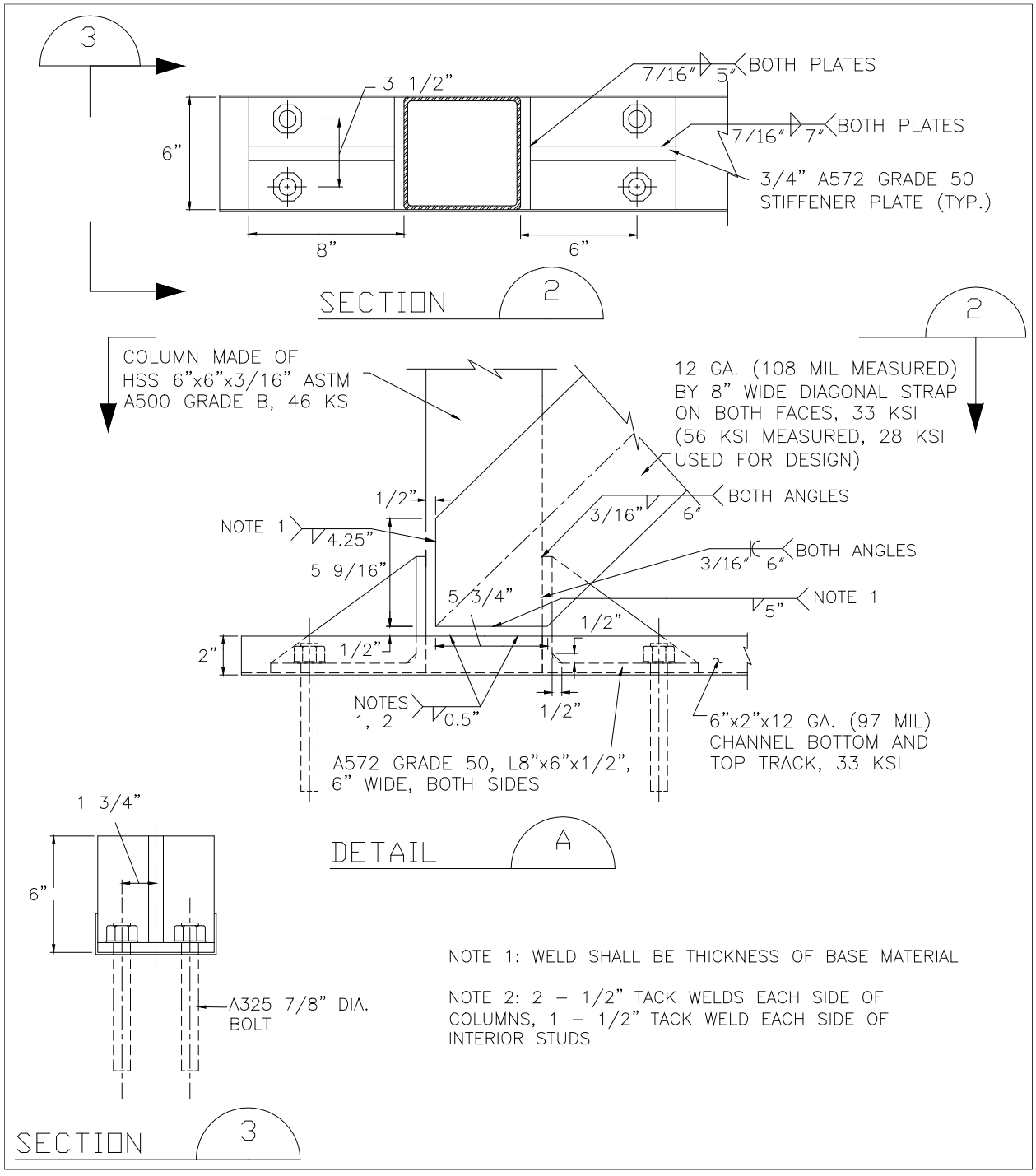

Appendix B: Cold-Formed Steel Test Observations

The following tables provide details on damage progression with respect to lateral deformation for all monotonically and cyclically loaded test panels.

Table B-1. Panel A1a monotonic observations.

Shear Deflection (in.)	Location	Failure or Other Observation
1.0	North (right) column, bottom corner	Local buckling at column knockouts – effectively redistributed loads to other portions of column cross-section.
1.4	South column, top corner	Top of tension strap began detaching, screws failed in shear at column/track connection. Column tearing in shear at column/track connection. Column began to twist at this connection because of column/track failure at the diagonal strap face of column while the other column face continued to carry shear forces to the track.
2.0	Top horizontal strap at south column	Buckling of horizontal strap.
2.1	South column, top corner	All screws at south column – top strap/column connection failed in shear.
3.5	Bottom of third stud in from north	Interior stud twisted and buckled.
3.5	North column	Buckling at two knockouts at the center and near the top of the exterior face of the north column.
3.8	First and third stud in from south column	Buckling of interior studs near their top at the diagonal and horizontal straps.
3.85	Second & third stud in from north column	Buckling of interior studs near their bottom at the diagonal and horizontal straps.
4.5	Second, third & fourth stud in from south column	Buckling of interior studs near their bottom at the horizontal strap.
4.8	North column, top corner	Column bending at the top (local buckling on the north face??).
5.0	South column, top corner	Shear failure of screws at back face of column/track connection.
5.4	North column	Buckling at two knockouts at the center and near the bottom of the interior face of the north column.
6.9	First stud in from south column – top	Screws at stud/track connection failed in shear.
7.8	Second stud in from south column – top	Screws at stud/track connection failed in shear.
8.3	Bottom of north column	Buckling at knockout at the south interior face of the north column.
9.0	Top of south column	Screws (3 or 4) failed in shear at the column/track connection.
9.7	North column, 1 ft down from top	Studs making up the column begin to separate.
10.4	Entire panel	Gross buckling of the columns and interior studs.

Table B-2. Panel A1b cyclic observations.

Shear Deflection (in.)	Location	Failure or Other Observations
0.4	Diagonal straps	Straps yield.
0.6	North and south columns	Buckling at column knockouts.
1.2	Second stud	Buckling of knockout near bottom of stud.
1.2	South column, upper corner	Column is twisting at top track (exterior face).
1.2	South column, lower corner	One screw sheared at lower south corner of column/strap connection
1.6	South column, upper and lower strap connections	Column is tearing between track flange tip and strap connection. There is large twisting at the column's midspan.
1.6	North column, upper corner	Buckling of column at the top track.
2.4	North column, upper corner	Kinking of column at top corner.
2.4	South column, upper and lower corners	Major tearing of column at track flange tip; screws, strap and track connection holding well.
2.4	South column at blocking stiffeners	Large buckling of columns at stiffeners.
2.4	6th stud	Buckling of middle knockout.
3.2	South column, upper corner	Tear halfway across column face between strap and track connections. All screws on strap side of track connection have failed. Screws on opposite side are beginning to fail.
3.2	South column, lower corner	All track screws have failed; only 2 strap screws have failed.
3.2	All studs	Twisting of interior studs near the strap connections (torsional buckling). All stud/bottom track connections have failed.
3.2	Fourth stud	Kinking of the column in the front face of stud near the knockout. Buckling of stud near the bottom track.
4.0	Bottom track	Buckling of stud flanges (front).
4.8	Bottom track	Buckling of stud flanges (back).
4.8	South column, upper corner	All track screws have failed; part of torn column still attached.
4.8	North column, upper corner	Kinking of exterior column flange (back).
5.6	Columns & interior studs	Total collapse of structure.

Table B-3. Panel A1c cyclic observations.

Shear Deflection (in.)	Location	Failure or Other Observations
0.4	Diagonal straps	Yielding of straps.
0.4	Sixth stud – top	Flange buckling in front; possible fabrication error.
0.4	South column, lower corner	Slight elastic shift in alignment of bottom track fasteners from strap connection fasteners. Column is still twisting at the connection.
0.6	North column, lower corner	See 0.4 in., south lower corner.
0.6	Fourth stud – top	Distortion around knockout.
0.6	North column	Column starting to twist at mid-height.
0.8	North column, upper corner	Local buckling of column knockout (interior face).
0.8	South column, lower corner	Permanent offset between strap and track connection.
1.2	North column, upper corner	Buckling of knockout on exterior face of column.
1.2	North column, lower corner	Buckling of column base at bottom track connection.

Shear Deflection (in.)	Location	Failure or Other Observations
1.2	South column, upper corner	Fasteners shearing in strap/column connection. Gaps are forming between the studs in the column. The top edge of the column/strap connection is pulling away from the plane.
1.2	South column, lower corner	Rotation and translation of bottom outer edge of column.
1.2	Strap on back of panel	Strap yielding on back of panel.
1.6	South column	Column has torn at top and bottom track connections.
1.6	North column, lower corner	Local deformation of top row of fasteners at joint. Pictures were taken of interior of column through the knockout.
1.6	South column, upper and lower column connections	Column is torn on face between track and strap connection.

Table B-4. Panel A2a monotonic observations.

Shear Deflection (in.)	Location	Failure or Other Observations
0.8	Diagonal strap	Buckling of strap.
2.1	North column, lower corner	Weld cracking at base (exterior front) of column at column/bottom track connection.
2.6	South column	Weld failure at lower column stiffener.
2.9	South column, upper corner	Weld fracture at column/track connection.
3.0	South column, upper corner	Fasteners breaking.
3.0	South column, lower column	Local buckling of knockout at exterior face.
3.6	North column, lower corner	Holes yielding at base of column.
4.1	Sixth stud – bottom	Stud rotated counterclockwise to the south.
4.4	North column	Local buckling of knockouts in exterior face of column.
5.3	North column, lower corner	Weld cracking at base of column (exterior face -back).
5.9	North column, lower corner	Weld failure along entire base of column/track connection.
6.2	South column, lower corner	Fasteners in column/strap connection failing in shear. Large buckling of column at track flange.
6.2	South column, upper column	Buckling of column flange at track.
7.1	First stud – top	Weld failure at nested stud connection.
7.4	North column, lower corner	Buckling of bottom track (back).
7.9	South column, upper corner	Weld failure at column/track connection.
8.2	North column, lower corner	Horizontal straps buckling.
9.2	South column, upper corner	Column is tearing at top track.
9.4	Interior studs – top	Fasteners failing in shear at top of studs (stud/track connection).
10.3	North column, lower corner	Bottom track yielding (buckling up) between sixth stud and column.
10.5	North column, lower corner	Tearing of web column at the base.
10.7	North column, upper corner	Fasteners connecting strap to studs on back shearing off.
11.2	North column, lower corner	Bottom track beginning to tear at column connection. (Front)
11.7	South column, upper corner	Column is pulling out of the connection.
12.6	Sixth stud – top	Fasteners shearing off at stud/top track connection.
13.2	Second stud	Second stud is twisting and fasteners are failing at both connections.

Shear Deflection (in.)	Location	Failure or Other Observations
14.2	South column	Local buckling of the knockouts.
14.2	South column, upper corner	Top track fractured at first column of fasteners.
Conclusion of test	North column, upper column	Weld at column/upper track connection fractured. Many fasteners at top and bottom of column sheared but the fastener heads remained affixed to the form.

Table B-5. Panel A2b trial cyclic observations (data are incomplete).

Shear Deflection (in.)	Location	Failure or Other Observations
0.5	Diagonal Straps	Buckling in both straps.
0.5	Sixth stud – bottom	Fasteners bending away from column at stud/ track connection.
0.5	Second stud – bracing	Fasteners on strap beginning to pull out.
0.5	First stud – bottom	Fasteners pulling away from base.
0.5	North column, lower corner	Slight bowing of second knockout from the bottom (exterior). Weld cracking at base of column at exterior face. Local buckling of knockouts near the bottom of the column.
0.5	North column, lower corner	Welds fracturing at top and base of column interior face. Buckling of all knockouts along exterior face.
0.5	South column, lower corner	Crack at welds in two directions into the column web (exterior).
0.5	South column, upper corner	Warping of knockouts. Local buckling of track near the back edge.
0.5	North column, upper corner	Large crack width at top of column across top weld. Buckling of top track near the back edge. Strap fasteners pulling out from studs.
6.4	North column, lower corner	Fracture through column at base.
6.4	Second stud – strap	Fasteners pulling out of studs.
6.4	North column, upper corner	Fasteners popping out of column/strap connection.
6.4	Fourth and fifth stud	Noticeable deformation of fastener holes in strap connections.
9.6	South column, upper corner	Bolts popping out of joint. Connection failure (back). Large web fracture at top of column at exterior face.
9.6	South column, lower corner	Buckling of column at base. Fasteners pulling out from column/strap connection.
9.6	Diagonal straps	Excessive buckling of bracing.
9.6	North column, upper corner	Fracture through column web on exterior face.
13.2	South column, upper corner	Column fracture completely through web. Fasteners popping out at joint
13.2	First, second, & third studs	Top fasteners in studs.
13.2	Stud –top	Failed.
15.0	South column, lower corner	Weld failure along bottom of track in nested stud. Column buckling on interior face.
15.0	Fourth & fifth studs - top	Studs twisting.

Table B-6. Panel A2b cyclic observations.

Shear Deflection (in.)	Location	Failure or Other Observations
0.6	Diagonal straps	Straps yielding.
1.2	South column, lower corner	Weld crack at stiffener front and back.
1.6	North column, upper/lower corner	Weld fracture at column.
2.4	South column, lower corner	Weld crack through stiffener.
3.2	North column, lower corner	Screw head sheared off (top row upper). Buckling of bottom track. Failure of 2 track screws at buckle point.
4.0	North column, lower corner	Buckling at column cutout. Buckling at column base.
4.8	North column, lower corner	Screw failure at top track (top row). Screw shearing at bottom track.
5.6	South column, upper corner	Fracture of column weld at top track. Tearing of column.
6.4	South column, lower corner	More weld failures at bottom of column. Column base beginning to bend.
6.4	South column, upper corner	Weld of nested stud failed.
6.4	South column	Weld fracture of column at track connection (interior).
6.4	South column, lower corner	Tearing of lower track near column intersection.
7.2	North column, lower corner	Upward buckling of track web at base of column at outer face. Tearing of track flange near weld at column base.
7.2	South column, lower corner	Fastener failure at column base. Bottom track lifting up off base beam (back).
8.0	South column, lower corner	Fasteners failing at column base (back).
8.0	Sixth stud - top	Fasteners failing at stud/strap connection.
8.0	South column, upper corner	Top track tearing at column intersection.
8.0	North column, lower corner	Fastener failed at track. Uplift of track is causing tearing of bottom track flange. Total failure of column base weld. Multiple fastener failure at north end (back).
8.8	North column - exterior	Buckling of exterior face between knockouts.
8.8	Sixth stud – top	Fastener connecting strap failed (back).
8.8	North column, upper corner	Weld tearing at column/top track connection (exterior).
9.6	North column, upper corner	Tearing of weld at column/top track connection (back).
9.6	Front diagonal strap	Various fasteners shearing at stud connections.
9.6	North column, upper corner	Four fasteners have failed in shear at top track/column connection.
9.6	North column, lower corner	Almost all fasteners in column/bottom track have failed (front).
10.4	Third stud	Fasteners shearing at stud connections.
11.2	North column, upper corner	Fasteners failing at column connection to upper stud.
11.2	Sixth stud – bottom	Fasteners failing at bracing connections.
11.2	North column, upper corner	Weld at column/top track connection failing (still maintaining some load). Fastener failed in shear at column/top track connection.
11.2	Sixth stud – bottom	Fastener failed at strap connection.
11.2	South column, upper corner	Top track tearing at column intersection (back).
11.2	Interior studs	Fasteners failing (back).
11.2	South column, upper corner	Top track tearing at top (back).

Table B-7. Panel A2c cyclic observations.

Shear Deflection (in.)	Location	Failure or Other Observations
0.4	Diagonal straps	Straps yielding.
0.6	North column, upper corner	Exterior weld crack at column/top track connection.
0.6	South column, lower corner	Weld beginning to fail at column/bottom track connection at panel exterior.
0.6	South column, lower corner	Fastener at strap/column connection failure.
1.2	North column, upper corner	Exterior weld continues to crack at column/top track connection.
1.6	Sixth stud - top	Strap fastener shear (front and back).
1.6	South column, lower corner	Bottom track beginning to buckle upwards, followed by screw failure.
2.4	North column, lower corner	Weld fracture at column/base track connection.
2.4	Track	Fasteners pulling out (back).
2.4	South column, lower corner Exterior	Weld at column/bottom track connection failed.
3.2	North column, lower corner	Base track torn from corner to fastener. Track buckling out at column intersection at back face.
3.2	South column, upper corner	Screws sheared at column/top track connection.
4.0	Diagonal strap	Strap buckling (front).
4.0	South column	Top track beginning to tear at column connections. Top weld at upper track/column connection (exterior).
4.0	South column, lower corner	Weld failure along bottom track connection (interior). Entire bottom track failing along exterior column face.
4.0	North column, upper corner	Top track buckling at column. Top track tearing along fastener line.
4.0	North column, lower corner	Welds fracturing at base. Fasteners shearing at bottom of track at back face.
4.0	Upper/north lower corners	Bending of top track away from beam at top and bottom.
4.8	North column, lower corner	Brittle weld fracture along entire base. Bottom track torn along fastener line at back face.
4.8	Sixth stud - bottom	Strap fastener failing.
5.6	Second stud	Fastener failed at strap connection.
5.6	North column, lower corner	Bottom track pulling up from beam.
5.6	North column, upper corner	Weld failure along base (exterior).
5.6	Right column	Local buckling near knockouts.
5.6	North column, lower corner	Column tearing at base near exterior weld.
5.6	South column, lower corner	Bottom track shearing and weld failure through track.
6.4	South column, upper corner	Exterior weld at upper track/column connection failed completely.
6.4	South column, lower corner	Slight buckling of column near base. Bottom track has failed (Back)
6.4	North column, lower corner	Buckling of interior track/column connection.
6.4	North column, upper corner	Column tearing near weld (exterior).
6.4	Sixth stud - top	Stud fastener to top track sheared off. Fasteners have sheared at top track – front and back face.
7.2	South column, upper corner	Fasteners failing at column connection – back face
8.0	South column, lower corner	Track is beginning to uplift from beam.
8.0	Third stud	Fastener failure at strap connection.
8.0	North column, lower corner	Column buckling at track (exterior). Column starting to gap at base.

Shear Deflection (in.)	Location	Failure or Other Observations
8.0	North column, upper corner	Fasteners shearing at track/column connection.
8.8	Third stud – strap	Fasteners shearing at strap connection.
9.6	Third stud – strap	Fasteners shearing at strap connection.
9.6	North column, lower corner	Bottom track flange beginning to tear.
9.6	South column, lower corner	Fasteners at column/strap connection failing.
10.4	North column, lower corner	Bottom track at column base has sheared. Tear continuing along the bottom track.
11.2	First stud- top	Fasteners at strap connection shearing.
12.8	Interior studs - bottom	Studs fail along bottom track at screws.

Table B-8. Panel A3a monotonic observations.

Shear Deflection (in.)	Location	Failure or Other Observations
Loading to the South – Positive Direction on Data Plots		
1.3	South column, top corner	Screws failed between column and track.
2.8	South column, top corner	Major distortion of column.
3.5	South column, top corner	Column pulled away from anchor.
4.0	South column, top corner	Screws between column and strap failing.
5.0	South column, top corner	Strap failed.
Loading to the North – Negative Direction on Data Plots		
0.7	North column, top corner	Screws failed between column and track.
1.15	South column, bottom corner	Screws failed between column and track.
2.2	South column, bottom corner	Column pulling away from strong-tie.
2.8	South column, bottom corner	Column buckling around strong-tie.
5.9	Interior	Studs buckle.
6.3	South column, bottom corner	Column pulling away from strong-tie.
10.0	South column, bottom corner	Slow progression of crushing of double stud between anchors.

Table B-9. Panel A3b cyclic observations.

Shear Deflection (in.)	Location	Failure or Other Observations
0.45	South column, bottom corner	Screws failed between column and track.
0.9	North column, bottom corner	Screws failed between column and track.
1.2	South column, top corner	Strap pulling away from column.
1.2	North column, bottom corner	Bowing of column.
1.8	South column, top corner	Buckling of column.
1.8	South column, bottom corner	Strap pulling away from column.
2.4	South column, bottom corner	Buckling of column.
2.4	North column, top corner	Buckling of column.
3.6	South column, top corner	Screws fail between strap and column.
3.6	Interior	Buckling of interior channels and partial screw pullout.

Shear Deflection (in.)	Location	Failure or Other Observations
3.6	North column, bottom corner	Screws fail between strap and column. Major tearing of column away from anchor
4.8	North column, top corner	Crushing of column against anchor.
4.8	South column, top corner	Channels of column start pulling apart.
4.8	South column, bottom corner	Screws pull out.
6.0	South column, bottom corner	Strap failure by pullout.
6.0	North column, bottom corner	Strap failure by pullout.

Table B-10. Panel A3c cyclic observations.

Shear Deflection (in.)	Location	Failure or Other Observations
0.45	North column, bottom corner	Column flexing with strap tension.
0.6	North column, top corner	Screws failed between column and track.
0.9	South column, Top/bottom corner	Screws failed between column and track.
0.9	North column, top corner	Screws failed between column and track.
1.2	North column, top corner	As connection is stressed, back of column wraps back around anchor.
2.4	North column, top/bottom corner	Screws between column and strap nearly pulling out.
3.6	North column, bottom corner	Strap net area failure at connection.
4.8	North column, top corner	Screws between column and strap pull out.
6.0	South column, bottom corner	Lots of screws showing between strap and column.
7.2	Interior	Interior studs well buckled.

Table B-11. Panel C1a monotonic observations.

Shear Deflection (in.)	Location	Failure or Other Observations
0	Unknown	Weld between track and column failed at application of vertical load.
0.5	North column, top corner	Weld between track and column failed.
0.75	South column, top corner; North column, bottom corner	Major deflection of strap (compression).
2.25	South column, bottom corner	Tearing of the strap.
3.5	South column, bottom corner	Rear strap failed.

Table B-12. Panel C1b cyclic observations.

Shear Deflection (in.)	Location	Failure or Other Observations
0.6	North column, top corner	Weld crack.
0.8	North column, bottom corner	Weld cracked on both sides
1.2	North column, bottom corner	Small cracking at top of angle/column connection.

Shear Deflection (in.)	Location	Failure or Other Observations
1.6	North column, bottom corner	First three welds cracked.
1.6	South column, bottom corner	Weld failure.
2.4	North column, top corner; North column, bottom corner	Complete tear of strap.
3.2	North column, bottom corner	Angle splitting from column.
4.8	North column, bottom corner	Complete tear at angle/column connection.

Table B-13. Panel C1c cyclic observations.

Shear Deflection (in.)	Location	Failure or Other Observations
0.3	North column, top corner	Track weld failure (front).
0.4	North column, top corner	Track weld failure (back).
0.6	North column, bottom corner	Track weld failure (front/back).
1.6	South column, bottom corner	Track weld failure (back).

Table B-14. Panel D1a monotonic observations.

Shear Deflection (in.)	Location	Failure or Other Observations
0.95	Diagonal straps	Straps yielding.
1.0	South column, upper corner	Crack forming in weld at column/top track connection. (Exterior) Track bowing away from beam.
1.37	North column, lower corner	Track pulling up.
1.6	North column, lower corner	Welds fracture at nested studs.
2.1	North column, lower corner	Bottom track tearing at weld (back). Weld at base of column fracture at exterior face.
3.8	South column, upper corner	Top track bowing away from beam.
4.0	South column, upper corner	Welds at nested stud have failed.
4.0	North column, lower corner	Track torn through to base.
4.43	North column, lower corner	Track base tearing. Track flanges bowing out between welds.
6.7	South column, lower corner	Bottom track pulling away from beam.
8.0	South column, lower corner	Weld failing at nested stud/column connection.
8.0	South column, upper corner	Top Track beginning to tear. Buckling of top track is causing it to crush against tube column.
8.46	Sixth stud - straps	Strap exhibiting a hump between welds on same stud.
9.3	North column, lower corner	Nested stud flanges are buckling against tube.
10.2	North column, lower corner - Strap	Strap tearing on back face.
10.68	North column, lower corner – Strap	Strap tom through on back.
10.68	Interior studs - bottom	Weld at base of interior stud fail.
11.24	North column, lower corner-strap	Front strap torn through on front.

Shear Deflection (in.)	Location	Failure or Other Observations
11.24	North column, lower corner	Bottom track bowing up.
11.24	Third stud	Strap weld fails.
12.0	First stud - bottom	Weld failure at strap connection.
12.5	Fifth stud - bottom	Stud buckling at base.
13.14	North column, lower corner	Bottom track buckling at base.
13.6	Interior studs - bottom	Massive buckling at stud/bottom track connections.
14.0	North column, lower corner	Weld fracture/tearing through track.
14.45	Diagonal strap	Strap weld failures at stud connections.
14.45	Base beam	Dishing effects at bolts.

Table B-15. Panel D1b cyclic observations.

Shear Deflection (in.)	Location	Failure or Other Observations
0.4	Diagonal straps	Straps yielding.
0.6	North column, upper corner	Weld begins to fail at column/top track connection at exterior face.
1.2	North column, upper corner	Welds across flanges fail at nested studs.
1.2	South column, upper corner	Welds across flanges fail at nested studs.
1.6	South column, lower corner	Welds across flanges fail at nested studs.
2.4	South column, lower corner	Bottom track beginning to uplift under outside of column.
2.4	South column, upper track	Tear in top track beginning to propagate in track near column at exterior face.
3.2	North column, lower corner	Weld begins to fail at flange of nested stud. Bottom track lifting up.
3.2	Second stud - strap	Weld at strap connection begins to fail at front and back face.
3.2	Third stud - strap	Weld failure at strap connection at back face.
4.0	North column, lower corner	Track tearing near column connection at front face. Tearing of bottom track along side at front face.
4.0	Second stud - strap	Weld at strap connection fails at front face.
4.0	North column, upper corner	Top track tearing. Flange of nested stud beginning to buckle.
4.0	South column, upper corner	Tears forming at column/top track weld connection at front and back faces. Buckling of nested stud flange due to prying action against column.
4.8	Sixth stud - bottom	Weld failure at strap connection.
4.8	Diagonal straps	Straps bowing between welds of same stud.
4.8	Second stud - bottom	Weld at strap connection failed at front and back faces.
5.6	North column, lower corner	Bottom track buckling out at column.
5.6	Sixth strap - bottom	Weld beginning to fail at strap connection.
5.6	North column, upper corner	Top track pulling away from beam.
5.6	South column, lower corner	Weld failure of column/bottom track connection at exterior face.
6.4	South column, upper corner	Weld failure of column/bottom track connection at exterior face.
6.4	North column, lower corner	Sudden weld fracture at column/bottom track connection at exterior face. Strap/column connection beginning to fail at back face. Bottom track buckling out at back face.
7.2	North column, upper corner	Strap/column connection beginning to fail. Weld failure at column/top track connection at exterior face.
7.2	Sixth stud - bottom	Stud beginning to tear near bottom track. Stud buckling at base.

Shear Deflection (in.)	Location	Failure or Other Observations
7.2	Fifth stud - bottom	Weld fails around strap.
8.0	South column, upper corner	Top track flanges beginning to buckle near column/top track connection.
8.0	Interior studs	Welds at strap/stud connection fail. Studs tearing near bottom track.
9.6	North column, lower corner	Strap beginning to tear.
9.6	North column, upper corner	Weld failure at column/top track connection at exterior face.
10.4	North column, lower corner	Strap tearing near column in two places. Weld failure near tear column/strap connection.
11.2	North column, lower corner	Sudden failure of back strap.
11.2	North column, upper corner	Strap beginning to tear.
12.0	North column, upper corner	Strap beginning to tear on back near column.
13.6	Interior studs	Local buckling near knockouts.
13.6	Diagonal straps	Three straps have failed.

Table B-16. Panel D1c cyclic observations.

Shear Deflection (in.)	Location	Failure or Other Observations
0.4	Diagonal straps	Straps yielding.
0.8	South column, lower corner	Inside weld of nested stud beginning to fracture.
1.2	South column, upper corner	Weld on top of nested stud beginning to fracture.
1.6	South column, lower corner	Tearing of bottom track at column interior.
1.6	North column, upper corner	Crack in weld at column/nested stud connection at front face.
2.4	North column, Lower Column	Weld at column/bottom track failed. Tear forming across nested stud near column connection at exterior face. Buckling of bottom track away from the nested studs. Uplift of track at column (front).
2.4	First stud	Strap weld fracturing (back).
3.2	North column, lower corner	Tear at weld propagating into bottom track.
3.2	South column, upper corner	Top track beginning to tear (exterior).
4.0	First & second stud	Welds to strap beginning to fail (back).
4.0	Third stud	Weld to strap failed (front).
4.0	North column, lower corner	Large crack through weld at the top of Bottom track near column connection at exterior face.
4.0	North column, Upper Column	Tear forming in top track at column connection at exterior face.
4.8	South column, lower corner	Bottom track beginning to lift off beam. Bottom track beginning to tear near column interior face.
4.8	First stud - bottom	Weld to bottom track beginning to fail.
4.8	South column, lower corner	Buckling of track at base.
4.8	First stud - top	Strap weld fails at back face.
5.6	North column, upper corner	Weld beginning to tear at strap/column connection at back face.
5.6	South column, lower corner	Weld at column base continues to fail.
5.6	First stud - bottom	Strap weld failure (back).
5.6	Third stud	Strap weld failure (front).
6.4	Sixth stud - top	Weld failure at strap connection at front and back face.
6.4	Fifth stud - top	Top track beginning to tear and twist at top track/stud connection.

Shear Deflection (in.)	Location	Failure or Other Observations
6.4	South column, upper corner	Top track tearing around column interior. Buckling of top track around column interior.
6.4	South column, lower corner	Small weld fracture of column/strap connection (front).
7.2	South column, lower corner	Total weld failure of column to bottom track connection at back face.
7.2	North column, upper corner	Weld failure along column/top track connection at back face.
7.2	Fourth and fifth stud	Welds to strap fails.
8.0	First stud	Strap bowing between welds on same stud. Short panel welds fail. Short panel near stud is rotating down.
8.0	Interior studs - bottom	Studs buckling near bottom track.
8.0	Second stud - strap	Strap beginning to tear (back).
8.0	First stud - bottom	Stud tearing near bottom track.
8.0	Second stud - top	Weld failing at stud/top track connection.
8.0	Fourth stud - top	Stud tearing near top track (front).
8.0	First stud - top	Stud tearing near top track (front).
8.0	Fifth stud - bottom	Stud tearing at stud/bottom track connection.
8.0	Sixth stud - top	Weld at strap connection failed (back).
8.0	Diagonal strap at fifth stud	Strap beginning to tear at stud connection on front face.
8.8	Second and third stud – top	Weld beginning to fail (track/top track connection).
8.8	Interior studs	All studs tearing along bottom track.
8.8	Diagonal strap – north column, upper corner	Strap beginning to tear at column connection (front).
9.6	North column, upper corner	Welds at strap connections beginning to tear at front & back faces.
9.6	South column, upper corner	Sudden weld failure at column/top track connection.
9.6	Interior studs	All studs tearing along top track.
9.6	South column, upper corner	Top track pulling away from beam.
12.0	North column, upper corner	Strap beginning to tear near column at back and front face.
12.8	Sixth stud at strap	Tear is propagating at first stud weld.
13.6	North column, lower corner	Two tears forming in straps near column at front face.
13.6	First stud	Short panel weld fails causing panel to swing down.

Table B-17. Panel D2a monotonic observations.

Shear Deflection (in.)	Location	Failure or Other Observations
Loading to the North – Positive Direction on Data Plot		
0.7	South column, bottom corner	Track weld failure.
0.8	North column, top corner	Track weld failure.
1.7	North column, top corner	Brittle fracture of strap.
1.9	South column, bottom corner	Brittle fracture of strap (back side).
Loading to the South – Negative Direction on Data Plot		
0.5	South column, top corner	Track weld failure.
1.2	South column, top corner	Vibration noise.

Table B-18. Panel D2b cyclic observations.

Shear Deflection (in.)	Location	Failure or Other Observations
0.4	North column, bottom corner	Track welds failed (back – north side of column).
0.6	North column, top corner	Track welds failed (back).
0.8	North column, bottom corner	Track welds failed (back – south side of column).
2.4	South column, top corner	Back strap failed.
2.4	South column, bottom corner	Front strap broke.
4.0	Unknown	Last strap broke.

Table B-19. Panel D2c cyclic observations.

Shear Deflection (in.)	Location	Failure or Other Observations
0.3	North column, top/bottom corner	Track weld failure (front and back).
2.4	North column, bottom corner	Brittle tear of strap.

Appendix C: Prototype Shear Panels for Cold-Formed Steel Seismic Design

This appendix provides tabular data for the selection of possible prototype shear panels that may be used in the seismic design of cold-formed steel structures. These panels were developed for the example problem presented in Chapter 12, using the design recommendations presented in Chapter 11. Each shear panel given in Table C-1 is defined in Figure 12-9, Figure 12-11, Figure 12-13 and Figure 12-12, as indicated in Table C-1. The panel shown in Figure 12-14 was not selected for the example problem, but meets all the requirements of these design recommendations.

Definition of terms

The prototype shear panels given in Table C-1 shall be used based on the following definition of terms. For these panels, the values of GL_{max} and GL_{min} were defined at which the demand reached the capacity for one of the limiting equations given below.

$\varphi_t Q_{sy}$ = the lateral shear panel design strength that must exceed the maximum story shear per shear panel, including the effects of torsion, defined and limited by Equation 11-37.

GL_{max} = the maximum gravity load per shear panel, defined by Equation 11-18 and limited by Equations 11-55 or 11-56.

GL_{min} = the minimum gravity load per shear panel, defined by Equation 11-19 and limited by Equations 11-100, 11-108, 11-116, 11-117, 11-118, 11-120, or 11-122.

Prototype panel load table

Table C-1 provides the tabular data needed to select prototype shear panels.

Table C-1. Prototype shear panel load capacities.

Panel Figure	Lateral Design Strength $\phi_t Q_{sy}$ (kips)	Max Gravity Load/ Panel GL_{max} (kips)	Min Gravity Load/ Panel GL_{min} (kips)
Figure 12-9	8.1	35.2	-3
Figure 12-11	19.0	36.5	-4
Figure 12-13	24.2	88.5	10
Figure 12-14	24.2	224	5

Appendix D: Seismic Qualification Procedure and Acceptance Criteria for Other Shear Panel Configurations

This appendix presents the test procedure, acceptance criteria, and documentation requirements needed to demonstrate the acceptability of cold-formed steel shear panel configurations that are different from the specific system defined in Chapter 11. Acceptable configurations are limited to cold-formed steel shear panels that use diagonal straps or full panel sheets as the lateral-load-resisting elements. The columns shall be constructed with cold-formed or hot-rolled structural steel. This procedure applies to the qualification of a prototype of the specific panel that will be used in construction. Qualification requires the testing of three specimens. All panel tests shall represent full panel system tests of all the panel components including connections and anchors.

Coupon tests of all test panel materials

Coupon tests shall be performed on all materials that may contribute to the structural performance of the test panels. At least three coupons shall be tested from each lot of each type of material. Coupons shall be prepared and tested following the provisions of ASTM A370 (ASTM 2014b). Materials that contribute to the ductility of the shear panels shall have a total elongation of at least 10% for a 2 in. gage length. All coupon test results shall be plotted in a test report, in terms of stress versus strain. All coupon test results shall also be summarized in a table in the format shown in Table D-1. The data in this table shall be the average value of the three or more coupons of the particular component.

Table D-1. Tabular format for coupon test results.

Structural Component of Coupon	Design Yield Stress (MPa or ksi)	0.2% Offset Yield Strain* (mm/mm)	0.2% Offset Yield Stress* (MPa or ksi)	Maximum Load Strain (mm/mm)	Maximum Stress (MPa or ksi)	Max Stress 0.2% Offset Yield Stress
Component #1						
Component #2						

See Chapter 4 for the definitions of 0.2% offset yield strain and stress.

Coupon test of all field panel materials

Coupon tests shall be performed on all materials that contribute to the structural performance of the field panels. The field panels shall be identical to the prototype-tested panels. At least three coupons of each material shall be tested. Coupons shall be prepared and tested following the provisions of ASTM A370 (ASTM 2014b). Materials that contribute to the ductility of the shear panels shall have a total elongation of at least 10% for a 2 in. gage length. All coupon test results shall be plotted in a test report, in terms of stress versus strain. All coupon test results shall also be summarized in a table in the format shown in Table D-1. The data in this table shall be the average value of the three or more coupons of the particular component. The field diagonal straps or full panel sheets shall have a coupon yield stress (0.2% offset) not greater than 5% above or not less than 10% below the test panel coupon yield stress (0.2% offset). The field material coupons for all other structural elements shall have coupon yield stress (0.2% offset) not less than the test panel coupon yield stress (0.2% offset).

Test configuration

Full-scale test panels shall be tested with both monotonic (push-over in one direction) and cyclic loading. The panels shall be anchored to a base beam and top beam in a manner representative of the field installation. The base beam shall resist any slippage, out-of-plane movement or rotation in any direction. Vertical load shall be applied to the shear panel through the top beam, at a level representative of potential gravity loads in the field. The amount of vertical load applied should consider the worst-case condition for the most vulnerable panel components. For example, the minimal vertical load may provide the most severe loading for the anchors, while the maximum vertical would provide the worst-case loading for column buckling. This vertical load shall be held constant throughout each test. The top beam shall be held horizontal during all tests, as this represents the field conditions when the panel is assembled in a building. Figure D-1 shows the test configuration and instrumentation plan for shear panels tested at ERDC-CERL, to illustrate the load configuration. In the ERDC-CERL tests, stroke control was used to keep the two vertical actuators at the same length, which held the top beam horizontal. The combined vertical force was held constant by using the test control system (which was done manually for earlier tests).

Figure D-1. Schematic drawing showing sensor locations.

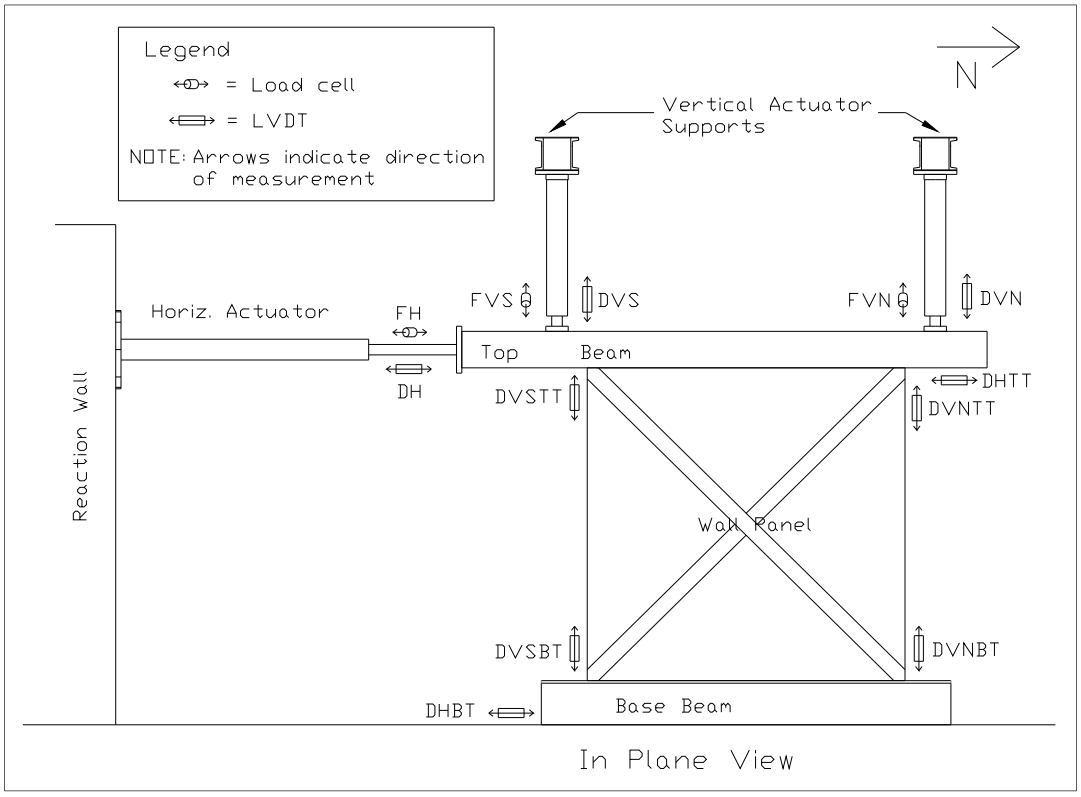

Instrumentation

Table D-2 defines the instrumentation required for all shear panel tests. Figure D-1 shows the location and orientation of all sensors, and Table D-2 describes the purpose of each sensor. The purpose of most gages is to ensure that no unwanted motion takes place and for test control. The only data used in reporting panel performance are the first, second, third, and fourth channels in Table D-2. The vertical actuator force measurements (FVS and FVN in Table D-2 and Figure D-1) are required to define total shear force when deflections reach large amplitudes, at which point the horizontal components of these forces become significant. This total shear force, TSF, is determined as follows:

$$TSF = FH - TVF\left\{sin\left[arctan\left(\frac{DH}{L}\right)\right]\right\} \quad \text{(Eq D1)}$$

where

FH = the measured horizontal actuator force (see Table D-2 or Figure D-1).

TVF = the total vertical actuator force, equal to FVS plus FVN (Table D-2 or Figure D-1).

DH = the measured horizontal displacement (Table D-2 or Figure D-1).

L = the length of the vertical actuators, with vertical load applied but no horizontal displacement.

Table D-2. Cold-formed steel shear panel instrumentation.

Channel #	Sensor Type	Measurement, Direction, Location and Symbol	Purpose
1	Load cell	Force Horizontal, FH	Horizontal actuator load measurement
2	LVDT	Deflection Horizontal, DH	Horizontal deflection, shear panel deformation
3	Load cell	Force Vertical South, FVS	Manual vertical load control (25k total load w/#5)
4	LVDT	Deflection Vertical South, DVS	Stroke (tied to #6)
5	Load cell	Force Vertical North, FVN	Load (summed with #3, for 25k total load)
6	LVDT	Deflection Vertical North, DVN	Controlled by #4 stroke feedback
7	LVDT	Defl Horiz Bot Track, DHBT	To ensure no slippage
8	LVDT	Defl Vert South Bot Track, DVSBT	To ensure no uplift
9	LVDT	Defl Vert North Bot Track, DVNBT	To ensure no uplift
10	LRDG* (20")	Defl Horiz Top Track, DHTT	Check for shear panel deformation - same as #2
11	LRDG (10")	Defl Vert South Top Track, DVSTT	Vertical panel/column deformation & rotation check
12	LRDG (10")	Defl Vert North Top Track, DVNTT	Vertical panel/column deformation & rotation check

*Linear resistance deflection gage, or cable-extension position transducer.

Test requirements

For each shear panel qualified, three specimens shall be fabricated and tested. This requirement assumes only minor variation in panel performance for a given shear panel. If large variations occur, more than three specimens shall be tested and a statistical evaluation of panel performance may be required. For panels with minor variation, one specimen shall be tested monotonically and two shall be tested cyclically, as defined below. All tests, both monotonic and cyclic, shall use stroke control, loading the panels laterally at a constant displacement per minute. The vertical load shall be held constant and the top beam shall be held horizontal throughout each test, as described previously under "Test Configuration." Both monotonic and cyclic tests shall be conducted up to deflections that cause ultimate failure of the shear panels or reach the limits of the test equipment, but shall not be less than 10 times the lateral yield displacement of the test panel, δ_y. These deflections are very large (well beyond acceptable drift limits), but they are needed to ensure that brittle failures (sudden loss of lateral or vertical load-carrying capacity) do not occur near the useful deflection range of the panel.

Monotonic test protocol

A single specimen of each shear panel shall be loaded in one direction (monotonic) at a constant stroke rate that is slow enough to allow careful observation of panel performance and failure progression.[25] These observations shall include documentation of panel behavior through a log of observations with respect to displacement and photographs. Load versus deflection (TSF versus DH) shall be plotted to determine the measured lateral yield displacement, δ_y, and this value shall be used in defining the cyclic test protocol.

Cyclic test protocol

A minimum of two specimens of each panel configuration shall be loaded cyclically at a constant stroke rate that is slow enough to allow careful observation of panel performance and failure progression[26]. These observations shall include documentation of panel behavior through a log of observations with respect to displacement and photographs. Load versus deflection (TSF versus DH) shall be plotted to create load/deflection hysteretic envelopes. The cyclic load protocol follows a standard method, so that test results may be compared with cyclic test results of other systems. The protocol defined here is similar to SAC Phase 2 guidelines (SAC 1997) that have been modified to scale to the lateral yield deflection, as described in ATC-24 (ATC 1992). The SAC-recommended loading histories call for loading with a deformation parameter based on interstory drift angle, θ, defined as interstory displacement over interstory height. The commentary to SAC (1997) explains that the interstory drift angle of 0.005 radians corresponds to a conservative estimate of the value that would cause yield deformation. Therefore, the load protocol defined by SAC in terms of drift angle is scaled to the measured lateral yield deflection, δ_y, to define the cyclic test steps shown in Table D-3. This protocol calls for a set number of cycles at each of the deformation amplitudes shown in Table D-3. This protocol is illustrated by the deformation time history shown in Figure D-2, which is based on a lateral yield deflection, δ_y of 0.4 in. and stroke rate of 6 in. per minute.

[25] Monotonic tests reported in Chapter 7 used a stroke rate of 0.5 in. per minute.

[26] Cyclic tests reported in Chapter 7 used a stroke rate of 3 and 6 in. per minute. The faster stroke rate was used for panels tested cyclically beyond 10 in. (20 in. peak to peak).

Table D-3. Cyclic test load protocol.

Load Step #	SAC-2		Modified SAC Amplitude
	Number of Cycles, n	Peak Deformation, θ (radians)	
1	6	0.00375	$0.75\delta_y$
2	6	0.005	$1.0\delta_y$
3	6	0.0075	$1.5\delta_y$
4	4	0.01	$2\delta_y$
5	2	0.015	$3\delta_y$
6	2	0.02	$4\delta_y$
7	2	0.03	$6\delta_y$
8	2	0.04	$8\delta_y$
9	2	0.05	$10\delta_y$
10	2	0.06	$12\delta_y$
11	2	0.07	$14\delta_y$
12	2	0.08	$16\delta_y$
13	2	0.09	$18\delta_y$
14	2	0.10	$20\delta_y$
15	2	0.11	$22\delta_y$
16	2	0.12	$24\delta_y$
17	2	0.13	$26\delta_y$
18	2	0.14	$28\delta_y$
19	2	0.15	$30\delta_y$
20	2	0.16	$32\delta_y$

Shear panel performance documentation

Shear panel performance from both monotonic and cyclic tests shall be documented in terms of load versus deflection plots (TSF versus DH). Cyclic tests plot load versus deflection to define load-versus-deflection hysteretic envelopes. Observations of panel performance and failure progression with respect to lateral displacement shall be documented in a spreadsheet format. Photographs that document these observations shall be included in the test report. Test results for each specimen tested shall be summarized in the format shown in Table D-4. Repeatability of panel performance of a given configuration is critical so that if only two cyclic tests are conducted, the poorest performance of the two shall form the basis for design. Therefore, special consideration shall be given to large variations in panel performance, especially failure type or displacement amplitude of each type of failure. Test procedures and results shall be documented in a test report.

Figure D-2. Modified SAC cyclic test time history, with δ_y = 0.4 in. and 6 in./min stroke rate.

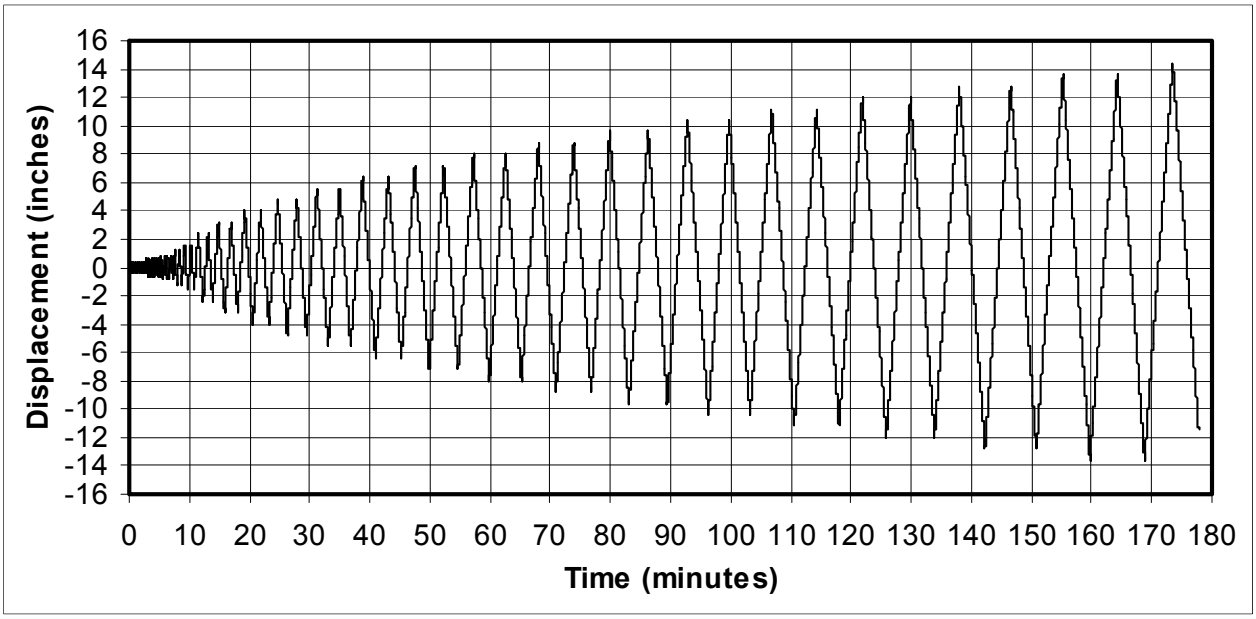

Table D-4. Summary of test panel performance (specified format).

Test Specimen	Load Type (Monotonic or Cyclic)	Load Rate (mm/min or in/min)	Linear Shear Stiffness (kN/mm) or (kips/in.)	Shear Load at δ_y Deflection (kip or kN)	Shear Deflection at Ultimate Shear Load (in. or mm)	Ultimate Shear Load (kip or kN)

Design recommendations

The measured load versus deflection data shall be used to define the design strength and stiffness of the shear panels. Resistance factors for each loading mechanism shall be defined that recognize the variation of the shear panel capacity. In other words, a panel shear capacity resistance factor, ϕ_v, shall reflect the variability of shear capacity of the tested panels. For example, ϕ_v = 0.9 if the strength variability is small and both mode and displacement of failures are consistent. The following criteria shall be defined from the shear panel cyclic test data:

1. The panel ductility, μ, the ultimate lateral deflection without loss of lateral or vertical load capacity, δ_u, over yield lateral deflection, δ_y, defined as follows:

$$\mu = \frac{\delta_u}{\delta_y} \quad \text{(Eq D2)}$$

2. The panel overstrength, Ω,[27] the maximum measured ultimate lateral panel capacity, Q_u, over the yield capacity, Q_y, defined as follows:

$$\Omega = \frac{Q_u}{Q_y} \quad \text{(Eq D3)}$$

3. The panel redundancy factor, ρ_1, of the individual shear panel tested[28]. This redundancy can be seen by comparing shear panel load/deflection data with coupon data, to determine if overstrength, Ω is due to strain hardening of the primary load-carrying element or due to the action of a secondary lateral load-resisting element. An example of this would be a panel with diagonal straps acting as the primary element with the columns effectively working to provide a significant moment frame. In this case the moment frame would provide redundancy for the shear panel. If the diagonal straps fail, this moment frame capacity would provide lateral resistance for the moment from the P-delta effect of the gravity load. This redundancy is critical to preventing building collapse for a structure whose lateral load-resisting system has failed. The panel redundancy factor, ρ_1 is calculated as follows:

$$\rho_1 = \frac{Q_u}{Q_p} = \frac{Q_p + Q_q}{Q_p} \quad \text{(Eq D4)}$$

where

Q_p = the portion of the shear panel ultimate lateral capacity carried by the primary lateral load-resisting element including the effects of strain hardening. For panels with full panel sheet(s), this contribution will increase with increasing deflection due to a widening of the panel tension field. This value can only be reasonably determined by measuring Q_c (as described below) and calculating Q_p as the difference between Q_u and Q_c.

Q_c = the portion of shear panel ultimate lateral capacity carried by the columns acting as moment frames. For panels with full

[27] This should not be confused with the system overstrength factor, Ω_0, as defined in ASCE 7-10 (ASCE 2010), Section 12.2.1.

[28] This should not be confused with the reliability factor, ρ or ρ_x, which is the extent of structural redundancy in the lateral-force-resisting system for an entire story of a building.

panel sheet(s), this value can only be obtained by testing the same exact panels with the full panel sheets removed. If these tests are not performed for full panel sheet shear panels, Q_c shall be set equal to zero.

4. The width of the cyclic test load/deflection hysteretic envelope. If the hysteretic envelope is significantly pinched (no or very little load resistance away from the peak excursions), much less energy is absorbed by the structural system so that building amplification grows. Pinched hysteretic envelopes occur when the primary lateral load-resisting element is stretched, and there is little redundant capacity from other elements to pick up load, so that little resistance is available away from the peak excursions of the load cycles. Panels with significantly pinched hysteretic envelopes, can experience high acceleration impact loading because the building will be free to sway with little resistance and then suddenly snap the lateral load-resisting element when another peak excursion is reached. This high acceleration snap can cause brittle failures. A shear panel with a great deal of redundancy within the panel, ρ_1 will tend to have a wide hysteretic envelope.

Table D-5 defines the acceptance criteria in terms of μ, Ω and ρ_1, based on data measured in the cyclic panel tests as defined by Equations D2 through D4.

Values for the system response modification coefficient, R; system overstrength factor, Ω_o; and deflection amplification factor, C_d, are defined in Table D-6. These values are used in the seismic design guidance defined in ASCE/SEI 7-10. Exceptions to these criteria shall require AISI approval or Corps of Engineers Headquarters (CEMP-ET) approval for Department of Defense construction.

Table D-5. Acceptance criteria for shear panels based on μ, Ω, and ρ_1.

Criteria	Acceptance Requirement
Panel ductility, μ	≥ 10
Panel overstrength, Ω	≥ 1.3
Panel redundancy factor, ρ_1	≥ 1.0
Hysteretic envelope width	Not required

Table D-6. Values for R, Ω_0, and C_d.

Factor	Value
System response modification coefficient, R	4
System overstrength factor, Ω_0	2
Deflection amplification factor, C_d	3.5